Relationship Between Atmospheric Rivers and the Dry Season Extreme Precipitation in Central-Western Mexico

Héctor Alejandro Inda Díaz[1] and Travis Allen O'Brien[2]

[1]Lawrence Berkeley National Laboratory
[2]Indiana University Bloomington

February 27, 2023

Abstract

Atmospheric rivers (AR) are long, narrow jets of moisture transport responsible for over 90% of moisture transport from the tropics to higher latitudes, covering only between 2% and 10% of the earth's surface. ARs have a significant impact on the hydrological cycle of midlatitudes and polar regions, which has resulted in a large effort to study ARs and their impacts on these regions. It is not until recently that ARs in tropical latitudes are starting to generate interest within the scientific AR community.

We use the ERA-20C reanalysis and the Bayesian AR detector TECA-BARD to show the relationship between extreme precipitation and atmospheric rivers in central-western Mexico (CWM) during the dry seasons (November-March) in the 1900-2010 period.

We find that more than 25% of extreme precipitation amount and frequency are associated with ARs, with a maximum of 60%-80% during December and January near the coast of Sinaloa (107.5W,25N). Composites of the mean meteorological state show "ideal" conditions for orographic precipitation due to landfalling ARs: high horizontal vapor transport perpendicular to the Sierra Madre. We observe a tropospheric wave pattern in vertical velocity, surface pressure, and geopotential height associated with these events. The nature and evolution of these waves need to be further studied. Our results suggest that TECA-BARD provides a reasonable estimation for AR presence in CWM. Nevertheless, we recommend using multiple AR detectors and one tuned explicitly for tropical latitudes. This will allow investigation of the response of CWM landfalling ARs and the region's hydroclimatology under future climate scenarios.

Relationship Between Atmospheric Rivers and the Dry Season Extreme Precipitation in Central-Western Mexico

H. A. Inda-Díaz[1], T. A. O'Brien[2,1]

[1]Climate and Ecosystem Sciences Division, Lawrence Berkeley National Laboratory, Berkeley, CA, USA
[2]Dept. of Earth and Atmospheric Sciences, Indiana University, Bloomington, IN, USA

Key Points:

- Extreme precipitation during the dry season in Central-Western Mexico is associated with atmospheric rivers (ARs)
- The meteorological state during extreme precipitation events shows ideal conditions for orographic precipitation over the Sierra Madre
- A detector designed for tropical latitudes could increase the correlation between ARs and dry season precipitation over Central-Western Mexico

Corresponding author: T.A. O'Brien, `obrienta@iu.edu`

Abstract

Atmospheric rivers (AR) are long, narrow jets of moisture transport responsible for over 90We use the ERA-20C reanalysis and the Bayesian AR detector TECA-BARD to show the relationship between extreme precipitation and atmospheric rivers in central-western Mexico (CWM) during the dry seasons (November-March) in the 1900-2010 period. We find that more than 25% of extreme precipitation amount and frequency are associated with ARs, with a maximum of 60%-80% during December and January near the coast of Sinaloa (107.5W,25N). Composites of the mean meteorological state show "ideal" conditions for orographic precipitation due to landfalling ARs: high horizontal vapor transport perpendicular to the Sierra Madre. We observe a tropospheric wave pattern in vertical velocity, surface pressure, and geopotential height associated with these events. The nature and evolution of these waves need to be further studied. Our results suggest that TECA-BARD provides a reasonable estimation for AR presence in CWM. Nevertheless, we recommend using multiple AR detectors and one tuned explicitly for tropical latitudes. This will allow investigation of the response of CWM landfalling ARs and the region's hydroclimatology under future climate scenarios.

Plain Language Summary

Atmospheric rivers (ARs) are a meteorological phenomenon with strong poleward water vapor transport. Due to their important role in the hydrological cycle and water availability of midlatitudes (like California, Europe, and Chile, among others) and polar regions, the scientific community has mainly focused AR research on these regions. It was not until recently that AR in lower tropical latitudes gathered more attention. This work focuses on the relationship between ARs and the dry season (November-March) precipitation over Central-Western Mexico (CWM), around 25 degrees north over the Pacific Coast of Mexico. We use precipitation data from the ERA-20C reanalysis, observational dataset, and a Bayesian AR detector to show that most of the precipitation over CWM during the November-March season is due to meteorological features with similar characteristics to midlatitude ARs. These events show typical conditions for ARs orographic precipitation: high water vapor transport perpendicular to the Sierra Madre that condensates into rain when the mountains lift it. We believe that an AR detector specifically designed for tropical latitudes could increase the relationship between AR and November-March precipitation in CWM and better allow us to study how these events might be modified by climate change.

1 Introduction

Atmospheric rivers (AR) are long, narrow jets of moisture transport typically associated with a low-level jet stream ahead of the cold front of an extratropical cyclone (F. M. Ralph et al., 2018). ARs account for over 90% of the water vapor transport from the subtropics to midlatitudes (Zhu & Newell, 1998). Over the last 20 years, there has been an increasing interest in the study and characterization of ARs. Numerous recent studies investigate AR and their relationship with extreme wind, precipitation, their impact on the regional hydrological cycles, water mass balance, and extreme hydrological events like flooding and droughts in midlatitude continental regions like North America, Europe, and South America (Neiman et al., 2002; F. M. Ralph et al., 2004, 2005, 2006; Dirmeyer & Brubaker, 2007; Neiman et al., 2008; Leung & Qian, 2009; Guan et al., 2010; Viale & Nuñez, 2011; M. Dettinger, 2011; F. M. Ralph & Dettinger, 2011; Warner et al., 2012; M. D. Dettinger, 2013; Lavers & Villarini, 2013b, 2013a; Kim et al., 2013; Neiman et al., 2013; F. M. Ralph et al., 2013; Rutz et al., 2014; Gimeno et al., 2016; Lavers, Waliser, et al., 2016; Lavers, Pappenberger, et al., 2016; Waliser & Guan, 2017; Gershunov et al., 2017; Goldenson et al., 2018; Viale et al., 2018; Eldardiry et al., 2019; F. M. Ralph et al., 2019; Huang et al., 2021). Some works have even investigated the structure of AR using *in situ* data and satellite observations (F. M. Ralph et al., 2005; Neiman et al., 2008; F. M. Ralph et al., 2010).

The significant impact of ARs on the climatology and hydrology of midlatitudes has generated great interest and community effort in studying ARs and their impacts on these regions. (F. Ralph et al., 2019) introduced a scale to categorize AR strength based on vapor transport intensity and landfall duration and show that there are beneficial and hazardous impacts associated with AR events. This scale is helpful for the scientific community, and it is a way of communication with the general public. The AR category scale can be applied to gridded datasets such as reanalysis, forecast, and climate projections. There is also an increasing interest in understanding how ARs and their impact will change in future climates. (Payne et al., 2020) concludes that AR response to climate change will have noticeable importance to water balance and regional water resources.

Most of the ARs research focuses on midlatitudes and polar regions. ARs in low latitudes are starting to generate interest within the scientific AR community. This work is motivated by the lack of study of tropical ARs. Moreover, we are also motivated by the direct observation of “unusual non-tropical” precipitation in the Winter of 2019-2020 in Nayarit, Mexico ∼21.5N,104.9W, during the dry season (November-March). We refer to “unusual non-tropical” precipitation as a low magnitude precipitation rate (compared to convective heavy tropical precipitation). During these days, we observed constant rainfall throughout one or two days, very similar to typical California winter precipitation (Figure 1(b) shows the IVT and horizontal wind speed at 700 hPa from one such event). The similarities in the IVT field with the typical characteristics of an AR raised the question: *is this an AR? Are there more events like this, and how are they associated with the extreme precipitation for the dry season in Central-Western Mexico (CWM)?* (thick black contour in Figure 1(a)).

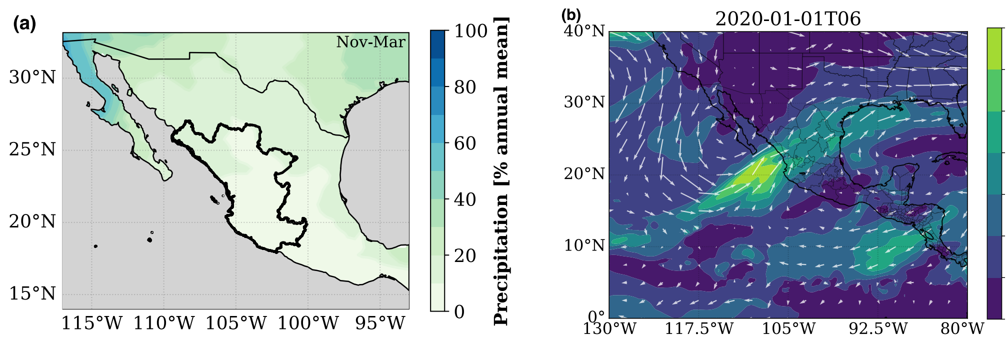

Figure 1. (a) Percentage of annual total precipitation from CPC Global Unified Gauge-Based Analysis of Daily Precipitation. Thick black contour is used to indicate what is considered as Central-Western Mexico throughout this work. (b) ERA5 reanalysis IVT in color contours. Vectors represent the 750 hPa wind velocity. 2020-01-01 is one of the times when the precipitation in CWM resembled the winter Californian AR-associated rainfall.

CWM is characterized by a dry season from November to March (García Amaro de Miranda, 2003), with a mean monthly accumulated precipitation of less than 10 mm[1] and over 75% of the annual precipitation from July-September, during the spring and

[1] `https://smn.conagua.gob.mx/es/climatologia/temperaturas-y-lluvias/resumenes-mensuales-de-temperaturas-y-lluvias`

summer months. Rainfall in CWM is mainly associated with the North American Monsoon. Less than 10% of the total annual mean rainfall occurs between November and March for most of CWM (Figure 1(a)), according to the CPC Global Unified Gauge-Based Analysis of Daily Precipitation[2] (Chen et al., 2008).

From a socio-economic point of view, it is important to study and quantify these events of atypical precipitation. CWM is one of the largest agricultural production regions in Mexico. It is common knowledge among CWM farmers that these rainfall events can be exploited to benefit agriculture; however, we could not find scientific quantification of it. There are even popular beliefs that they can be predicted following a set of heuristic rules (Cruz López, 2011). There is also some evidence that different crops, like beans, coffee, and corn, are sensitive to changes in environmental conditions, like precipitation and humidity (Viguera et al., 2017). Therefore, changes in climate conditions can affect the productivity and quality of the crops (Porter & Semenov, 2005).

Moreover, changes in wind speed and direction, moisture transport, and the location of the intertropical convergence zone (ITCZ) can modify the energy exchange between the atmosphere and the ocean. These changes could generate a displacement northward of the oxygen minimum zone (OMZ), which can affect ocean species distribution and the productivity of regional aquaculture and fisheries (Breitburg, Denise; Grégoire, Marilaure and Isensee, Kirsten, 2018). Furthermore, other studies have observed that dry season rainfall events can change the coastal environment. Coastal water chlorophyll concentration, turbidity, temperature, and salinity, due to increased river discharge, can impact the sustainability of coastal ecosystems and their biological production (Domínguez-Hernández et al., 2020; Romero-Rodríguez et al., 2020).

Although there are numerous possible effects of anomalous winter precipitation in the CWM region, there is still a lack of documentation about these events and their impacts. Moreover, no existing research links these events with ARs. We investigate the relationship between lower latitudes ARs "dry season" (November-March) rainfall in CWM. We use data from the European Centre for Medium-Range Weather Forecasts (ECMWF) Atmospheric Reanalysis of the Twentieth Century ERA-20C[3] (Poli et al., 2016) and the Bayesian AR Detector `TECA-BARD v1.0.1`. We aim to quantify how much of the CWM winter precipitation is associated with ARs and the meteorological state of the atmosphere during these events.

2 Data and Methods

ERA-20C output is 3-hourly with a of ∼125 km on 37 pressure levels. We use data at pressure level: geopotential `z`, wind velocity `u`, `v`, and `w`, specific humidity `q`, temperature `t`, and surface level: mean sea level pressure `mslp`, surface pressure `ps`, total precipitation `tp`, vertical integral of northward water vapor flux `vinwvf`, vertical integral of eastward water vapor flux `viewvf`, and total column water vapor `tcwv`. According to the ERA-20C documentation, the vertically integrated vapor fluxes are calculated in the model coordinates following:

$$\text{VIEWVF} = -\frac{1}{g}\int_0^1 qu\frac{\partial p}{\partial \eta}d\eta \approx -\frac{1}{g}\sum_{k=1}^{N} u_k\, q_k \Delta p_k, \tag{1}$$

$$\text{VINWVF} = -\frac{1}{g}\int_0^1 qv\frac{\partial p}{\partial \eta}d\eta \approx -\frac{1}{g}\sum_{k=1}^{N} v_k\, q_k \Delta p_k, \tag{2}$$

[2] `https://psl.noaa.gov/data/gridded/data.cpc.globalprecip.html`
[3] `https://www.ecmwf.int/en/forecasts/datasets/reanalysis-datasets/era-20c`

where u and v are the components of the horizontal wind vector, q is the specific humidity, p is pressure, η is the hybrid coordinate (Simmons & Burridge, 1981), index k corresponds to model levels going from the surface ($k = 1$) to the top of the model atmosphere ($k = N$), and Δp_k is the difference in level pressures, estimated at level k. ERA-20C daily forecasted precipitation accumulation has been converted to a 3-hourly precipitation rate (with units of mm/d); IWV is used directly from ERA-20C total column water vapor `tcwv`. IVT is calculated as the magnitude of the vertically integrated moisture-weighted wind (horizontal vapor flux vector) $\vec{u_q}$, directly from ERA-20C eastward and northward water vapor fluxes:

$$\vec{u_q} = (\mathrm{VIEWVF}, \mathrm{VINWVF}), \tag{3}$$

$$\mathrm{IVT} = |\vec{u_q}| = \sqrt{\mathrm{VIEWVF}^2 + \mathrm{VINWVF}^2}. \tag{4}$$

Additionally, we compare the ERA-20C reanalysis data with observational precipitation, using precipitation data from the Livneh gridded precipitation for the continental US, Mexico, and Southern Canada (Livneh, Ben & National Center for Atmospheric Research Staff (Eds), Last modified 12 Dec 2019). The (Livneh et al., 2015) dataset is a long-term gridded daily dataset at fine 1/16° (∼6 km) horizontal resolution for the period 1950-2013. We use bilinear interpolation to regrid the AR detection from TECA-BARD in ERA-20C data to the Livneh dataset grid.

2.1 AR probability from ERA-20C and TECA-BARD

To calculate the probability of the presence of an atmospheric river (AR probability) we use the Bayesian AR Detector `TECA-BARD v1.0.1`, a probabilistic AR detector implemented in the Toolkit for Extreme Climate Analysis `TECA`. TECA-BARD uses a Bayesian framework to sample from the set of AR detector parameters that yield AR counts similar to the expert database of AR counts; this yields a set of "plausible" AR detectors from which we can assess quantitative uncertainty (O'Brien et al., 2020). We apply TECA-BARD to the ERA-20C data, and asses the plausible presence of an AR at a grid point where where AR probability$>$ 0.05. While 0.05 is a low probability threshold, this indicates a non-zero probability of the existence of an AR in a given grid cell. Since TECA-BARD is inherently designed to detect ARs in mid-latitudes, it filters the IVT field near the tropics, resulting in AR probability that would have lower values in the presence of an AR in tropical latitudes than one in higher latitudes. We hypothesize that AR probability$>$ 0.05 represents a reasonable indication of the presence of an AR in lower latitudes. We test and show this in Sections 5 and 6.

2.2 Extreme Precipitation

We calculate the monthly 98th percentile precipitation rate value for ERA-20C and Livneh datasets at each grid cell. We define an *extreme precipitation event* for a given grid cell as the time when the precipitation is above the 98th percentile. We calculate the AR-associated extreme precipitation for each grid cell as the precipitation above the 98th percentile when AR probability$>$ 0.05. Since the data record is sufficiently long (1900-2010 for ERA-20C and 1950-2013 for Livneh), we calculate all means and extreme precipitation quantiles monthly. The same holds for the atmospheric state composites described in Section 2.3.

2.3 Atmospheric State Composites

Following the methodology of (Neiman et al., 2008), we create composites of meteorological variables to study the state of the atmosphere at the time of extreme precipitation and AR events at two locations: `Loc1` = 107.5W,25N, and `Loc2` = 105.0W,21N (Figure 2, `Loc1` denoted circle marker, `Loc2` by the triangle). `Loc1` is located close to the maximum area of AR-associated precipitation and close to Culiacán Sinaloa, one of the most productive agricultural states of México. `Loc2` is around the most southern region with AR-associated precipitation fraction ∼0.5, and in the state of Jalisco, another important agricultural producer in CWM. Both locations are close to the *Sierra Madre Occidental*, a mountain range that extends through Northwestern and Central-Western Mexico, as a part of the North American Cordillera, parallel to the coast. We hypothesize that if there is IVT normal to the *Sierra Madre* during the dry season, it could produce precipitation due to orographic lifting. The methodology to select the time steps to composite is as follows: we find the times when the AR probability is > 0.05 (ar), then we find all the times when the precipitation is above the 98th percentile (pr). We define then AR + extreme precipitation conditions as the times where both conditions ar and pr are met (ar_pr), times when there is ar but no pr (ar_nopr), and times when there is pr but no ar (pr_noar). Finally, the long-term mean is the monthly climatology for 1900-2010 (ltm). We average in time for all the time in each composite and create monthly composites. Anomalies are calculated as the specific composite minus the long-term mean. Table 1 summarizes the different composite sampling.

Table 1. Atmospheric state composites. Composites are created monthly. The number of events at each location is the total number of events for all November-March months.

Atmospheric state composites

Conditions	Name	Anomaly	Events at `Loc1`	Events at `Loc2`
Climatology (long term mean)	*ltm*		134304	134304
AR	*ar*	*ar* - *ltm*	8886	4650
Extreme precipitation	*pr*	*pr* - *ltm*	2690	2688
AR/extreme precipitation	*ar_pr*	*ar_pr* - *ltm*	1549	1003
AR/no extreme precipitation	*ar_nopr*	*ar_nopr* - *ltm*	7337	3647
Extreme precipitation/no AR	*pr_noar*	*pr_noar* - *ltm*	1141	1685

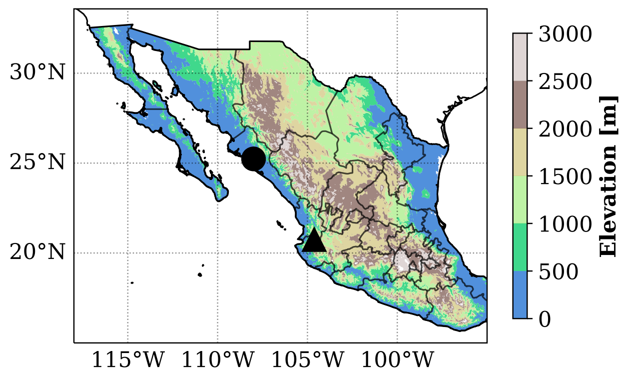

Figure 2. Orography of CWM. `Loc1` and `Loc2` are show in circle and triangle markers, respectively. The *Sierra Madre Occidental* is the mountain range that runs through Northwestern and Central-Western Mexico.

3 Results

In Section 3.1 we present the results of the AR-associated precipitation in CWM during the dry season (November-March) in the 1900-2010 period. We present the frac-tional contribution of ARs to the precipitation, using ERA-20C data and the Livneh *et al.* gridded dataset. Sections 5 through 6 focus on the meteorological state of the atmosphere during extreme precipitation and AR events and the difference between different composites. In the supplemental information, we include additional plots related to the meteorological state of the atmosphere and differences between composites.

3.1 AR-associated extreme precipitation

Figure 3 shows how much of the CWM dry season precipitation is associated with ARs. Figure 3(a) shows the fraction of ERA-20C total extreme precipitation amount associated with ARs, and (b) shows the same for Livneh precipitation. Figure 3(c) shows the fraction of ERA-20C extreme precipitation frequency associated with ARs, and Figure 3(d) shows the same for Livneh precipitation. The results are highly condensed in these figures, but they are clear and relevant: The influence of ARs in the dry season extreme precipitation in CWM extends as far as $\sim$17N. December has the highest AR-associated precipitation, with $\sim$75% of the frequency and amount 0.75 near `Loc1`, and between 50% and 60% near `Loc2`. In general, we can say that in the Nov-March, more than half of the extreme rainfall at `Loc1` (more than 30% at `Loc2`) is associated with ARs, both in total amount and frequency.

We have shown the results based on two facts: the total amount of precipitation (and frequency) higher than the monthly 98th percentile for November-March; and the "plausible" presence of an AR in CWM given the `ar_probability`$\geq$0.05. We hypothesize that this precipitation is associated with low latitudes ARs and that `TECA_bard` provides a good insight into the presence of ARs in CWM. This becomes clearer in Section 5, where we present composites of the state of the atmosphere during `ar_probability`$\geq$0.05 events at `Loc1` and `Loc2`. For simplicity, in Section 4 and 5, we show the results for January. The supplemental information contains the results for the long-term mean and *ar_pr* composites.

4 Long-term Mean

We briefly show the climatological state of the atmosphere (*ltm*) for January. The long-term mean is calculated based using ERA-20C data. Figure 4(a) shows IWV between 10 and 15 kg m^{-2} in CWM, with a maximum of 45 kg m^{-2} near the ITCZ (between 5S and 5N). IVT is shown in Figure 4(b), with values between 0 and 100 kg m^{-1}s^{-1} in CWM (IVT direction shown with vectors). We note a high IVT plume over the Pacific storm track and higher IVT values between 5S and 5N associated with the ITCZ. Mean sea level pressure depicts the North Pacific High with its maximum at 130W,30N, shown in Figure 4(c). Geopotential height at 650 hPa, shown in Figure 4(d), has a large gradient between 30N and 60N, associated with the jet stream over midlatitudes, with very little or no spatial patterns over CWM and the central Pacific Ocean. The long-term means for Nov-March are shown in the supplemental information (Figures S1 through Figure S5). The general structure of the atmosphere is similar to 4(Low IVT and IWV over CWM with the North Pacific High west of the coast of California and Baja California), with slight differences in the locations of the ITCZ, storm track, North Pacific High, etc.

5 Extreme Precipitation and AR Events Composite

In this section, we focus on the state of the atmosphere for the *ar_pr* composite (events with extreme precipitation + AR probability $\pm$0.05).

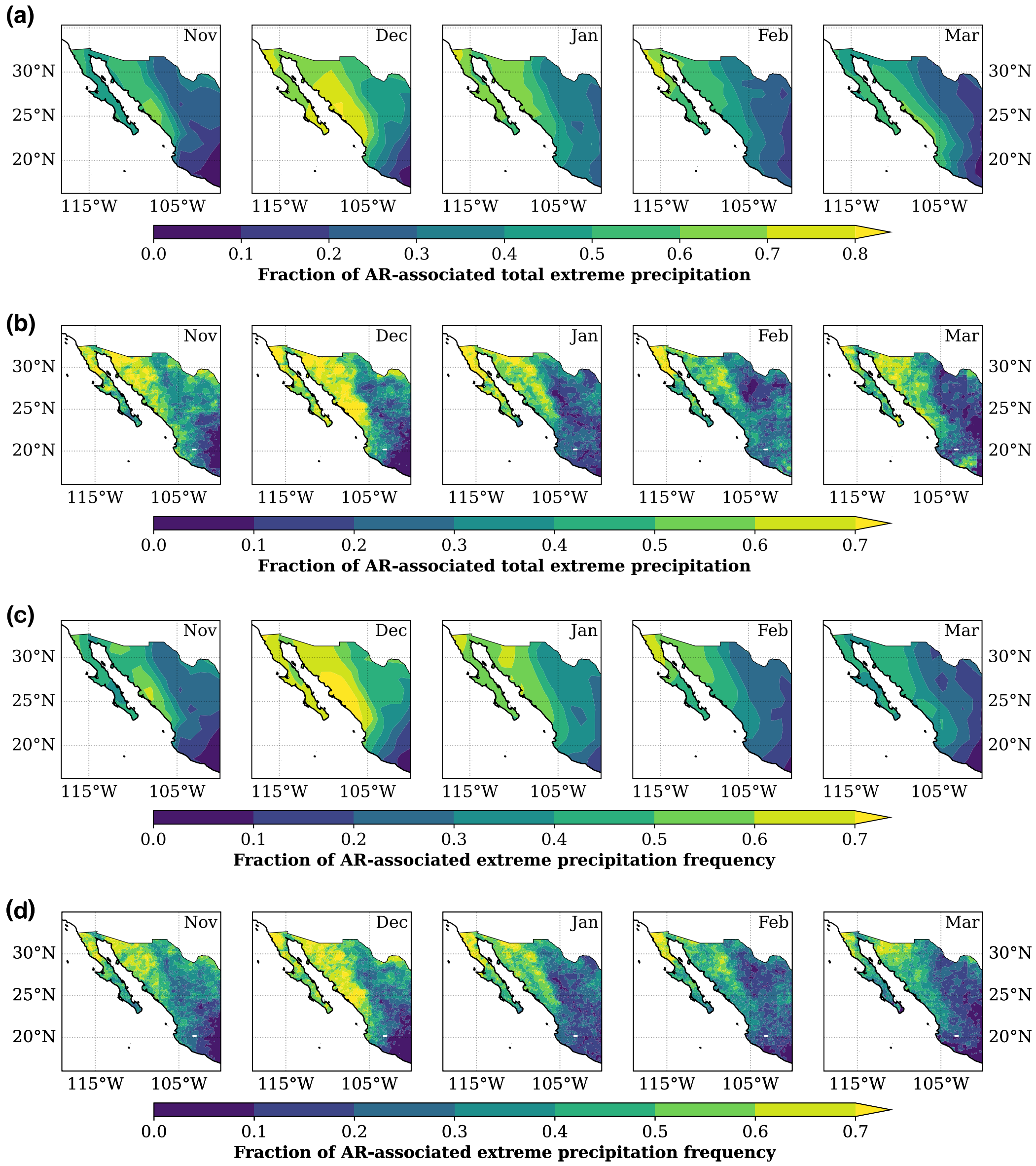

Figure 3. (a-b) Fraction of the total precipitation extreme precipitation (>98th percentile) associated with ARs. (a) ERA-20C 1900-2010. (b) Livneh 1950-2010. (c-d) Fraction of AR-associated to the total extreme (>98th) precipitation frequency. (c) ERA-20C 1900-2010. (d) Livneh 1950-2010

5.1 *ar_pr* composite at Loc1: Sinaloa, (107.5W,25N)

Figure 5(a) shows IVT in colored contours and IWV in dashed white contours. We observe an elongated region of high IWV extending from the ITCZ into CWM, with values up to 30 kg m^{-2} at `Loc1`; as well as a ridge-like structure of high IVT (between 200 and 400 kg m^{-1}s^{-1} centered at `Loc1`, similar to mid-latitude landfalling ARs (Neiman et al., 2008). Figure 5(b) shows IVT anomalies higher than 200 kg m^{-1}s^{-1}, and IWV anomalies up to 15 kg m^{-2} near`Loc1`. Mean sea level pressure (gray-filled contours in Figure 5(c)) shows the presence of the North Pacific High. Moreover, in 5(d), we observe a low in sea level pressure and geopotential height at 850 hPa anomalies centered near

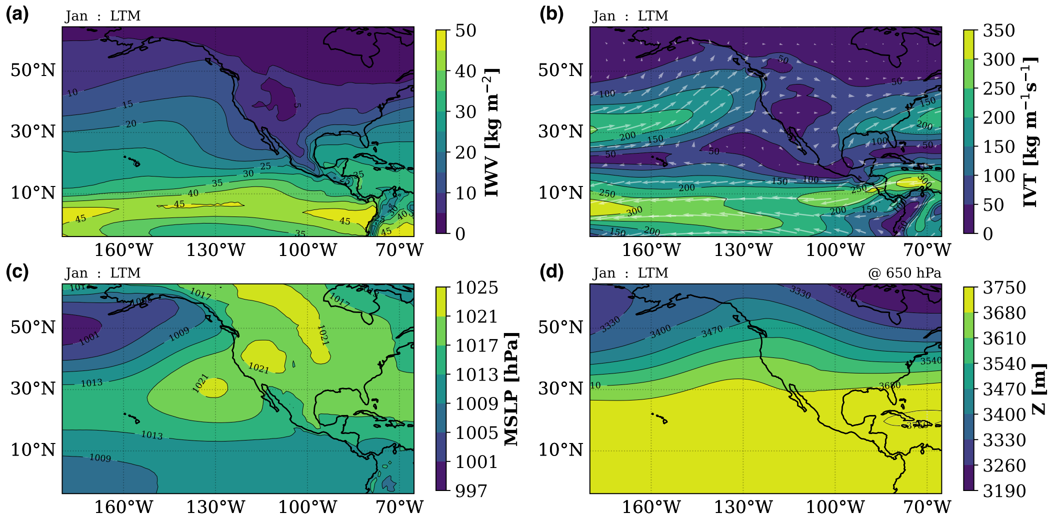

Figure 4. Long-term mean for 1900-2010 in December. (a) Integrated water vapor (IWV), (b) integrated vapor transport (IVT), (c) mean sea level pressure (MSLP), (d) geopotential height at 650 hPa. The vectors in panel (b) represent the direction of IVT.

115W,30N. This wave pattern is more noticeable in Figures 5(e) and (f) (geopotential height at 500 hPa). It is worth noticing that the low-pressure system at the surface is approximately aligned with the mid-troposphere low. This could imply that the wave producing this AR-pattern and anomalous dry season precipitation is barotropic. However, more analysis is needed to determine the nature and characteristics of these waves. Figures 5(g) and (h) show a mean negative vertical velocity (ascending) over the high IVT plume, ahead of the mid-tropospheric low (with anomalies $\sim$6 hPa s^{-1}). Vectors show the direction of IVT and its anomalies in Figures 5(g) and (h). IVT is normal to the mountain range and `Loc1`, with a weakening of the westward moisture transport near the Equator.

5.2 *ar_pr* composite at Loc2: Jalisco and Nayarit (105.0W,21N)

The *ar_pr* at `Loc2` has a similar general structure to the `Loc1`, with slightly weaker IVT and higher IWV than the `Loc1` composite. Figure 6(a) shows a high IVT ridge near `Loc2` with a maximum value of $\sim$350 kg m^{-1}s^{-1} and IWV $\sim$35 kg m^{-2} near `Loc2`. The mean sea level pressure and geopotential show negative anomalies centered near 26N,110W, with lower magnitude than the `Loc1` composite anomalies (Figures 6(c-f)). An upward 650 hPa wind velocity (and its anomaly) ahead of the tropospheric through, with high IVT normal to the Sierra Madre at `Loc2` (Figures 6(g) and (h)). The genesis and nature of the waves responsible for this weather pattern need to be further explored.

6 Difference between composites

This work focuses on the relationship between ARs and extreme precipitation during the dry season in CWM. In Section 5, we show the results for the *ar_pr* composite, *i.e.* when extreme precipitation and AR are present. This naturally raises the questions: *what about the other composites?*, *what is the difference between composites?*. For example, what is the difference between the climatology of events with extreme precipitation but no ARs detected (*pr_noar*)? What drives this anomalous rainfall? For simplicity, we focus the results in this section on composites over `Loc1`.

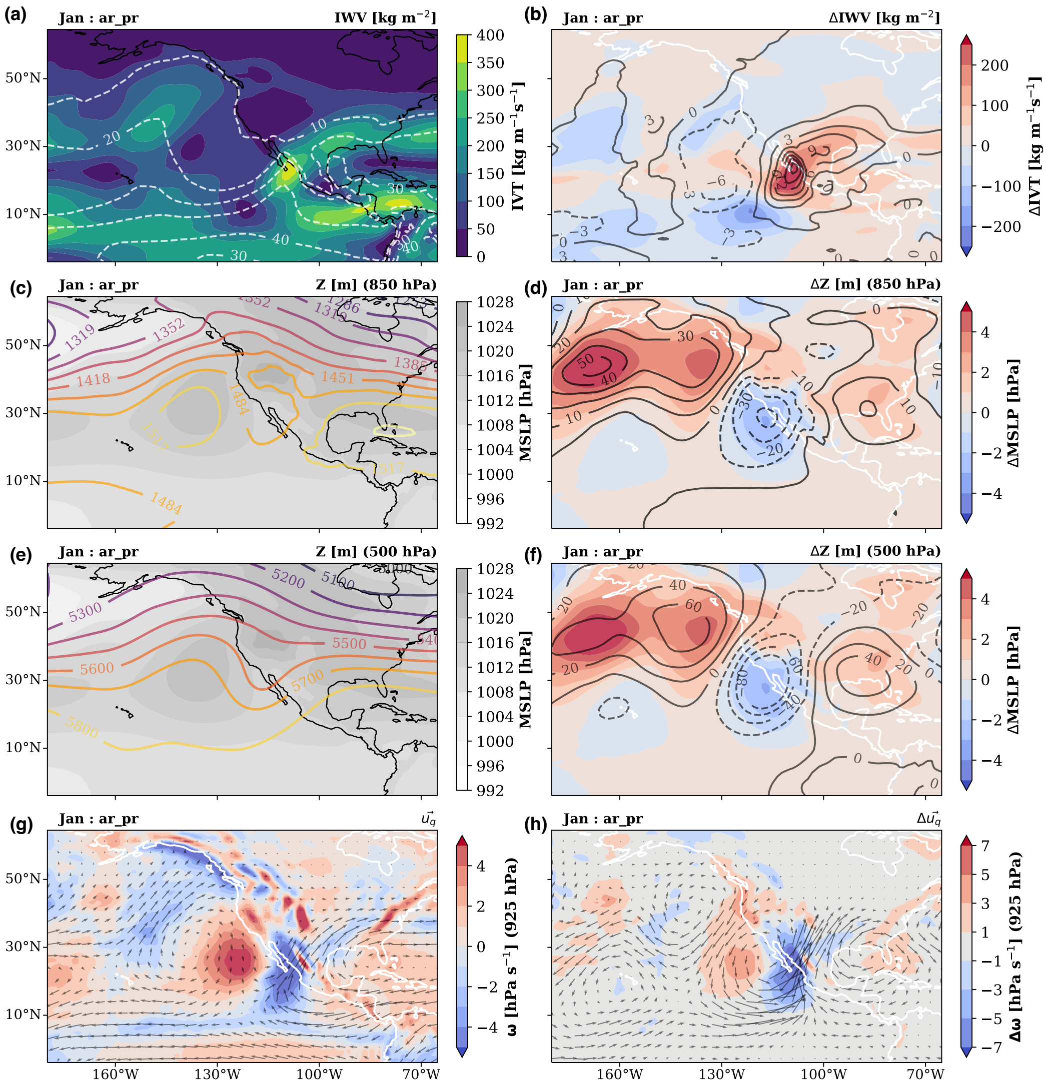

Figure 5. State of the atmosphere during AR landfalling and extreme precipitation at `Loc1` in January. Contours variables are specified on the top-right of each plot. Left column: IWV, IVT, mean sea level pressure, geopotential height at 850 and 500 hPA, IVT direction (u_q), and ω at 650 hPa. Right column: anomalies with respect to the long-term mean for the same variables.

The IWV and IVT for January during extreme precipitation without detection of ARs (*pr_noar*) is shown in Figure 7(a,b). We observe that the general structure of IVT and IWV are similar to the *ar_pr* composite (surface pressure, geopotential height, and vertical velocity plots are shown in Figure S17). So, how different are they? In Figure 7(c,d), we observe little variation between the two composites for the pressure and 850 hPa geopotential height near CWM. The main differences in the pressure/geopotential fields are in the north part of the domain, where the wave pattern, present in both *ar_pr* and *pr_noar* is stronger for *ar_pr* (positive differences in Figure 7 (d)). Nevertheless, the spatial patterns are similar between the two composites. Figure 7(c) shows moisture fields similar to *ar_pr*, although with weaker magnitudes in IVT and IWV for the *pr_noar* composite (Figure 7(c)), probably due to the weakening of the mid-troposphere wave pattern (Figure 7(d)).

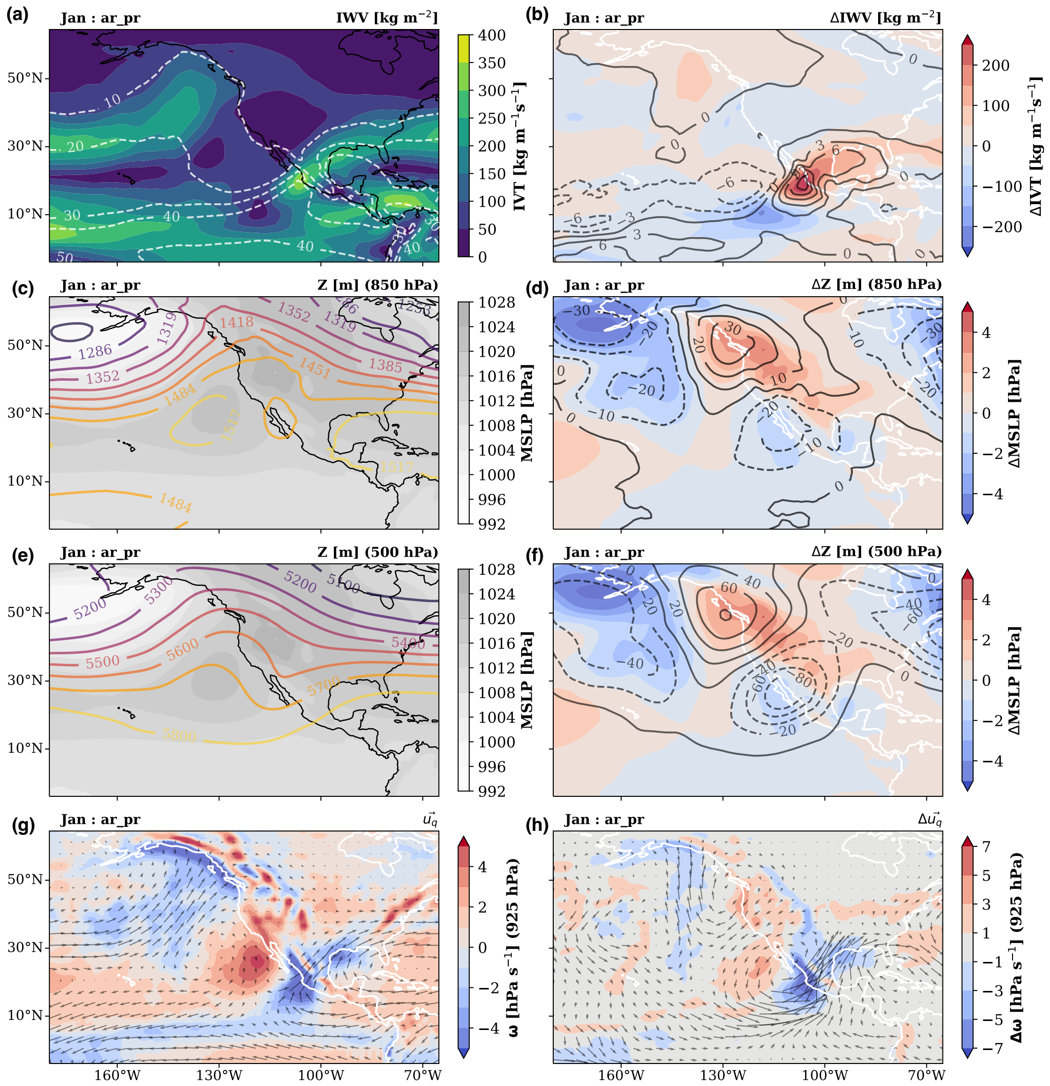

Figure 6. State of the atmosphere during AR landfalling and extreme precipitation at `Loc2` in January. Contours variables are specified on the top-right of each plot. Left column: IWV, IVT, mean sea level pressure, geopotential height at 850 and 500 hPA, IVT direction (u_q), and ω at 650 hPa. Right column: anomalies with respect to the long-term mean for the same variables.

Figure 8(a,b) show the IWV and IVT for the *ar_nopr* composite in January, *i.e.* during AR detection without extreme precipitation present. We note a moisture transport into `Loc1` (surface pressure, geopotential height, and vertical velocity plots are shown in Figure S16). In Figure 8, we notice differences between the *ar_nopr* and the *ar_pr* composites in surface pressure. The *ar_nopr* has a stronger pressure high in the northwest part of the domain but a weaker low high near CWM (Figure 8(d)). Moreover, a tilting in the geopotential height wave pattern (show in the supplemental information, Figure S16), and differences in its magnitude create a much weaker IVT magnitude and a difference in IVT direction at `Loc1` (8(c)). This could be due to a stronger mid-troposphere wave associated with the jet stream meandering or the superposition of two or more waves. Again, the nature of the wave producing these weather patterns still needs to be explored and would make an exciting work by itself. Ultimately, the main consequence of these

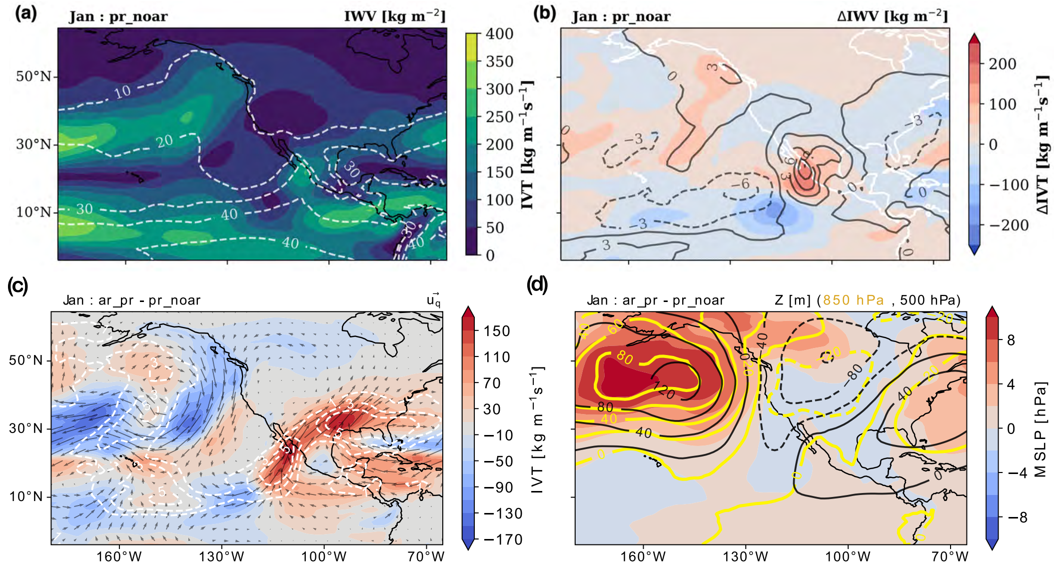

Figure 7. (a) IVT and IWV *pr_noar* composites for January and and their anomalies (`Loc1`). (c and d) Differences in the atmospheric mean state between *ar_pr* and *pr_noar*. (c) IVT magnitude in filled contours, vectors represent IVT direction IVT, and white dashed contours denote changes in IWV. (d) Filled contours show mean sea level pressure differences, thick yellow contours show geopotential height at 850 hPa, and black contours geopotential height at 500 hPa.

wave differences is that they result in a much weaker IVT magnitude with a different direction, both directly related to orographic precipitation.

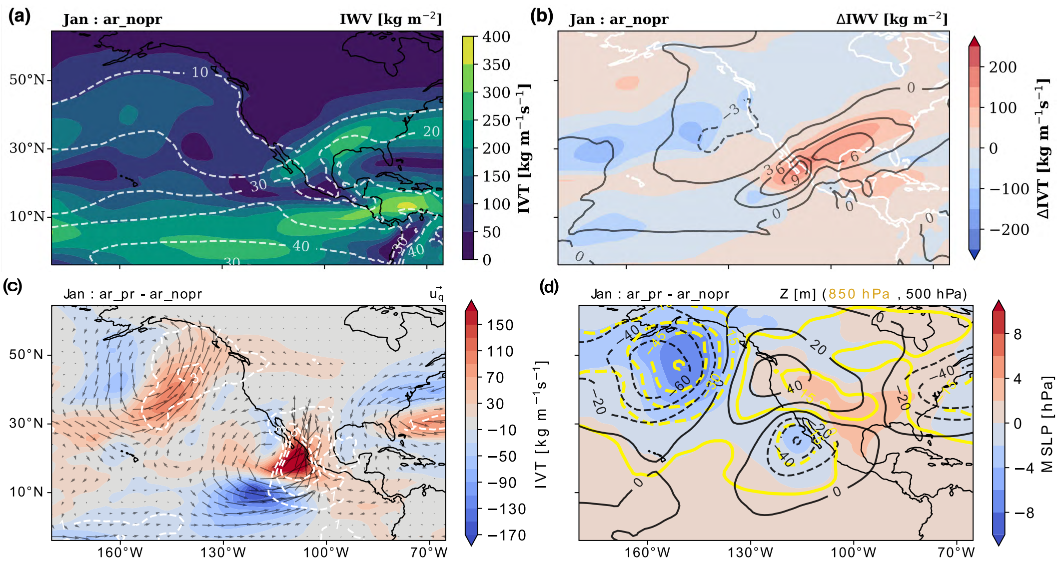

Figure 8. (a) IVT and IWV *pr_noar* composites for January and and their anomalies (`Loc1`). (c and d) Differences in the atmospheric mean state between *ar_pr* and *ar_nopr*. (c) IVT magnitude in filled contours, vectors represent IVT direction IVT, and white dashed contours denote changes in IWV. (d) Filled contours show mean sea level pressure differences, thick yellow contours show geopotential height at 850 hPa, and black contours geopotential height at 500 hPa.

Figures 7(c,d) and 8(c,d) suggest that the different composites might be related to the same or similar weather events or different phases in the same weather event or wave. To explore this, we plot the occurrence time of the events for each composite, shown in the supplemental information's Figures S18-S25 (full 1900-2010 event composites time of occurrence at `Loc1`). There is, in fact, an overlap between composites; in some cases, precipitation events occur before or after ARs but around the same dates in general. This suggests that while we have acceptably identified AR events, an ARDT tuned for tropical latitudes could improve the AR detection in CWM, which could result in a greater correlation between ARs and dry season precipitation in CWM.

7 Discussion and Conclusions

There is a large amount of literature regarding the impacts of ARs in mid-latitudes and polar regions ((Gimeno et al., 2014; F. M. Ralph et al., 2017; Paltan et al., 2017; Rutz et al., 2019; Lora et al., 2020), and references therein) and AR changes with climate change ((Lavers et al., 2015; Payne et al., 2020; O'Brien et al., 2021), and references therein). Nonetheless, there is less research about ARs and their effects in lower latitudes (M. De Luna et al., 2020; M. I. De Luna, 2021). It is not until recently that tropical ARs have started to gather scientific interest. Moreover, since the summer precipitation (June-October) dominates the total precipitation of CWM, a significant part of the research has focused on the role of tropical storms, and tropical cyclones (Farfán & Fogel, 2007; Díaz et al., 2008; Agustín Breña-Naranjo et al., 2015; Dominguez, Christian and Magaña, Victor, 2018; Dominguez et al., 2020), and the role of the North American Monsoon (Adams & Comrie, 1997; Douglas & Englehart, 2007; Cavazos, Tereza and Arriaga-Ramírez, Sarahí, 2012). Furthermore, some studies associate the fluctuations and trends in precipitation in CWM with large-scale climate features like El Niño Southern Oscillation, Pacific Decadal Oscillation, and the Atlantic Multidecadal Oscillation (Magaña, Víctor and Pérez, Joel and Vázquez, Jorge and Pérez, José, 2003; Matías Méndez and Víctor Magaña, 2010; Curtis, 2007; Arriaga-Ramírez, Sarahí and Cavazos, Tereza, 2010). In particular, CWM appears to be a transition region between the Mediterranean rainfall regime in California and northern Baja California and the summer-dominated tropical rainfall regime and the North American Monsoon. This, together with the relatively developed AR research, has resulted in an overlook of the dry season (winter) precipitation and its association with tropical ARs.

Here, we present clear evidence of the relationship between CWM dry season precipitation and ARs. Our composites reflect a high degree of similarity with other compositing studios in higher latitudes (Neiman et al., 2008). Nevertheless, many aspects of these tropical ARs still need to be studied. Investigating the characteristics of the waves that create these anomalous IVT filaments and rainfall is key to understanding these weather patterns and their implications in the CWM dry season hydrological cycle. Moreover, ARs have been typically associated with mid-latitude baroclinic waves and extratropical cyclones (ETC). However, recently (Zhang et al., 2019) showed that nearly 20% of ARs are not nearby an ETC. Here we have presented evidence that aligned surface and mid-troposphere weaves are associated with tropical ARs in CWM, and could possibly denote a barotropic nature of these waves. There is no doubt that we still have a lot to learn and explore about ARs, particularly lower latitudes ARs. We still need to determine the genesis of these events. Are they more related to extratropical weather patterns like an amplification of mid-latitude waves? or maybe to tropical dynamics, energy balance, and responses to shifts in the ITCZ (Haffke & Magnusdottir, 2013; Choi et al., 2015; Lintner & Boos, 2019). In other words, *are these events, in fact, atmospheric rivers, or are they another weather phenomenon?*. We show clear evidence that there is a reasonable degree of similarity between winter ARs in CWM and typical mid-latitude ARs, so a more reasonable question may be *how similar or how different are tropical and mid-latitude ARs?*.

Although ARs in CWM do not dominate the total annual precipitation like on the US West Coast, they regulate extreme precipitation during the dry season. The water vapor in ARs frequently leads to heavy precipitation where they are forced upward by mountains (F. M. Ralph et al., 2018; Smith et al., 2009; F. Ralph et al., 2019). The presence of the *Sierra Madre Occidental* in CWM provides creates an ideal mechanism for orographic rainfall during high IVT events in CWM. Therefore, it is relevant to quantify and understand these tropical ARs and their influence on the regional hydrological cycle of CWM. We recognize that this study (and future studies) could benefit from an ARDT tuned for tropical latitude, which brings back the question of how similar these ARs are to "traditional" mid-latitude ARs. The uncertainty in AR detection is key to answering this question. It has been discussed the possibility that there is more than one type of dynamical phenomenon that produces AR-like objects and that different definitions for these processes could help in future studies (Inda-Díaz et al., 2021; O'Brien et al., 2021). This gains particular relevance for the study of future ARs in CWM, because, in general, different "types" of AR-like phenomena (including CWM landfalling tropical ARs) could have different responses to climate change. There is some evidence of future AR frequency increases in lower latitudes (M. De Luna et al., 2020). Although the frequency increase magnitude is lower than for higher latitudes, there is no assurance on how the local hydrology will be impacted by changes in other AR quantities (intensity, size, orientation, geometry, among others).

In summary, we use data from the Atmospheric Reanalysis of the Twentieth Century ERA-20C and the TECA-BARD AR detector to demonstrate the relationship between extreme precipitation and atmospheric rivers in central-western Mexico during the dry season (November-March) of 1900-2010. We find that more than 25% of extreme precipitation amount and frequency are associated with ARs, with a maximum of 60%-80% during December and January near the coast of Sinaloa ($\sim$107.5W,$\sim$25N).

We calculate composites of the mean state of the atmosphere during AR and extreme precipitation events. We find that for the AR and precipitation composite (ar_pr), there is a positive anomaly in IWV and IVT. Horizontal vapor transport is normal to the coast and the mountain range of the Sierra Madre. Vertical velocity has upward anomalies alongside the high IVT envelope. Besides, changes in horizontal moisture transport, sea level pressure, and geopotential height anomaly fields show a wave pattern associated with the ar_pr composite. A weakening of the surface pressure high and the presence of geopotential lows (above 850 hPa) suggest that the moisture transport occurs at a higher level than typical mid-latitude ARs.

Additionally, we examine the differences between composites. Our results suggest that the AR events without precipitation have a lower IVT magnitude. Furthermore, they show a tilted wave pattern in the geopotential height field with respect to the AR with precipitation composite. Taken together, this translates into lower horizontal vapor transport values with different orientations with respect to the mountain range, resulting in lower precipitation rates. Furthermore, we show that the main difference between the precipitation events with/and without ARs composite is IVT magnitude. Both composites have similar pressure and geopotential wave patterns near the coast of CWM. The pressure and low atmosphere geopotential main differences are located north of 30N. These results suggest that the precipitation without AR events, in fact, is related to the AR events. Both composites could be part of the same weather pattern that our ARDT failed to detect due to the lower IVT magnitude and its inherent design to filter out the tropics.

The nature and genesis of these anomalous IVT events and dry season precipitation –or apparent tropical ARs– still need to be determined, and we plan to explore them in future work. We recommend using more than one ARDT or one tuned explicitly for tropical latitudes, which could sharpen the correlation between ARs and CWM winter precipitation. This will allow investigating the response of CWM landfalling ARs to climate change, which could be critical for studying the region's hydroclimatology under future climate scenarios.

Acknowledgments

The authors thank the multiple reviewers and editors whose feedback and commentary greatly improved the quality and presentation of this manuscript.

This study was supported by the Director, Office of Science, Office of Biological and Environmental Research of the U.S. Department of Energy Regional and Global Modeling and Analysis (RGMA) and used resources of the National Energy Research Scientific Computing Center (NERSC), also supported by the Office of Science of the U.S. Department of Energy under Contract no. DE-AC02-05CH11231.

This project was supported by the Environmental Resilience Institute, funded by Indiana University's Prepared for Environmental Change Grand Challenge initiative.

CPC Global Unified Precipitation data provided by the NOAA/OAR/ESRL PSL, Boulder, Colorado, USA, from their Web site at `https://psl.noaa.gov/data/gridded/data.cpc.globalprecip.html`.

We would like to acknowledge the European Centre for Medium-Range Weather Forecasts and ERA-20C Project (`https://www.ecmwf.int/en/forecasts/datasets/reanalysis-datasets/era-20c`). ERA-20C was accessed through the Copernicus Climate Change Service (C3S) Climate Data Store (CDS) - `https://apps.ecmwf.int/datasets/data/era20c-ofa/`.

We acknowledge Livneh, Ben & National Center for Atmospheric Research Staff (Eds). Last modified 12 Dec 2019. "The Climate Data Guide: Livneh gridded precipitation and other meteorological variables for continental US, Mexico and southern Canada." Retrieved from `https://climatedataguide.ucar.edu/climate-data/livneh-gridded-precipitation-and-other-meteorological-variables-continental-us-mexico`.

This manuscript has been authored by authors at Lawrence Berkeley National Laboratory under Contract No. DE-AC02-05CH11231 with the U.S. Department of Energy. The U.S. Government retains, and the publisher, by accepting the article for publication, acknowledges, that the U.S. Government retains a non-exclusive, paid-up, irrevocable, worldwide license to publish or reproduce the published form of this manuscript, or allow others to do so, for U.S. Government purposes

References

Magaña, Víctor and Pérez, Joel and Vázquez, Jorge and Pérez, José. (2003). Impact of el niño on precipitation in mexico. *Geofísica Internacional*. Retrieved from `https://www.redalyc.org/articulo.oa?id=56842304`

Adams, D. K., & Comrie, A. C. (1997). The north american monsoon. *Bulletin of the American Meteorological Society*, *78*(10), 2197 - 2214. Retrieved from `https://journals.ametsoc.org/view/journals/bams/78/10/1520-0477_1997_078_2197_tnam_2_0_co_2.xml` doi: 10.1175/1520-0477(1997)078⟨2197:TNAM⟩2.0.CO;2

Agustín Breña-Naranjo, J., Pedrozo-Acuña, A., Pozos-Estrada, O., Jiménez-López, S. A., & López-López, M. R. (2015). The contribution of tropical cyclones to rainfall in mexico. *Physics and Chemistry of the Earth, Parts A/B/C*, *83-84*, 111-122. Retrieved from `https://www.sciencedirect.com/science/article/pii/S1474706515000704` (Emerging science and applications with microwave remote sensing data) doi: https://doi.org/10.1016/j.pce.2015.05.011

Arriaga-Ramírez, Sarahí and Cavazos, Tereza. (2010). Regional trends of daily precipitation indices in northwest mexico and southwest united states. *Journal of Geophysical Research: Atmospheres*, *115*(D14). Retrieved from `https://agupubs.onlinelibrary.wiley.com/doi/abs/10.1029/2009JD013248` doi: https://doi.org/10.1029/2009JD013248

Breitburg, Denise; Grégoire, Marilaure and Isensee, Kirsten. (2018). *The ocean is losing its breath: declining oxygen in the world's ocean and coastal waters; summary for policy makers.* Retrieved from `https://unesdoc.unesco.org/ark:/48223/pf0000265196`

Cavazos, Tereza and Arriaga-Ramírez, Sarahí. (2012). Downscaled climate change scenarios for baja california and the north american monsoon during the twenty-first century. *Journal of Climate*, *25*(17), 5904 - 5915. Retrieved from `https://journals.ametsoc.org/view/journals/clim/25/17/jcli-d-11-00425.1.xml` doi: 10.1175/JCLI-D-11-00425.1

Chen, M., Shi, W., Xie, P., Silva, V. B. S., Kousky, V. E., Wayne Higgins, R., & Janowiak, J. E. (2008). Assessing objective techniques for gauge-based analyses of global daily precipitation. *Journal of Geophysical Research: Atmospheres*, *113*(D4). Retrieved from `https://agupubs.onlinelibrary.wiley.com/doi/abs/10.1029/2007JD009132` doi: https://doi.org/10.1029/2007JD009132

Choi, K.-Y., Vecchi, G. A., & Wittenberg, A. T. (2015). Nonlinear zonal wind response to enso in the cmip5 models: Roles of the zonal and meridional shift of the itcz/spcz and the simulated climatological precipitation. *Journal of Climate*, *28*(21), 8556 - 8573. Retrieved from `https://journals.ametsoc.org/view/journals/clim/28/21/jcli-d-15-0211.1.xml` doi: 10.1175/JCLI-D-15-0211.1

Cruz López, M. (2011). Comparación del ciclo agrícola actual con el de hace unos diez anos en San Juan Jalpa municipio San Felipe Del Progreso Estado de México: Evidencia de adapatación al cambio climático. *Ra Ximhai. Revista de Sociedad, Cultura y Desarrollo Sustentable*, *7*(1), 95–106.

Curtis, S. (2007, August). The atlantic multidecadal oscillation and extreme daily precipitation over the US and mexico during the hurricane season. *Climate Dynamics*, *30*(4), 343–351. Retrieved from `https://doi.org/10.1007/s00382-007-0295-0` doi: 10.1007/s00382-007-0295-0

De Luna, M., Waliser, D., Guan, B., Sengupta, A., Raymond, C., & Ye1, H. (2020). *Tropical atmospheric rivers.* Paper presented at the Virtual Symposium by the International Atmospheric Rivers Conference (IARC) Community, 5-9 October, 2020.

De Luna, M. I. (2021). Tropical atmospheric rivers. *Ph.D. dissertation, California State University, Los Angeles*, *ProQuest Dissertations Publishing*. Retrieved from `https://www.proquest.com/dissertations-theses/tropical-atmospheric-rivers/docview/2562506390/se-2?accountid=14505`

Dettinger, M. (2011). Climate change, atmospheric rivers, and floods in California - a multimodel analysis of storm frequency and magnitude changes. *Journal of the American Water Resources Association*, *47*(3), 514–523. doi: 10.1111/j.1752-1688.2011.00546.x

Dettinger, M. D. (2013). Atmospheric Rivers as Drought Busters on the U.S. West Coast. *Journal of Hydrometeorology*, *14*(6), 1721–1732. doi: 10.1175/jhm-d-13-02.1

Dirmeyer, P. A., & Brubaker, K. L. (2007). Characterization of the Global Hydrologic Cycle from a Back-Trajectory Analysis of Atmospheric Water Vapor. *Journal of Hydrometeorology*, *8*(1), 20–37. doi: 10.1175/jhm557.1

Dominguez, C., Done, J. M., & Bruyère, C. L. (2020). Easterly wave con-tributions to seasonal rainfall over the tropical americas in observations and a regional climate model. *Climate Dynamics*, *54*(1), 191–209. Retrieved from https://doi.org/10.1007/s00382-019-04996-7 doi: 10.1007/s00382-019-04996-7

Dominguez, Christian and Magaña, Victor. (2018). The role of tropical cyclones in precipitation over the tropical and subtropical north america. *Frontiers in Earth Science*, *6*. Retrieved from https://www.frontiersin.org/article/10.3389/feart.2018.00019 doi: 10.3389/feart.2018.00019

Domínguez-Hernández, G., Cepeda-Morales, J., Soto-Mardones, L., Rivera-Caicedo, J. P., Romero-Rodríguez, D. A., Inda-Díaz, E. A., ... Romero-Bañuelos, C. (2020, June). Semi-annual variations of chlorophyll concentration on the Eastern Tropical Pacific coast of Mexico. *Advances in Space Research*, *65*(11), 2595–2607. Retrieved 2020-08-14, from https://linkinghub.elsevier.com/retrieve/pii/S0273117720301113 doi: 10.1016/j.asr.2020.02.019

Douglas, A. V., & Englehart, P. J. (2007). A climatological perspective of transient synoptic features during name 2004. *Journal of Climate*, *20*(9), 1947 - 1954. Retrieved from https://journals.ametsoc.org/view/journals/clim/20/9/jcli4095.1.xml doi: 10.1175/JCLI4095.1

Díaz, S., Salinas-Zavala, C., & Hernández-Vázquez, S. (2008, 04). Variability of rainfall from tropical cyclones in northwestern México and its relation to SOI and PDO. *Atmósfera*, *21*, 213 - 223. Retrieved from http://www.scielo.org.mx/scielo.php?script=sci_arttext&pid=S0187-62362008000200006&nrm=iso

Eldardiry, H., Mahmood, A., Chen, X., Hossain, F., Nijssen, B., & Lettenmaier, D. P. (2019). Atmospheric River–Induced Precipitation and Snowpack during the Western United States Cold Season. *Journal of Hydrometeorology*, *20*(4), 613–630. doi: 10.1175/jhm-d-18-0228.1

European Centre for Medium-Range Weather Forecasts. (2014). *Era-20c project (ecmwf atmospheric reanalysis of the 20th century).* https://doi.org/10.5065/D6VQ30QG. Boulder CO: Research Data Archive at the National Center for Atmospheric Research, Computational and Information Systems Laboratory. ((Updated daily.) Accessed January 2022)

Farfán, L. M., & Fogel, I. (2007, April). Influence of tropical cyclones on humidity patterns over southern baja california, mexico. *Monthly Weather Review*, *135*(4), 1208–1224. Retrieved from https://doi.org/10.1175/mwr3356.1 doi: 10.1175/mwr3356.1

García Amaro de Miranda, E. (2003, 04). Distribución de la precipitación en la República Mexicana. *Investigaciones geográficas*, 67 - 76. Retrieved from http://www.scielo.org.mx/scielo.php?script=sci_arttext&pid=S0188-46112003000100009&nrm=iso

Gershunov, A., Shulgina, T., Ralph, F. M., Lavers, D. A., & Rutz, J. J. (2017, aug). Assessing the climate-scale variability of atmospheric rivers affecting western North America. *Geophysical Research Letters*, *44*(15), 7900–7908. Retrieved from http://doi.wiley.com/10.1002/2017GL074175 doi: 10.1002/2017GL074175

Gimeno, L., Dominguez, F., Nieto, R., Trigo, R., Drumond, A., Reason, C. J., ... Marengo, J. (2016). Major Mechanisms of Atmospheric Moisture Transport and Their Role in Extreme Precipitation Events. *Annual Review of Environment and Resources*, *41*(1), 117–141. doi: 10.1146/annurev-environ-110615-085558

Gimeno, L., Nieto, R., Vázquez, M., & Lavers, D. A. (2014). Atmospheric rivers: a mini-review. *Frontiers in Earth Science*, *2*(March), 1–6. doi: 10.3389/feart.2014.00002

Goldenson, N., Leung, L. R., Bitz, C. M., & Blanchard-Wrigglesworth, E. (2018). Influence of atmospheric rivers on mountain snowpack in the western United States. *Journal of Climate*, *31*(24), 9921–9940. doi:

10.1175/JCLI-D-18-0268.1

Guan, B., Molotch, N. P., Waliser, D. E., Fetzer, E. J., & Neiman, P. J. (2010). Extreme snowfall events linked to atmospheric rivers and surface air temperature via satellite measurements. *Geophysical Research Letters*, *37*(20), 2–7. doi: 10.1029/2010GL044696

Haffke, C., & Magnusdottir, G. (2013). The south pacific convergence zone in three decades of satellite images. *Journal of Geophysical Research: Atmospheres*, *118*(19), 10,839-10,849. Retrieved from `https://agupubs.onlinelibrary.wiley.com/doi/abs/10.1002/jgrd.50838` doi: https://doi.org/10.1002/jgrd.50838

Huang, H., Patricola, C. M., Bercos-Hickey, E., Zhou, Y., Rhoades, A., Risser, M. D., & Collins, W. D. (2021). Sources of subseasonal-to-seasonal predictability of atmospheric rivers and precipitation in the western United States. *Journal of Geophysical Research: Atmospheres*, *126*, e2020JD034053. doi: 10.1029/2020JD034053

Inda-Díaz, H. A., O'Brien, T. A., Zhou, Y., & Collins, W. D. (2021). Constraining and characterizing the size of atmospheric rivers: A perspective independent from the detection algorithm. *Journal of Geophysical Research: Atmospheres*, *126*(16), e2020JD033746. Retrieved from `https://agupubs.onlinelibrary.wiley.com/doi/abs/10.1029/2020JD033746` (e2020JD033746 2020JD033746) doi: https://doi.org/10.1029/2020JD033746

Kim, J., Waliser, D. E., Neiman, P. J., Guan, B., Ryoo, J. M., & Wick, G. A. (2013). Effects of atmospheric river landfalls on the cold season precipitation in California. *Climate Dynamics*, *40*(1-2), 465–474. doi: 10.1007/s00382-012-1322-3

Lavers, D. A., Pappenberger, F., Richardson, D. S., & Zsoter, E. (2016). ECMWF Extreme Forecast Index for water vapor transport: A forecast tool for atmospheric rivers and extreme precipitation. *Geophysical Research Letters*, *43*(22), 11,852–11,858. doi: 10.1002/2016GL071320

Lavers, D. A., Ralph, F. M., Waliser, D. E., Gershunov, A., & Dettinger, M. D. (2015, jul). Climate change intensification of horizontal water vapor transport in CMIP5. *Geophysical Research Letters*, *42*(13), 5617–5625. Retrieved from `http://doi.wiley.com/10.1002/2015GL064672` doi: 10.1002/2015GL064672

Lavers, D. A., & Villarini, G. (2013a). Atmospheric rivers and flooding over the central United States. *Journal of Climate*, *26*(20), 7829–7836. doi: 10.1175/JCLI-D-13-00212.1

Lavers, D. A., & Villarini, G. (2013b). The nexus between atmospheric rivers and extreme precipitation across Europe. *Geophysical Research Letters*, *40*(12), 3259–3264. doi: 10.1002/grl.50636

Lavers, D. A., Waliser, D. E., Ralph, F. M., & Dettinger, M. D. (2016). Predictability of horizontal water vapor transport relative to precipitation: Enhancing situational awareness for forecasting western U.S. extreme precipitation and flooding. *Geophysical Research Letters*, *43*(5), 2275–2282. doi: 10.1002/2016GL067765

Leung, L.-R., & Qian, Y. (2009). Atmospheric rivers induced heavy precipitation and flooding in the western U.S. simulated by the WRF regional climate model. *Geophysical Research Letters*, *36*(3), 1–6. doi: 10.1029/2008GL036445

Lintner, B. R., & Boos, W. R. (2019). Using atmospheric energy transport to quantitatively constrain south pacific convergence zone shifts during enso. *Journal of Climate*, *32*(6), 1839 - 1855. Retrieved from `https://journals.ametsoc.org/view/journals/clim/32/6/jcli-d-18-0151.1.xml` doi: 10.1175/JCLI-D-18-0151.1

Livneh, B., Bohn, T. J., Pierce, D. W., Munoz-Arriola, F., Nijssen, B., Vose, R., ... Brekke, L. (2015, August). A spatially comprehensive, hydrometeorological data set for mexico, the u.s., and southern canada 1950–2013. *Scientific Data*, *2*(1). Retrieved from `https://doi.org/10.1038/sdata.2015.42` doi: 10.1038/sdata.2015.42

Livneh, Ben & National Center for Atmospheric Research Staff (Eds). (Last modified 12 Dec 2019). *ERA5: Fifth generation of ECMWF atmospheric reanalyses of the global climate.* https://climatedataguide.ucar.edu/climate-data/livneh-gridded-precipitation-and-other-meteorological-variables-continental-us-mexico.

Lora, J. M., Shields, C. A., & Rutz, J. J. (2020, oct). Consensus and Disagreement in Atmospheric River Detection: ARTMIP Global Catalogues. *Geophysical Research Letters*, *47*(20), 1–10. Retrieved from `https://onlinelibrary.wiley.com/doi/10.1029/2020GL089302` doi: 10.1029/2020GL089302

Matías Méndez and Víctor Magaña. (2010). Regional aspects of prolonged meteorological droughts over mexico and central america. *Journal of Climate*, *23*(5), 1175 - 1188. Retrieved from `https://journals.ametsoc.org/view/journals/clim/23/5/2009jcli3080.1.xml` doi: 10.1175/2009JCLI3080.1

Neiman, P. J., Ralph, F. M., White, A. B., Kingsmill, D. E., & Persson, P. O. (2002). The statistical relationship between upslope flow and rainfall in California's coastal mountains: Observations during CALJET. *Monthly Weather Review*, *130*(6), 1468–1492. doi: 10.1175/1520-0493(2002)130⟨1468:TSRBUF⟩2.0.CO;2

Neiman, P. J., Ralph, F. M., Wick, G. A., Lundquist, J. D., & Dettinger, M. D. (2008). Meteorological Characteristics and Overland Precipitation Impacts of Atmospheric Rivers Affecting the West Coast of North America Based on Eight Years of SSM/I Satellite Observations. *Journal of Hydrometeorology*, *9*(1), 22–47. doi: 10.1175/2007jhm855.1

Neiman, P. J., Ralph, M. F., Moore, B. J., Hughes, M., Mahoney, K. M., Cordeira, J. M., & Dettinger, M. D. (2013). The landfall and inland penetration of a flood-producing atmospheric river in Arizona. Part I: Observed synoptic-scale, orographic, and hydrometeorological characteristics. *Journal of Hydrometeorology*, *14*(2), 460–484. doi: 10.1175/JHM-D-12-0101.1

NOAA Physical Science Laboratory. (2008). *CPC global unified gauge-based analysis of daily precipitation.* Retrieved from `https://psl.noaa.gov/data/gridded/data.cpc.globalprecip.html`

O'Brien, T. A., Risser, M. D., Loring, B., Elbashandy, A. A., Krishnan, H., Johnson, J., ... Collins, W. D. (2020, dec). Detection of atmospheric rivers with inline uncertainty quantification: TECA-BARD v1.0.1. *Geoscientific Model Development*, *13*(12), 6131–6148. Retrieved from `https://www.geosci-model-dev-discuss.net/gmd-2020-55/#discussionhttps://gmd.copernicus.org/articles/13/6131/2020/` doi: 10.5194/gmd-13-6131-2020

O'Brien, T. A., Wehner, M. F., Payne, A. E., Shields, C. A., Rutz, J. J., Leung, L. R., ... Zhou, Y. (2021). Increases in future ar count and size: Overview of the artmip tier 2 cmip5/6 experiment. *Journal of Geophysical Research: Atmospheres*, e2021JD036013. Retrieved from `https://agupubs.onlinelibrary.wiley.com/doi/abs/10.1029/2021JD036013` doi: https://doi.org/10.1029/2021JD036013

Paltan, H., Waliser, D., Lim, W. H., Guan, B., Yamazaki, D., Pant, R., & Dadson, S. (2017). Global Floods and Water Availability Driven by Atmospheric Rivers. *Geophysical Research Letters*, *44*(20), 10,387–10,395. doi: 10.1002/2017GL074882

Payne, A. E., Demory, M.-E., Leung, L. R., Ramos, A. M., Shields, C. A., Rutz, J. J., ... Ralph, F. M. (2020, mar). Responses and impacts of atmospheric rivers to climate change. *Nature Reviews Earth & Environment*, *1*(3), 143–157. Retrieved from `http://dx.doi.org/10.1038/s43017-020-0030-5http://www.nature.com/articles/s43017-020-0030-5` doi:

10.1038/s43017-020-0030-5

Poli, P., Hersbach, H., Dee, D. P., Berrisford, P., Simmons, A. J., Vitart, F., ... Fisher, M. (2016). Era-20c: An atmospheric reanalysis of the twentieth century. *Journal of Climate*, *29*(11), 4083 - 4097. Retrieved from `https://journals.ametsoc.org/view/journals/clim/29/11/jcli-d-15-0556.1.xml` doi: 10.1175/JCLI-D-15-0556.1

Porter, J. R., & Semenov, M. A. (2005, November). Crop responses to climatic variation. *Philosophical Transactions of the Royal Society B: Biological Sciences*, *360*(1463), 2021–2035. Retrieved 2020-08-13, from `https://royalsocietypublishing.org/doi/10.1098/rstb.2005.1752` doi: 10.1098/rstb.2005.1752

Ralph, F., Rutz, J. J., Cordeira, J. M., Dettinger, M., Anderson, M., Reynolds, D., ... Smallcomb, C. (2019, feb). A scale to characterize the strength and impacts of atmospheric rivers. *Bulletin of the American Meteorological Society*, *100*(2), 269–289. doi: 10.1175/BAMS-D-18-0023.1

Ralph, F. M., Coleman, T., Neiman, P. J., Zamora, R. J., & Dettinger, M. D. (2013, apr). Observed Impacts of Duration and Seasonality of Atmospheric-River Landfalls on Soil Moisture and Runoff in Coastal Northern California. *Journal of Hydrometeorology*, *14*(2), 443–459. Retrieved from `https://journals.ametsoc.org/jhm/article/14/2/443/5819/Observed-Impacts-of-Duration-and-Seasonality-of` doi: 10.1175/JHM-D-12-076.1

Ralph, F. M., Dettinger, M., Lavers, D., Gorodetskaya, I. V., Martin, A., Viale, M., ... Cordeira, J. (2017). Atmospheric rivers emerge as a global science and applications focus. *Bulletin of the American Meteorological Society*, *98*(9), 1969 - 1973. Retrieved from `https://journals.ametsoc.org/view/journals/bams/98/9/bams-d-16-0262.1.xml` doi: 10.1175/BAMS-D-16-0262.1

Ralph, F. M., & Dettinger, M. D. (2011, aug). Storms, floods, and the science of atmospheric rivers. *Eos, Transactions American Geophysical Union*, *92*(32), 265–266. Retrieved from `https://onlinelibrary.wiley.com/doi/abs/10.1029/2011EO320001` doi: 10.1029/2011EO320001

Ralph, F. M., Dettinger, M. D., Cairns, M. M., Galarneau, T. J., & Eylander, J. (2018, apr). Defining "Atmospheric River": How the Glossary of Meteorology Helped Resolve a Debate. *Bulletin of the American Meteorological Society*, *99*(4), 837–839. Retrieved from `http://journals.ametsoc.org/doi/10.1175/BAMS-D-17-0157.1` doi: 10.1175/BAMS-D-17-0157.1

Ralph, F. M., Neiman, P. J., Kiladis, G. N., Weickmann, K., & Reynolds, D. W. (2010, nov). A Multiscale Observational Case Study of a Pacific Atmospheric River Exhibiting Tropical–Extratropical Connections and a Mesoscale Frontal Wave. *Monthly Weather Review*, *139*(4), 1169–1189. doi: 10.1175/2010mwr3596.1

Ralph, F. M., Neiman, P. J., & Rotunno, R. (2005). Dropsonde observations in low-level jets over the northeastern Pacific Ocean from CALJET-1998 and PACJET-2001: Mean vertical-profile and atmospheric-river characteristics. *Monthly Weather Review*, *133*(4), 889–910. doi: 10.1175/MWR2896.1

Ralph, F. M., Neiman, P. J., & Wick, G. A. (2004). Satellite and CALJET Aircraft Observations of Atmospheric Rivers over the Eastern North Pacific Ocean during the Winter of 1997/98. *Monthly Weather Review*, *132*(7), 1721–1745. Retrieved from `http://journals.ametsoc.org/doi/abs/10.1175/1520-0493{\%}282004{\%}29132{\%}3C1721{\%}3ASACAOO{\%}3E2.0.CO{\%}3B2` doi: 10.1175/1520-0493(2004)132⟨1721:SACAOO⟩2.0.CO;2

Ralph, F. M., Neiman, P. J., Wick, G. A., Gutman, S. I., Dettinger, M. D., Cayan, D. R., & White, A. B. (2006). Flooding on California's Russian River: Role of atmospheric rivers. *Geophysical Research Letters*, *33*(13), 3–7. doi: 10.1029/2006GL026689

Ralph, F. M., Rutz, J. J., Cordeira, J. M., Dettinger, M., Anderson, M., Reynolds, D., … Smallcomb, C. (2019, feb). A Scale to Characterize the Strength and Impacts of Atmospheric Rivers. *Bulletin of the American Meteorological Society*, *100*(2), 269–289. Retrieved from https://journals.ametsoc.org/bams/article/100/2/269/69196/A-Scale-to-Characterize-the-Strength-and-Impacts doi: 10.1175/BAMS-D-18-0023.1

Romero-Rodríguez, D. A., Soto-Mardones, L. A., Cepeda-Morales, J., Rivera Caicedo, J. P., & Inda Díaz, E. A. (2020). Satellite-derived turbidity influence factors at small river mouths, tropical Pacific coast off México. *Advances in Space Research*. (Aceptado el 3 de agosto de 2020)

Rutz, J. J., James Steenburgh, W., & Martin Ralph, F. (2014, feb). Climatological characteristics of atmospheric rivers and their inland penetration over the western united states. *Monthly Weather Review*, *142*(2), 905–921. Retrieved from https://journals.ametsoc.org/mwr/article/142/2/905/71947/Climatological-Characteristics-of-Atmospheric doi: 10.1175/MWR-D-13-00168.1

Rutz, J. J., Shields, C. A., Lora, J. M., Payne, A. E., Guan, B., Ullrich, P., … Viale, M. (2019, dec). The Atmospheric River Tracking Method Intercomparison Project (ARTMIP): Quantifying Uncertainties in Atmospheric River Climatology. *Journal of Geophysical Research: Atmospheres*, *124*(24), 13777–13802. Retrieved from https://onlinelibrary.wiley.com/doi/abs/10.1029/2019JD030936 doi: 10.1029/2019JD030936

Simmons, A. J., & Burridge, D. M. (1981). An energy and angular-momentum conserving vertical finite-difference scheme and hybrid vertical coordinates. *Monthly Weather Review*, *109*(4), 758 - 766. Retrieved from https://journals.ametsoc.org/view/journals/mwre/109/4/1520-0493_1981_109_0758_aeaamc_2_0_co_2.xml doi: 10.1175/1520-0493(1981)109⟨0758:AEAAMC⟩2.0.CO;2

Smith, B. L., Yuter, S. E., Neiman, P. J., & Kingsmill, D. E. (2009). Water Vapor Fluxes and Orographic Precipitation over Northern California Associated with a Landfalling Atmospheric River. *Monthly Weather Review*, *138*(1), 74–100. doi: 10.1175/2009mwr2939.1

Viale, M., & Nuñez, M. N. (2011). Climatology of winter orographic precipitation over the subtropical central Andes and associated synoptic and regional characteristics. *Journal of Hydrometeorology*, *12*(4), 481–507. doi: 10.1175/2010JHM1284.1

Viale, M., Valenzuela, R., Garreaud, R. D., & Ralph, F. M. (2018). Impacts of Atmospheric Rivers on Precipitation in Southern South America. *Journal of Hydrometeorology*, *19*(10), 1671–1687. doi: 10.1175/jhm-d-18-0006.1

Viguera, B., Martínez-Rodríguez, M., Donatti, C., Harvey, C., & Alpízar, F. (2017). *Impactos del cambio climático en la agricultura de centroamérica, estrategias de mitigación y adaptación. materiales de fortalecimiento de capacidades técnicas del proyecto cascada (conservación internacional-catie).* Conservación Internacional. Retrieved from https://www.conservation.org/docs/default-source/publication-pdfs/cascade_modulo-2-impactos-del-cambio-climatico-en-la-agricultura-de-centroamerica.pdf

Waliser, D., & Guan, B. (2017). Extreme winds and precipitation during landfall of atmospheric rivers. *Nature Geoscience*, *10*(3), 179–183. doi: 10.1038/ngeo2894

Warner, M. D., Mass, C. F., & Salatheé, E. P. (2012). Wintertime extreme precipitation events along the Pacific Northwest Coast: Climatology and synoptic evolution. *Monthly Weather Review*, *140*(7), 2021–2043. doi: 10.1175/MWR-D-11-00197.1

Zhang, Z., Ralph, F. M., & Zheng, M. (2019). The Relationship Between Extratropical Cyclone Strength and Atmospheric River Intensity and Position. *Geophysical Research Letters*, *46*(3), 1814–1823. doi: 10.1029/2018GL079071

Zhu, Y., & Newell, R. E. (1998). A Proposed Algorithm for Moisture Fluxes from Atmospheric Rivers. *Monthly Weather Review*, *126*(3), 725–735. doi: 10.1175/1520-0493(1998)126⟨0725:apafmf⟩2.0.co;2

Relationship Between Atmospheric Rivers and the Dry Season Extreme Precipitation in Central-Western Mexico

H. A. Inda-Díaz[1], T. A. O'Brien[2,1]

[1]Climate and Ecosystem Sciences Division, Lawrence Berkeley National Laboratory, Berkeley, CA, USA
[2]Dept. of Earth and Atmospheric Sciences, Indiana University, Bloomington, IN, USA

Key Points:

- Extreme precipitation during the dry season in Central-Western Mexico is associated with atmospheric rivers (ARs)
- The meteorological state during extreme precipitation events shows ideal conditions for orographic precipitation over the Sierra Madre
- A detector designed for tropical latitudes could increase the correlation between ARs and dry season precipitation over Central-Western Mexico

Corresponding author: T.A. O'Brien, `obrienta@iu.edu`

Abstract

Atmospheric rivers (AR) are long, narrow jets of moisture transport responsible for over 90We use the ERA-20C reanalysis and the Bayesian AR detector TECA-BARD to show the relationship between extreme precipitation and atmospheric rivers in central-western Mexico (CWM) during the dry seasons (November-March) in the 1900-2010 period. We find that more than 25% of extreme precipitation amount and frequency are associated with ARs, with a maximum of 60%-80% during December and January near the coast of Sinaloa (107.5W,25N). Composites of the mean meteorological state show "ideal" conditions for orographic precipitation due to landfalling ARs: high horizontal vapor transport perpendicular to the Sierra Madre. We observe a tropospheric wave pattern in vertical velocity, surface pressure, and geopotential height associated with these events. The nature and evolution of these waves need to be further studied. Our results suggest that TECA-BARD provides a reasonable estimation for AR presence in CWM. Nevertheless, we recommend using multiple AR detectors and one tuned explicitly for tropical latitudes. This will allow investigation of the response of CWM landfalling ARs and the region's hydroclimatology under future climate scenarios.

Plain Language Summary

Atmospheric rivers (ARs) are a meteorological phenomenon with strong poleward water vapor transport. Due to their important role in the hydrological cycle and water availability of midlatitudes (like California, Europe, and Chile, among others) and polar regions, the scientific community has mainly focused AR research on these regions. It was not until recently that AR in lower tropical latitudes gathered more attention. This work focuses on the relationship between ARs and the dry season (November-March) precipitation over Central-Western Mexico (CWM), around 25 degrees north over the Pacific Coast of Mexico. We use precipitation data from the ERA-20C reanalysis, observational dataset, and a Bayesian AR detector to show that most of the precipitation over CWM during the November-March season is due to meteorological features with similar characteristics to midlatitude ARs. These events show typical conditions for ARs orographic precipitation: high water vapor transport perpendicular to the Sierra Madre that condensates into rain when the mountains lift it. We believe that an AR detector specifically designed for tropical latitudes could increase the relationship between AR and November-March precipitation in CWM and better allow us to study how these events might be modified by climate change.

1 Introduction

Atmospheric rivers (AR) are long, narrow jets of moisture transport typically associated with a low-level jet stream ahead of the cold front of an extratropical cyclone (F. M. Ralph et al., 2018). ARs account for over 90% of the water vapor transport from the subtropics to midlatitudes (Zhu & Newell, 1998). Over the last 20 years, there has been an increasing interest in the study and characterization of ARs. Numerous recent studies investigate AR and their relationship with extreme wind, precipitation, their impact on the regional hydrological cycles, water mass balance, and extreme hydrological events like flooding and droughts in midlatitude continental regions like North America, Europe, and South America (Neiman et al., 2002; F. M. Ralph et al., 2004, 2005, 2006; Dirmeyer & Brubaker, 2007; Neiman et al., 2008; Leung & Qian, 2009; Guan et al., 2010; Viale & Nuñez, 2011; M. Dettinger, 2011; F. M. Ralph & Dettinger, 2011; Warner et al., 2012; M. D. Dettinger, 2013; Lavers & Villarini, 2013b, 2013a; Kim et al., 2013; Neiman et al., 2013; F. M. Ralph et al., 2013; Rutz et al., 2014; Gimeno et al., 2016; Lavers, Waliser, et al., 2016; Lavers, Pappenberger, et al., 2016; Waliser & Guan, 2017; Gershunov et al., 2017; Goldenson et al., 2018; Viale et al., 2018; Eldardiry et al., 2019; F. M. Ralph et al., 2019; Huang et al., 2021). Some works have even investigated the structure of AR using *in situ* data and satellite observations (F. M. Ralph et al., 2005; Neiman et al., 2008; F. M. Ralph et al., 2010).

The significant impact of ARs on the climatology and hydrology of midlatitudes has generated great interest and community effort in studying ARs and their impacts on these regions. (F. Ralph et al., 2019) introduced a scale to categorize AR strength based on vapor transport intensity and landfall duration and show that there are beneficial and hazardous impacts associated with AR events. This scale is helpful for the scientific community, and it is a way of communication with the general public. The AR category scale can be applied to gridded datasets such as reanalysis, forecast, and climate projections. There is also an increasing interest in understanding how ARs and their impact will change in future climates. (Payne et al., 2020) concludes that AR response to climate change will have noticeable importance to water balance and regional water resources.

Most of the ARs research focuses on midlatitudes and polar regions. ARs in low latitudes are starting to generate interest within the scientific AR community. This work is motivated by the lack of study of tropical ARs. Moreover, we are also motivated by the direct observation of "unusual non-tropical" precipitation in the Winter of 2019-2020 in Nayarit, Mexico ∼21.5N,104.9W, during the dry season (November-March). We refer to "unusual non-tropical" precipitation as a low magnitude precipitation rate (compared to convective heavy tropical precipitation). During these days, we observed constant rainfall throughout one or two days, very similar to typical California winter precipitation (Figure 1(b) shows the IVT and horizontal wind speed at 700 hPa from one such event). The similarities in the IVT field with the typical characteristics of an AR raised the question: *is this an AR? Are there more events like this, and how are they associated with the extreme precipitation for the dry season in Central-Western Mexico (CWM)?* (thick black contour in Figure 1(a)).

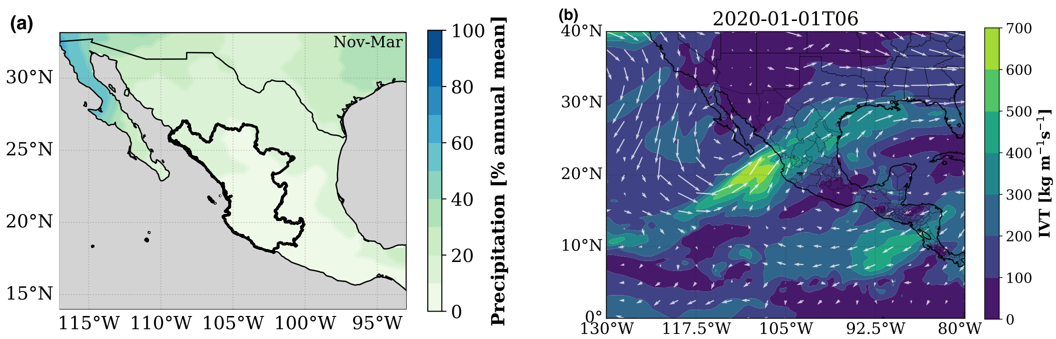

Figure 1. (a) Percentage of annual total precipitation from CPC Global Unified Gauge-Based Analysis of Daily Precipitation. Thick black contour is used to indicate what is considered as Central-Western Mexico throughout this work. (b) ERA5 reanalysis IVT in color contours. Vectors represent the 750 hPa wind velocity. 2020-01-01 is one of the times when the precipitation in CWM resembled the winter Californian AR-associated rainfall.

CWM is characterized by a dry season from November to March (García Amaro de Miranda, 2003), with a mean monthly accumulated precipitation of less than 10 mm[1] and over 75% of the annual precipitation from July-September, during the spring and

[1] `https://smn.conagua.gob.mx/es/climatologia/temperaturas-y-lluvias/resumenes-mensuales-de-temperaturas-y-lluvias`

summer months. Rainfall in CWM is mainly associated with the North American Monsoon. Less than 10% of the total annual mean rainfall occurs between November and March for most of CWM (Figure 1(a)), according to the CPC Global Unified Gauge-Based Analysis of Daily Precipitation[2] (Chen et al., 2008).

From a socio-economic point of view, it is important to study and quantify these events of atypical precipitation. CWM is one of the largest agricultural production regions in Mexico. It is common knowledge among CWM farmers that these rainfall events can be exploited to benefit agriculture; however, we could not find scientific quantification of it. There are even popular beliefs that they can be predicted following a set of heuristic rules (Cruz López, 2011). There is also some evidence that different crops, like beans, coffee, and corn, are sensitive to changes in environmental conditions, like precipitation and humidity (Viguera et al., 2017). Therefore, changes in climate conditions can affect the productivity and quality of the crops (Porter & Semenov, 2005).

Moreover, changes in wind speed and direction, moisture transport, and the location of the intertropical convergence zone (ITCZ) can modify the energy exchange between the atmosphere and the ocean. These changes could generate a displacement northward of the oxygen minimum zone (OMZ), which can affect ocean species distribution and the productivity of regional aquaculture and fisheries (Breitburg, Denise; Grégoire, Marilaure and Isensee, Kirsten, 2018). Furthermore, other studies have observed that dry season rainfall events can change the coastal environment. Coastal water chlorophyll concentration, turbidity, temperature, and salinity, due to increased river discharge, can impact the sustainability of coastal ecosystems and their biological production (Domínguez-Hernández et al., 2020; Romero-Rodríguez et al., 2020).

Although there are numerous possible effects of anomalous winter precipitation in the CWM region, there is still a lack of documentation about these events and their impacts. Moreover, no existing research links these events with ARs. We investigate the relationship between lower latitudes ARs "dry season" (November-March) rainfall in CWM. We use data from the European Centre for Medium-Range Weather Forecasts (ECMWF) Atmospheric Reanalysis of the Twentieth Century ERA-20C[3] (Poli et al., 2016) and the Bayesian AR Detector `TECA-BARD v1.0.1`. We aim to quantify how much of the CWM winter precipitation is associated with ARs and the meteorological state of the atmosphere during these events.

2 Data and Methods

ERA-20C output is 3-hourly with a of ∼125 km on 37 pressure levels. We use data at pressure level: geopotential `z`, wind velocity `u`, `v`, and `w`, specific humidity `q`, temperature `t`, and surface level: mean sea level pressure `mslp`, surface pressure `ps`, total precipitation `tp`, vertical integral of northward water vapor flux `vinwvf`, vertical integral of eastward water vapor flux `viewvf`, and total column water vapor `tcwv`. According to the ERA-20C documentation, the vertically integrated vapor fluxes are calculated in the model coordinates following:

$$\mathrm{VIEWVF} = -\frac{1}{g}\int_0^1 qu\frac{\partial p}{\partial \eta}d\eta \approx -\frac{1}{g}\sum_{k=1}^{N} u_k\, q_k \Delta p_k, \tag{1}$$

$$\mathrm{VINWVF} = -\frac{1}{g}\int_0^1 qv\frac{\partial p}{\partial \eta}d\eta \approx -\frac{1}{g}\sum_{k=1}^{N} v_k\, q_k \Delta p_k, \tag{2}$$

[2] `https://psl.noaa.gov/data/gridded/data.cpc.globalprecip.html`
[3] `https://www.ecmwf.int/en/forecasts/datasets/reanalysis-datasets/era-20c`

where u and v are the components of the horizontal wind vector, q is the specific humidity, p is pressure, η is the hybrid coordinate (Simmons & Burridge, 1981), index k corresponds to model levels going from the surface ($k = 1$) to the top of the model atmosphere ($k = N$), and Δp_k is the difference in level pressures, estimated at level k. ERA-20C daily forecasted precipitation accumulation has been converted to a 3-hourly precipitation rate (with units of mm/d); IWV is used directly from ERA-20C total column water vapor `tcwv`. IVT is calculated as the magnitude of the vertically integrated moisture-weighted wind (horizontal vapor flux vector) $\vec{u_q}$, directly from ERA-20C eastward and northward water vapor fluxes:

$$\vec{u_q} = (\text{VIEWVF}, \text{VINWVF}), \tag{3}$$

$$\text{IVT} = |\vec{u_q}| = \sqrt{\text{VIEWVF}^2 + \text{VINWVF}^2}. \tag{4}$$

Additionally, we compare the ERA-20C reanalysis data with observational precipitation, using precipitation data from the Livneh gridded precipitation for the continental US, Mexico, and Southern Canada (Livneh, Ben & National Center for Atmospheric Research Staff (Eds), Last modified 12 Dec 2019). The (Livneh et al., 2015) dataset is a long-term gridded daily dataset at fine 1/16° (∼6 km) horizontal resolution for the period 1950-2013. We use bilinear interpolation to regrid the AR detection from TECA-BARD in ERA-20C data to the Livneh dataset grid.

2.1 AR probability from ERA-20C and TECA-BARD

To calculate the probability of the presence of an atmospheric river (AR probability) we use the Bayesian AR Detector `TECA-BARD v1.0.1`, a probabilistic AR detector implemented in the Toolkit for Extreme Climate Analysis `TECA`. TECA-BARD uses a Bayesian framework to sample from the set of AR detector parameters that yield AR counts similar to the expert database of AR counts; this yields a set of "plausible" AR detectors from which we can assess quantitative uncertainty (O'Brien et al., 2020). We apply TECA-BARD to the ERA-20C data, and asses the plausible presence of an AR at a grid point where where AR probability$>$ 0.05. While 0.05 is a low probability threshold, this indicates a non-zero probability of the existence of an AR in a given grid cell. Since TECA-BARD is inherently designed to detect ARs in mid-latitudes, it filters the IVT field near the tropics, resulting in AR probability that would have lower values in the presence of an AR in tropical latitudes than one in higher latitudes. We hypothesize that AR probability$>$ 0.05 represents a reasonable indication of the presence of an AR in lower latitudes. We test and show this in Sections 5 and 6.

2.2 Extreme Precipitation

We calculate the monthly 98th percentile precipitation rate value for ERA-20C and Livneh datasets at each grid cell. We define an *extreme precipitation event* for a given grid cell as the time when the precipitation is above the 98th percentile. We calculate the AR-associated extreme precipitation for each grid cell as the precipitation above the 98th percentile when AR probability$>$ 0.05. Since the data record is sufficiently long (1900-2010 for ERA-20C and 1950-2013 for Livneh), we calculate all means and extreme precipitation quantiles monthly. The same holds for the atmospheric state composites described in Section 2.3.

2.3 Atmospheric State Composites

Following the methodology of (Neiman et al., 2008), we create composites of meteorological variables to study the state of the atmosphere at the time of extreme precipitation and AR events at two locations: `Loc1` = 107.5W,25N, and `Loc2` = 105.0W,21N (Figure 2, `Loc1` denoted circle marker, `Loc2` by the triangle). `Loc1` is located close to the maximum area of AR-associated precipitation and close to Culiacán Sinaloa, one of the most productive agricultural states of México. `Loc2` is around the most southern region with AR-associated precipitation fraction ∼0.5, and in the state of Jalisco, another important agricultural producer in CWM. Both locations are close to the *Sierra Madre Occidental*, a mountain range that extends through Northwestern and Central-Western Mexico, as a part of the North American Cordillera, parallel to the coast. We hypothesize that if there is IVT normal to the *Sierra Madre* during the dry season, it could produce precipitation due to orographic lifting. The methodology to select the time steps to composite is as follows: we find the times when the AR probability is > 0.05 (ar), then we find all the times when the precipitation is above the 98th percentile (pr). We define then AR + extreme precipitation conditions as the times where both conditions ar and pr are met (ar_pr), times when there is ar but no pr (ar_nopr), and times when there is pr but no ar (pr_noar). Finally, the long-term mean is the monthly climatology for 1900-2010 (ltm). We average in time for all the time in each composite and create monthly composites. Anomalies are calculated as the specific composite minus the long-term mean. Table 1 summarizes the different composite sampling.

Table 1. Atmospheric state composites. Composites are created monthly. The number of events at each location is the total number of events for all November-March months.

Atmospheric state composites

Conditions	Name	Anomaly	Events at `Loc1`	Events at `Loc2`
Climatology (long term mean)	ltm		134304	134304
AR	ar	ar - ltm	8886	4650
Extreme precipitation	pr	pr - ltm	2690	2688
AR/extreme precipitation	ar_pr	ar_pr - ltm	1549	1003
AR/no extreme precipitation	ar_nopr	ar_nopr - ltm	7337	3647
Extreme precipitation/no AR	pr_noar	pr_noar - ltm	1141	1685

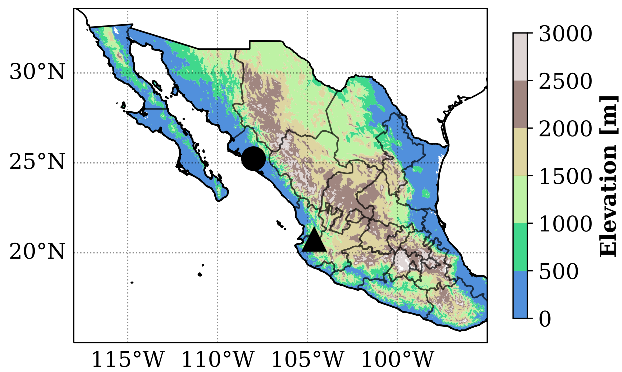

Figure 2. Orography of CWM. `Loc1` and `Loc2` are show in circle and triangle markers, respectively. The *Sierra Madre Occidental* is the mountain range that runs through Northwestern and Central-Western Mexico.

3 Results

In Section 3.1 we present the results of the AR-associated precipitation in CWM during the dry season (November-March) in the 1900-2010 period. We present the frac-tional contribution of ARs to the precipitation, using ERA-20C data and the Livneh *et al.* gridded dataset. Sections 5 through 6 focus on the meteorological state of the atmosphere during extreme precipitation and AR events and the difference between different composites. In the supplemental information, we include additional plots related to the meteorological state of the atmosphere and differences between composites.

3.1 AR-associated extreme precipitation

Figure 3 shows how much of the CWM dry season precipitation is associated with ARs. Figure 3(a) shows the fraction of ERA-20C total extreme precipitation amount associated with ARs, and (b) shows the same for Livneh precipitation. Figure 3(c) shows the fraction of ERA-20C extreme precipitation frequency associated with ARs, and Figure 3(d) shows the same for Livneh precipitation. The results are highly condensed in these figures, but they are clear and relevant: The influence of ARs in the dry season extreme precipitation in CWM extends as far as $\sim$17N. December has the highest AR-associated precipitation, with $\sim$75% of the frequency and amount 0.75 near `Loc1`, and between 50% and 60% near `Loc2`. In general, we can say that in the Nov-March, more than half of the extreme rainfall at `Loc1` (more than 30% at `Loc2`) is associated with ARs, both in total amount and frequency.

We have shown the results based on two facts: the total amount of precipitation (and frequency) higher than the monthly 98th percentile for November-March; and the "plausible" presence of an AR in CWM given the `ar_probability`$\geq$0.05. We hypothesize that this precipitation is associated with low latitudes ARs and that `TECA_bard` provides a good insight into the presence of ARs in CWM. This becomes clearer in Section 5, where we present composites of the state of the atmosphere during `ar_probability`$\geq$0.05 events at `Loc1` and `Loc2`. For simplicity, in Section 4 and 5, we show the results for January. The supplemental information contains the results for the long-term mean and *ar_pr* composites.

4 Long-term Mean

We briefly show the climatological state of the atmosphere (*ltm*) for January. The long-term mean is calculated based using ERA-20C data. Figure 4(a) shows IWV between 10 and 15 kg m^{-2} in CWM, with a maximum of 45 kg m^{-2} near the ITCZ (between 5S and 5N). IVT is shown in Figure 4(b), with values between 0 and 100 kg m^{-1}s^{-1} in CWM (IVT direction shown with vectors). We note a high IVT plume over the Pacific storm track and higher IVT values between 5S and 5N associated with the ITCZ. Mean sea level pressure depicts the North Pacific High with its maximum at 130W,30N, shown in Figure 4(c). Geopotential height at 650 hPa, shown in Figure 4(d), has a large gradient between 30N and 60N, associated with the jet stream over midlatitudes, with very little or no spatial patterns over CWM and the central Pacific Ocean. The long-term means for Nov-March are shown in the supplemental information (Figures S1 through Figure S5). The general structure of the atmosphere is similar to 4(Low IVT and IWV over CWM with the North Pacific High west of the coast of California and Baja California), with slight differences in the locations of the ITCZ, storm track, North Pacific High, etc.

5 Extreme Precipitation and AR Events Composite

In this section, we focus on the state of the atmosphere for the *ar_pr* composite (events with extreme precipitation + AR probability $\pm$0.05).

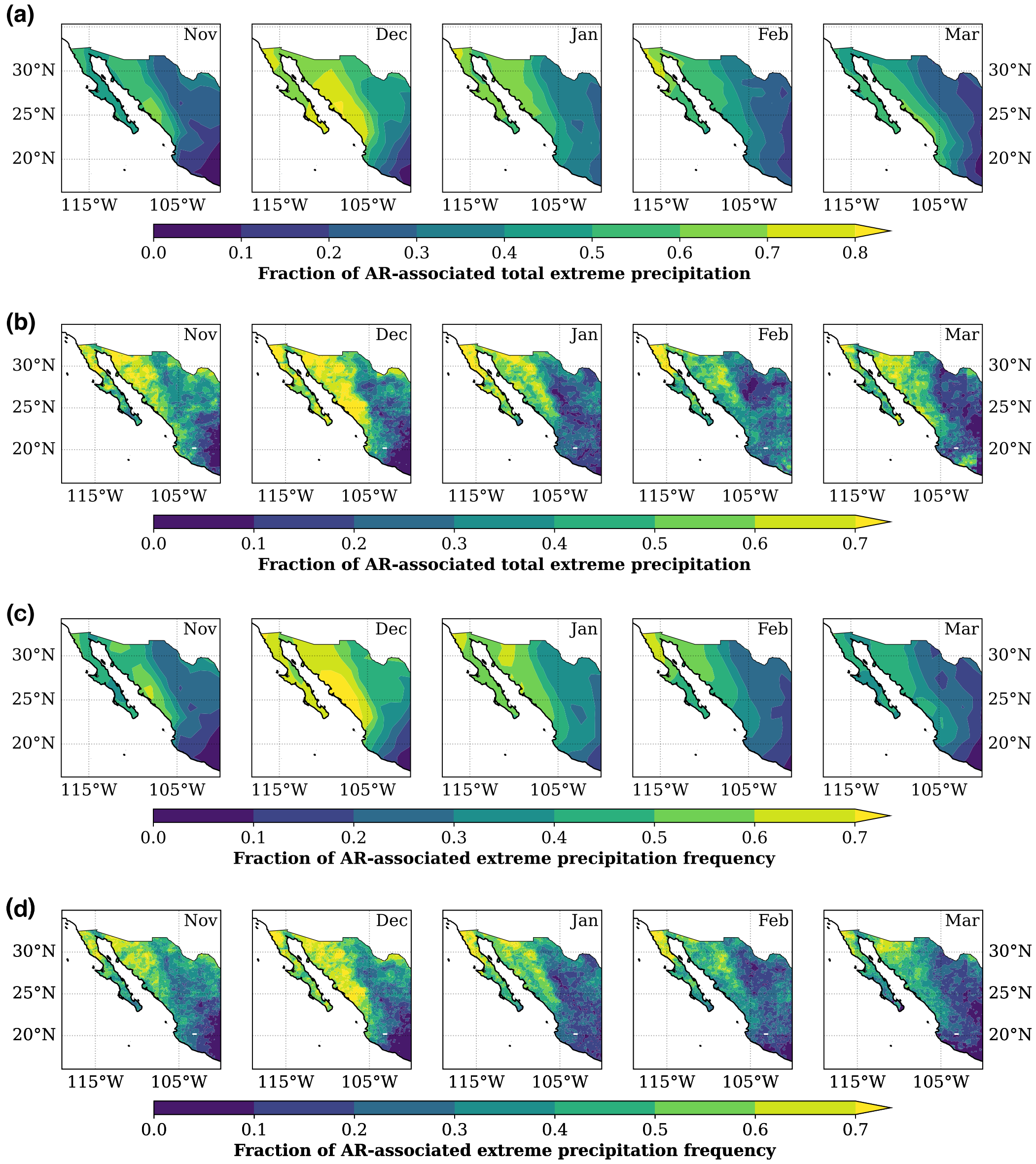

Figure 3. (a-b) Fraction of the total precipitation extreme precipitation (>98th percentile) associated with ARs. (a) ERA-20C 1900-2010. (b) Livneh 1950-2010. (c-d) Fraction of AR-associated to the total extreme (>98th) precipitation frequency. (c) ERA-20C 1900-2010. (d) Livneh 1950-2010

5.1 *ar_pr* composite at Loc1: Sinaloa, (107.5W,25N)

Figure 5(a) shows IVT in colored contours and IWV in dashed white contours. We observe an elongated region of high IWV extending from the ITCZ into CWM, with values up to 30 kg m^{-2} at `Loc1`; as well as a ridge-like structure of high IVT (between 200 and 400 kg m^{-1}s^{-1} centered at `Loc1`, similar to mid-latitude landfalling ARs (Neiman et al., 2008). Figure 5(b) shows IVT anomalies higher than 200 kg m^{-1}s^{-1}, and IWV anomalies up to 15 kg m^{-2} near`Loc1`. Mean sea level pressure (gray-filled contours in Figure 5(c)) shows the presence of the North Pacific High. Moreover, in 5(d), we observe a low in sea level pressure and geopotential height at 850 hPa anomalies centered near

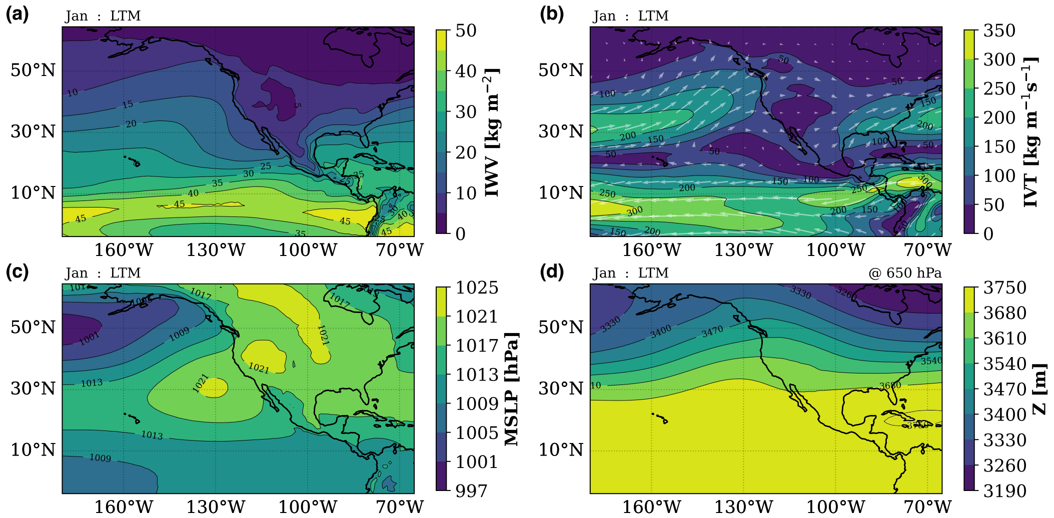

Figure 4. Long-term mean for 1900-2010 in December. (a) Integrated water vapor (IWV), (b) integrated vapor transport (IVT), (c) mean sea level pressure (MSLP), (d) geopotential height at 650 hPa. The vectors in panel (b) represent the direction of IVT.

115W,30N. This wave pattern is more noticeable in Figures 5(e) and (f) (geopotential height at 500 hPa). It is worth noticing that the low-pressure system at the surface is approximately aligned with the mid-troposphere low. This could imply that the wave producing this AR-pattern and anomalous dry season precipitation is barotropic. However, more analysis is needed to determine the nature and characteristics of these waves. Figures 5(g) and (h) show a mean negative vertical velocity (ascending) over the high IVT plume, ahead of the mid-tropospheric low (with anomalies $\sim$6 hPa s^{-1}). Vectors show the direction of IVT and its anomalies in Figures 5(g) and (h). IVT is normal to the mountain range and `Loc1`, with a weakening of the westward moisture transport near the Equator.

5.2 *ar_pr* composite at Loc2: Jalisco and Nayarit (105.0W,21N)

The *ar_pr* at `Loc2` has a similar general structure to the `Loc1`, with slightly weaker IVT and higher IWV than the `Loc1` composite. Figure 6(a) shows a high IVT ridge near `Loc2` with a maximum value of $\sim$350 kg m^{-1}s^{-1} and IWV $\sim$35 kg m^{-2} near `Loc2`. The mean sea level pressure and geopotential show negative anomalies centered near 26N,110W, with lower magnitude than the `Loc1` composite anomalies (Figures 6(c-f)). An upward 650 hPa wind velocity (and its anomaly) ahead of the tropospheric through, with high IVT normal to the Sierra Madre at `Loc2` (Figures 6(g) and (h)). The genesis and nature of the waves responsible for this weather pattern need to be further explored.

6 Difference between composites

This work focuses on the relationship between ARs and extreme precipitation during the dry season in CWM. In Section 5, we show the results for the *ar_pr* composite, *i.e.* when extreme precipitation and AR are present. This naturally raises the questions: *what about the other composites?*, *what is the difference between composites?*. For example, what is the difference between the climatology of events with extreme precipitation but no ARs detected (*pr_noar*)? What drives this anomalous rainfall? For simplicity, we focus the results in this section on composites over `Loc1`.

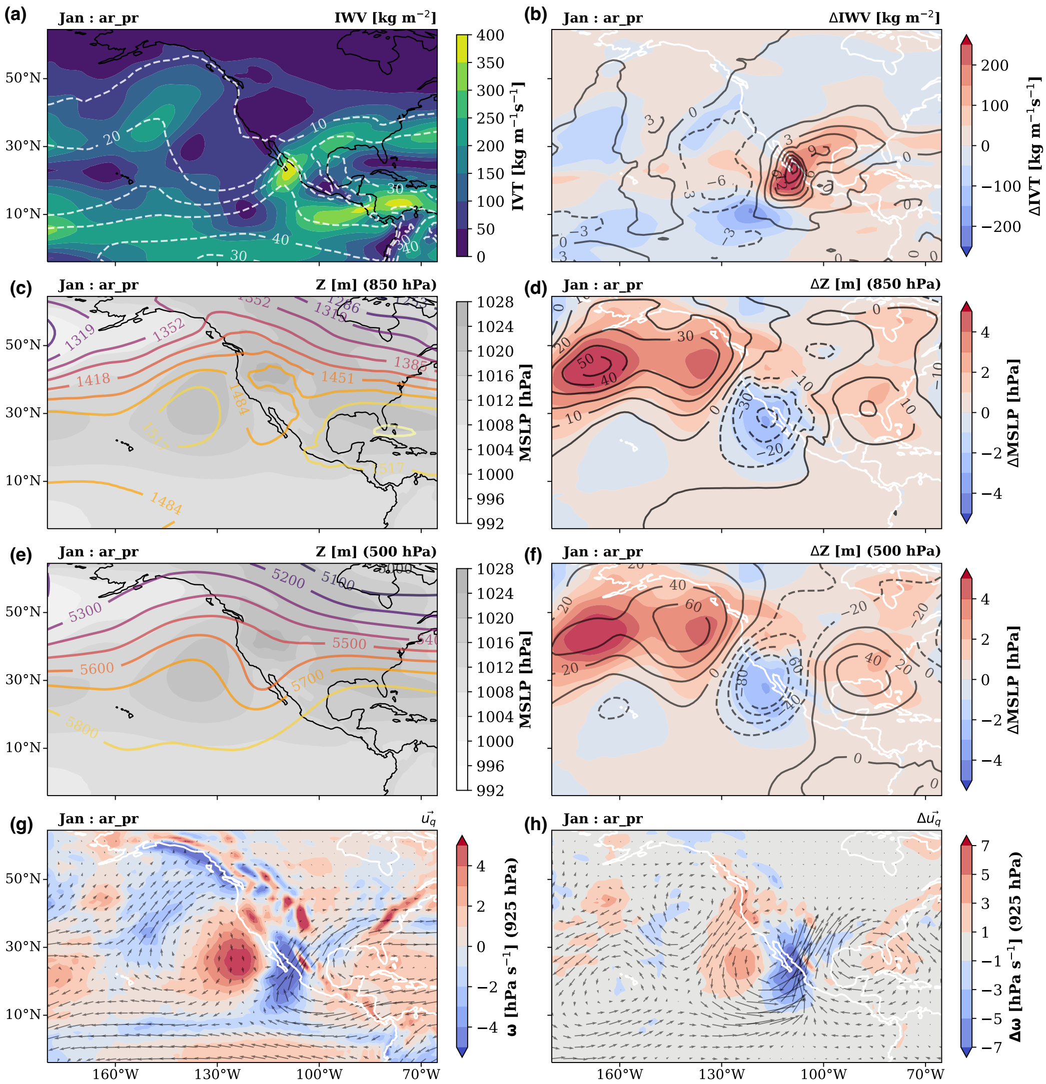

Figure 5. State of the atmosphere during AR landfalling and extreme precipitation at `Loc1` in January. Contours variables are specified on the top-right of each plot. Left column: IWV, IVT, mean sea level pressure, geopotential height at 850 and 500 hPA, IVT direction (u_q), and ω at 650 hPa. Right column: anomalies with respect to the long-term mean for the same variables.

The IWV and IVT for January during extreme precipitation without detection of ARs (*pr_noar*) is shown in Figure 7(a,b). We observe that the general structure of IVT and IWV are similar to the *ar_pr* composite (surface pressure, geopotential height, and vertical velocity plots are shown in Figure S17). So, how different are they? In Figure 7(c,d), we observe little variation between the two composites for the pressure and 850 hPa geopotential height near CWM. The main differences in the pressure/geopotential fields are in the north part of the domain, where the wave pattern, present in both *ar_pr* and *pr_noar* is stronger for *ar_pr* (positive differences in Figure 7 (d)). Nevertheless, the spatial patterns are similar between the two composites. Figure 7(c) shows moisture fields similar to *ar_pr*, although with weaker magnitudes in IVT and IWV for the *pr_noar* composite (Figure 7(c)), probably due to the weakening of the mid-troposphere wave pattern (Figure 7(d)).

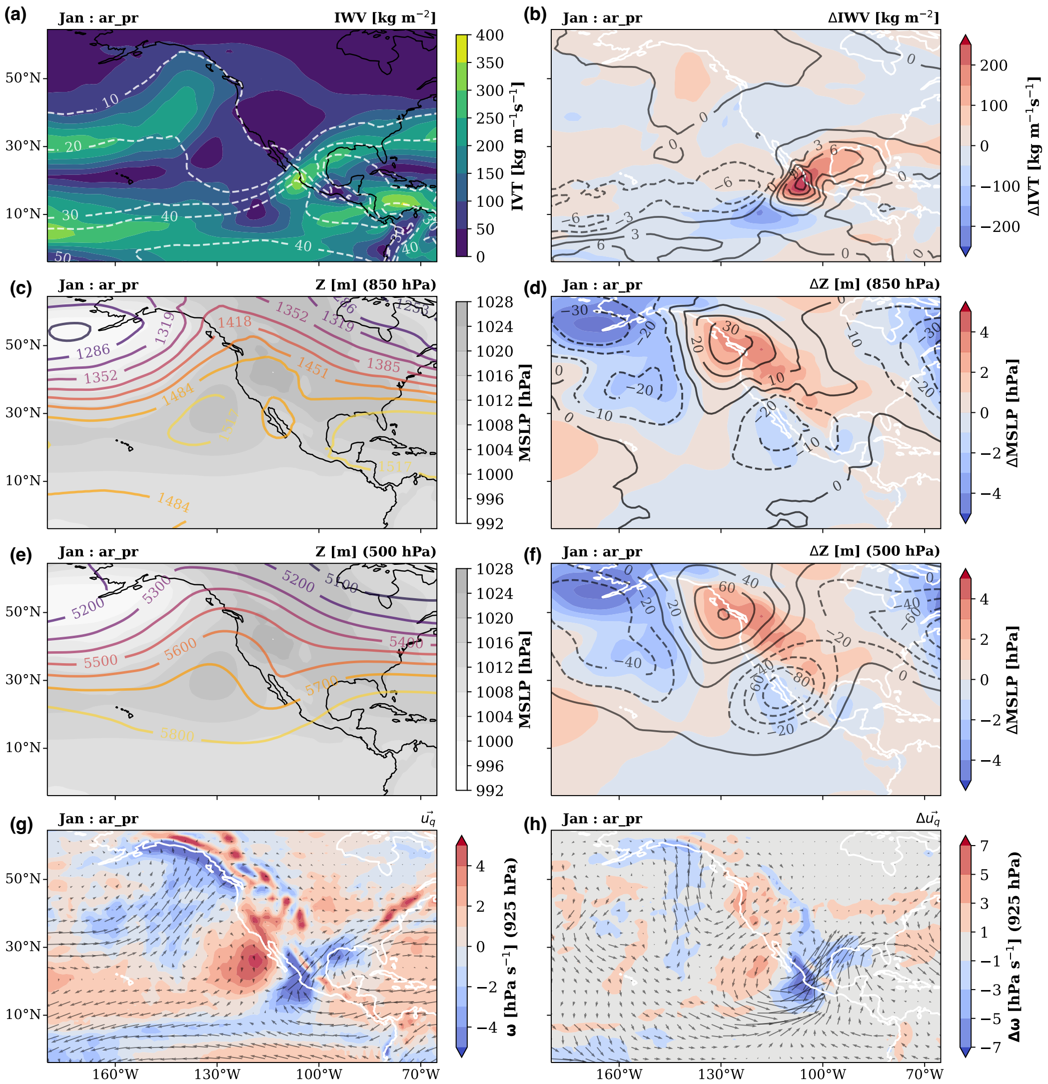

Figure 6. State of the atmosphere during AR landfalling and extreme precipitation at `Loc2` in January. Contours variables are specified on the top-right of each plot. Left column: IWV, IVT, mean sea level pressure, geopotential height at 850 and 500 hPA, IVT direction (u_q), and ω at 650 hPa. Right column: anomalies with respect to the long-term mean for the same variables.

Figure 8(a,b) show the IWV and IVT for the *ar_nopr* composite in January, *i.e.* during AR detection without extreme precipitation present. We note a moisture transport into `Loc1` (surface pressure, geopotential height, and vertical velocity plots are shown in Figure S16). In Figure 8, we notice differences between the *ar_nopr* and the *ar_pr* composites in surface pressure. The *ar_nopr* has a stronger pressure high in the northwest part of the domain but a weaker low high near CWM (Figure 8(d)). Moreover, a tilting in the geopotential height wave pattern (show in the supplemental information, Figure S16), and differences in its magnitude create a much weaker IVT magnitude and a difference in IVT direction at `Loc1` (8(c)). This could be due to a stronger mid-troposphere wave associated with the jet stream meandering or the superposition of two or more waves. Again, the nature of the wave producing these weather patterns still needs to be explored and would make an exciting work by itself. Ultimately, the main consequence of these

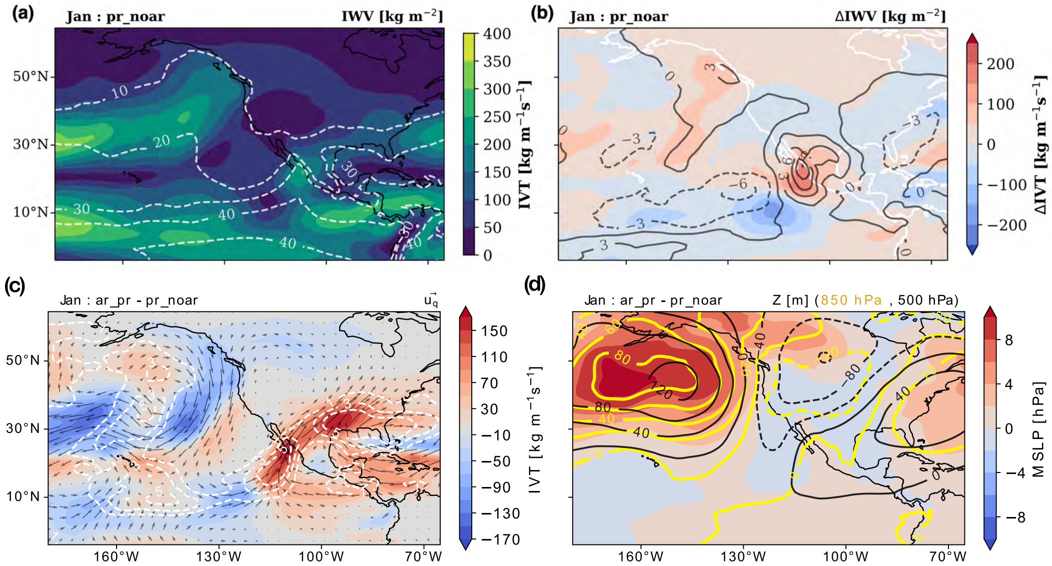

Figure 7. (a) IVT and IWV *pr_noar* composites for January and and their anomalies (`Loc1`). (c and d) Differences in the atmospheric mean state between *ar_pr* and *pr_noar*. (c) IVT magnitude in filled contours, vectors represent IVT direction IVT, and white dashed contours denote changes in IWV. (d) Filled contours show mean sea level pressure differences, thick yellow contours show geopotential height at 850 hPa, and black contours geopotential height at 500 hPa.

wave differences is that they result in a much weaker IVT magnitude with a different direction, both directly related to orographic precipitation.

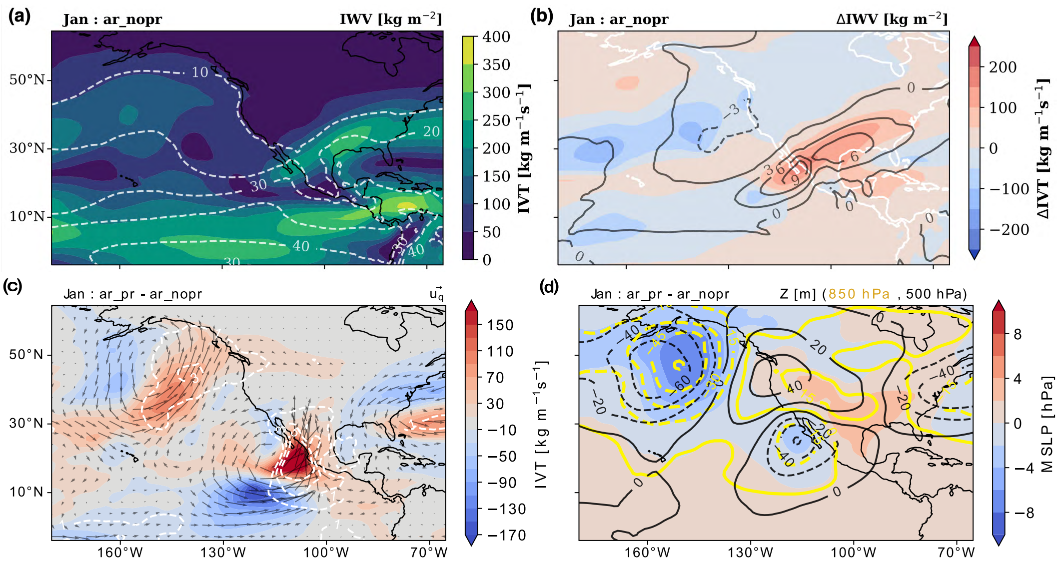

Figure 8. (a) IVT and IWV *pr_noar* composites for January and and their anomalies (`Loc1`). (c and d) Differences in the atmospheric mean state between *ar_pr* and *ar_nopr*. (c) IVT magnitude in filled contours, vectors represent IVT direction IVT, and white dashed contours denote changes in IWV. (d) Filled contours show mean sea level pressure differences, thick yellow contours show geopotential height at 850 hPa, and black contours geopotential height at 500 hPa.

Figures 7(c,d) and 8(c,d) suggest that the different composites might be related to the same or similar weather events or different phases in the same weather event or wave. To explore this, we plot the occurrence time of the events for each composite, shown in the supplemental information's Figures S18-S25 (full 1900-2010 event composites time of occurrence at `Loc1`). There is, in fact, an overlap between composites; in some cases, precipitation events occur before or after ARs but around the same dates in general. This suggests that while we have acceptably identified AR events, an ARDT tuned for tropical latitudes could improve the AR detection in CWM, which could result in a greater correlation between ARs and dry season precipitation in CWM.

7 Discussion and Conclusions

There is a large amount of literature regarding the impacts of ARs in mid-latitudes and polar regions ((Gimeno et al., 2014; F. M. Ralph et al., 2017; Paltan et al., 2017; Rutz et al., 2019; Lora et al., 2020), and references therein) and AR changes with climate change ((Lavers et al., 2015; Payne et al., 2020; O'Brien et al., 2021), and references therein). Nonetheless, there is less research about ARs and their effects in lower latitudes (M. De Luna et al., 2020; M. I. De Luna, 2021). It is not until recently that tropical ARs have started to gather scientific interest. Moreover, since the summer precipitation (June-October) dominates the total precipitation of CWM, a significant part of the research has focused on the role of tropical storms, and tropical cyclones (Farfán & Fogel, 2007; Díaz et al., 2008; Agustín Breña-Naranjo et al., 2015; Dominguez, Christian and Magaña, Victor, 2018; Dominguez et al., 2020), and the role of the North American Monsoon (Adams & Comrie, 1997; Douglas & Englehart, 2007; Cavazos, Tereza and Arriaga-Ramírez, Sarahí, 2012). Furthermore, some studies associate the fluctuations and trends in precipitation in CWM with large-scale climate features like El Niño Southern Oscillation, Pacific Decadal Oscillation, and the Atlantic Multidecadal Oscillation (Magaña, Víctor and Pérez, Joel and Vázquez, Jorge and Pérez, José, 2003; Matías Méndez and Víctor Magaña, 2010; Curtis, 2007; Arriaga-Ramírez, Sarahí and Cavazos, Tereza, 2010). In particular, CWM appears to be a transition region between the Mediterranean rainfall regime in California and northern Baja California and the summer-dominated tropical rainfall regime and the North American Monsoon. This, together with the relatively developed AR research, has resulted in an overlook of the dry season (winter) precipitation and its association with tropical ARs.

Here, we present clear evidence of the relationship between CWM dry season precipitation and ARs. Our composites reflect a high degree of similarity with other compositing studios in higher latitudes (Neiman et al., 2008). Nevertheless, many aspects of these tropical ARs still need to be studied. Investigating the characteristics of the waves that create these anomalous IVT filaments and rainfall is key to understanding these weather patterns and their implications in the CWM dry season hydrological cycle. Moreover, ARs have been typically associated with mid-latitude baroclinic waves and extratropical cyclones (ETC). However, recently (Zhang et al., 2019) showed that nearly 20% of ARs are not nearby an ETC. Here we have presented evidence that aligned surface and mid-troposphere weaves are associated with tropical ARs in CWM, and could possibly denote a barotropic nature of these waves. There is no doubt that we still have a lot to learn and explore about ARs, particularly lower latitudes ARs. We still need to determine the genesis of these events. Are they more related to extratropical weather patterns like an amplification of mid-latitude waves? or maybe to tropical dynamics, energy balance, and responses to shifts in the ITCZ (Haffke & Magnusdottir, 2013; Choi et al., 2015; Lintner & Boos, 2019). In other words, *are these events, in fact, atmospheric rivers, or are they another weather phenomenon?*. We show clear evidence that there is a reasonable degree of similarity between winter ARs in CWM and typical mid-latitude ARs, so a more reasonable question may be *how similar or how different are tropical and mid-latitude ARs?*.

Although ARs in CWM do not dominate the total annual precipitation like on the US West Coast, they regulate extreme precipitation during the dry season. The water vapor in ARs frequently leads to heavy precipitation where they are forced upward by mountains (F. M. Ralph et al., 2018; Smith et al., 2009; F. Ralph et al., 2019). The presence of the *Sierra Madre Occidental* in CWM provides creates an ideal mechanism for orographic rainfall during high IVT events in CWM. Therefore, it is relevant to quantify and understand these tropical ARs and their influence on the regional hydrological cycle of CWM. We recognize that this study (and future studies) could benefit from an ARDT tuned for tropical latitude, which brings back the question of how similar these ARs are to "traditional" mid-latitude ARs. The uncertainty in AR detection is key to answering this question. It has been discussed the possibility that there is more than one type of dynamical phenomenon that produces AR-like objects and that different definitions for these processes could help in future studies (Inda-Díaz et al., 2021; O'Brien et al., 2021). This gains particular relevance for the study of future ARs in CWM, because, in general, different "types" of AR-like phenomena (including CWM landfalling tropical ARs) could have different responses to climate change. There is some evidence of future AR frequency increases in lower latitudes (M. De Luna et al., 2020). Although the frequency increase magnitude is lower than for higher latitudes, there is no assurance on how the local hydrology will be impacted by changes in other AR quantities (intensity, size, orientation, geometry, among others).

In summary, we use data from the Atmospheric Reanalysis of the Twentieth Century ERA-20C and the TECA-BARD AR detector to demonstrate the relationship between extreme precipitation and atmospheric rivers in central-western Mexico during the dry season (November-March) of 1900-2010. We find that more than 25% of extreme precipitation amount and frequency are associated with ARs, with a maximum of 60%-80% during December and January near the coast of Sinaloa (∼107.5W,∼25N).

We calculate composites of the mean state of the atmosphere during AR and extreme precipitation events. We find that for the AR and precipitation composite (ar_pr), there is a positive anomaly in IWV and IVT. Horizontal vapor transport is normal to the coast and the mountain range of the Sierra Madre. Vertical velocity has upward anomalies alongside the high IVT envelope. Besides, changes in horizontal moisture transport, sea level pressure, and geopotential height anomaly fields show a wave pattern associated with the ar_pr composite. A weakening of the surface pressure high and the presence of geopotential lows (above 850 hPa) suggest that the moisture transport occurs at a higher level than typical mid-latitude ARs.

Additionally, we examine the differences between composites. Our results suggest that the AR events without precipitation have a lower IVT magnitude. Furthermore, they show a tilted wave pattern in the geopotential height field with respect to the AR with precipitation composite. Taken together, this translates into lower horizontal vapor transport values with different orientations with respect to the mountain range, resulting in lower precipitation rates. Furthermore, we show that the main difference between the precipitation events with/and without ARs composite is IVT magnitude. Both composites have similar pressure and geopotential wave patterns near the coast of CWM. The pressure and low atmosphere geopotential main differences are located north of 30N. These results suggest that the precipitation without AR events, in fact, is related to the AR events. Both composites could be part of the same weather pattern that our ARDT failed to detect due to the lower IVT magnitude and its inherent design to filter out the tropics.

The nature and genesis of these anomalous IVT events and dry season precipitation –or apparent tropical ARs– still need to be determined, and we plan to explore them in future work. We recommend using more than one ARDT or one tuned explicitly for tropical latitudes, which could sharpen the correlation between ARs and CWM winter precipitation. This will allow investigating the response of CWM landfalling ARs to climate change, which could be critical for studying the region's hydroclimatology under future climate scenarios.

Acknowledgments

The authors thank the multiple reviewers and editors whose feedback and commentary greatly improved the quality and presentation of this manuscript.

This study was supported by the Director, Office of Science, Office of Biological and Environmental Research of the U.S. Department of Energy Regional and Global Modeling and Analysis (RGMA) and used resources of the National Energy Research Scientific Computing Center (NERSC), also supported by the Office of Science of the U.S. Department of Energy under Contract no. DE-AC02-05CH11231.

This project was supported by the Environmental Resilience Institute, funded by Indiana University's Prepared for Environmental Change Grand Challenge initiative.

CPC Global Unified Precipitation data provided by the NOAA/OAR/ESRL PSL, Boulder, Colorado, USA, from their Web site at `https://psl.noaa.gov/data/gridded/data.cpc.globalprecip.html`.

We would like to acknowledge the European Centre for Medium-Range Weather Forecasts and ERA-20C Project (`https://www.ecmwf.int/en/forecasts/datasets/reanalysis-datasets/era-20c`). ERA-20C was accessed through the Copernicus Climate Change Service (C3S) Climate Data Store (CDS) - `https://apps.ecmwf.int/datasets/data/era20c-ofa/`.

We acknowledge Livneh, Ben & National Center for Atmospheric Research Staff (Eds). Last modified 12 Dec 2019. "The Climate Data Guide: Livneh gridded precipitation and other meteorological variables for continental US, Mexico and southern Canada." Retrieved from `https://climatedataguide.ucar.edu/climate-data/livneh-gridded-precipitation-and-other-meteorological-variables-continental-us-mexico`.

This manuscript has been authored by authors at Lawrence Berkeley National Laboratory under Contract No. DE-AC02-05CH11231 with the U.S. Department of Energy. The U.S. Government retains, and the publisher, by accepting the article for publication, acknowledges, that the U.S. Government retains a non-exclusive, paid-up, irrevocable, worldwide license to publish or reproduce the published form of this manuscript, or allow others to do so, for U.S. Government purposes

References

Magaña, Víctor and Pérez, Joel and Vázquez, Jorge and Pérez, José. (2003). Impact of el niño on precipitation in mexico. *Geofísica Internacional*. Retrieved from `https://www.redalyc.org/articulo.oa?id=56842304`

Adams, D. K., & Comrie, A. C. (1997). The north american monsoon. *Bulletin of the American Meteorological Society*, *78*(10), 2197 - 2214. Retrieved from `https://journals.ametsoc.org/view/journals/bams/78/10/1520-0477_1997_078_2197_tnam_2_0_co_2.xml` doi: 10.1175/1520-0477(1997)078⟨2197:TNAM⟩2.0.CO;2

Agustín Breña-Naranjo, J., Pedrozo-Acuña, A., Pozos-Estrada, O., Jiménez-López, S. A., & López-López, M. R. (2015). The contribution of tropical cyclones to rainfall in mexico. *Physics and Chemistry of the Earth, Parts A/B/C*, *83-84*, 111-122. Retrieved from `https://www.sciencedirect.com/science/article/pii/S1474706515000704` (Emerging science and applications with microwave remote sensing data) doi: https://doi.org/10.1016/j.pce.2015.05.011

Arriaga-Ramírez, Sarahí and Cavazos, Tereza. (2010). Regional trends of daily precipitation indices in northwest mexico and southwest united states. *Journal of Geophysical Research: Atmospheres*, *115*(D14). Retrieved from `https://agupubs.onlinelibrary.wiley.com/doi/abs/10.1029/2009JD013248` doi: https://doi.org/10.1029/2009JD013248

Breitburg, Denise; Grégoire, Marilaure and Isensee, Kirsten. (2018). *The ocean is losing its breath: declining oxygen in the world's ocean and coastal waters; summary for policy makers.* Retrieved from `https://unesdoc.unesco.org/ark:/48223/pf0000265196`

Cavazos, Tereza and Arriaga-Ramírez, Sarahí. (2012). Downscaled climate change scenarios for baja california and the north american monsoon during the twenty-first century. *Journal of Climate*, *25*(17), 5904 - 5915. Retrieved from `https://journals.ametsoc.org/view/journals/clim/25/17/jcli-d-11-00425.1.xml` doi: 10.1175/JCLI-D-11-00425.1

Chen, M., Shi, W., Xie, P., Silva, V. B. S., Kousky, V. E., Wayne Higgins, R., & Janowiak, J. E. (2008). Assessing objective techniques for gauge-based analyses of global daily precipitation. *Journal of Geophysical Research: Atmospheres*, *113*(D4). Retrieved from `https://agupubs.onlinelibrary.wiley.com/doi/abs/10.1029/2007JD009132` doi: https://doi.org/10.1029/2007JD009132

Choi, K.-Y., Vecchi, G. A., & Wittenberg, A. T. (2015). Nonlinear zonal wind response to enso in the cmip5 models: Roles of the zonal and meridional shift of the itcz/spcz and the simulated climatological precipitation. *Journal of Climate*, *28*(21), 8556 - 8573. Retrieved from `https://journals.ametsoc.org/view/journals/clim/28/21/jcli-d-15-0211.1.xml` doi: 10.1175/JCLI-D-15-0211.1

Cruz López, M. (2011). Comparación del ciclo agrícola actual con el de hace unos diez anos en San Juan Jalpa municipio San Felipe Del Progreso Estado de México: Evidencia de adapatación al cambio climático. *Ra Ximhai. Revista de Sociedad, Cultura y Desarrollo Sustentable*, *7*(1), 95–106.

Curtis, S. (2007, August). The atlantic multidecadal oscillation and extreme daily precipitation over the US and mexico during the hurricane season. *Climate Dynamics*, *30*(4), 343–351. Retrieved from `https://doi.org/10.1007/s00382-007-0295-0` doi: 10.1007/s00382-007-0295-0

De Luna, M., Waliser, D., Guan, B., Sengupta, A., Raymond, C., & Ye1, H. (2020). *Tropical atmospheric rivers.* Paper presented at the Virtual Symposium by the International Atmospheric Rivers Conference (IARC) Community, 5-9 October, 2020.

De Luna, M. I. (2021). Tropical atmospheric rivers. *Ph.D. dissertation, California State University, Los Angeles*, *ProQuest Dissertations Publishing*. Retrieved from `https://www.proquest.com/dissertations-theses/tropical-atmospheric-rivers/docview/2562506390/se-2?accountid=14505`

Dettinger, M. (2011). Climate change, atmospheric rivers, and floods in California - a multimodel analysis of storm frequency and magnitude changes. *Journal of the American Water Resources Association*, *47*(3), 514–523. doi: 10.1111/j.1752-1688.2011.00546.x

Dettinger, M. D. (2013). Atmospheric Rivers as Drought Busters on the U.S. West Coast. *Journal of Hydrometeorology*, *14*(6), 1721–1732. doi: 10.1175/jhm-d-13-02.1

Dirmeyer, P. A., & Brubaker, K. L. (2007). Characterization of the Global Hydrologic Cycle from a Back-Trajectory Analysis of Atmospheric Water Vapor. *Journal of Hydrometeorology*, *8*(1), 20–37. doi: 10.1175/jhm557.1

Dominguez, C., Done, J. M., & Bruyère, C. L. (2020). Easterly wave con-tributions to seasonal rainfall over the tropical americas in observations and a regional climate model. *Climate Dynamics*, *54*(1), 191–209. Retrieved from https://doi.org/10.1007/s00382-019-04996-7 doi: 10.1007/s00382-019-04996-7

Dominguez, Christian and Magaña, Victor. (2018). The role of tropical cyclones in precipitation over the tropical and subtropical north america. *Frontiers in Earth Science*, *6*. Retrieved from https://www.frontiersin.org/article/10.3389/feart.2018.00019 doi: 10.3389/feart.2018.00019

Domínguez-Hernández, G., Cepeda-Morales, J., Soto-Mardones, L., Rivera-Caicedo, J. P., Romero-Rodríguez, D. A., Inda-Díaz, E. A., ... Romero-Bañuelos, C. (2020, June). Semi-annual variations of chlorophyll concentration on the Eastern Tropical Pacific coast of Mexico. *Advances in Space Research*, *65*(11), 2595–2607. Retrieved 2020-08-14, from https://linkinghub.elsevier.com/retrieve/pii/S0273117720301113 doi: 10.1016/j.asr.2020.02.019

Douglas, A. V., & Englehart, P. J. (2007). A climatological perspective of transient synoptic features during name 2004. *Journal of Climate*, *20*(9), 1947 - 1954. Retrieved from https://journals.ametsoc.org/view/journals/clim/20/9/jcli4095.1.xml doi: 10.1175/JCLI4095.1

Díaz, S., Salinas-Zavala, C., & Hernández-Vázquez, S. (2008, 04). Variability of rainfall from tropical cyclones in northwestern México and its relation to SOI and PDO. *Atmósfera*, *21*, 213 - 223. Retrieved from http://www.scielo.org.mx/scielo.php?script=sci_arttext&pid=S0187-62362008000200006&nrm=iso

Eldardiry, H., Mahmood, A., Chen, X., Hossain, F., Nijssen, B., & Lettenmaier, D. P. (2019). Atmospheric River–Induced Precipitation and Snowpack during the Western United States Cold Season. *Journal of Hydrometeorology*, *20*(4), 613–630. doi: 10.1175/jhm-d-18-0228.1

European Centre for Medium-Range Weather Forecasts. (2014). *Era-20c project (ecmwf atmospheric reanalysis of the 20th century).* https://doi.org/10.5065/D6VQ30QG. Boulder CO: Research Data Archive at the National Center for Atmospheric Research, Computational and Information Systems Laboratory. ((Updated daily.) Accessed January 2022)

Farfán, L. M., & Fogel, I. (2007, April). Influence of tropical cyclones on humidity patterns over southern baja california, mexico. *Monthly Weather Review*, *135*(4), 1208–1224. Retrieved from https://doi.org/10.1175/mwr3356.1 doi: 10.1175/mwr3356.1

García Amaro de Miranda, E. (2003, 04). Distribución de la precipitación en la República Mexicana. *Investigaciones geográficas*, 67 - 76. Retrieved from http://www.scielo.org.mx/scielo.php?script=sci_arttext&pid=S0188-46112003000100009&nrm=iso

Gershunov, A., Shulgina, T., Ralph, F. M., Lavers, D. A., & Rutz, J. J. (2017, aug). Assessing the climate-scale variability of atmospheric rivers affecting western North America. *Geophysical Research Letters*, *44*(15), 7900–7908. Retrieved from http://doi.wiley.com/10.1002/2017GL074175 doi: 10.1002/2017GL074175

Gimeno, L., Dominguez, F., Nieto, R., Trigo, R., Drumond, A., Reason, C. J., ... Marengo, J. (2016). Major Mechanisms of Atmospheric Moisture Transport and Their Role in Extreme Precipitation Events. *Annual Review of Environment and Resources*, *41*(1), 117–141. doi: 10.1146/annurev-environ-110615-085558

Gimeno, L., Nieto, R., Vázquez, M., & Lavers, D. A. (2014). Atmospheric rivers: a mini-review. *Frontiers in Earth Science*, *2*(March), 1–6. doi: 10.3389/feart.2014.00002

Goldenson, N., Leung, L. R., Bitz, C. M., & Blanchard-Wrigglesworth, E. (2018). Influence of atmospheric rivers on mountain snowpack in the western United States. *Journal of Climate*, *31*(24), 9921–9940. doi:

10.1175/JCLI-D-18-0268.1

Guan, B., Molotch, N. P., Waliser, D. E., Fetzer, E. J., & Neiman, P. J. (2010). Extreme snowfall events linked to atmospheric rivers and surface air temperature via satellite measurements. *Geophysical Research Letters*, *37*(20), 2–7. doi: 10.1029/2010GL044696

Haffke, C., & Magnusdottir, G. (2013). The south pacific convergence zone in three decades of satellite images. *Journal of Geophysical Research: Atmospheres*, *118*(19), 10,839-10,849. Retrieved from https://agupubs.onlinelibrary.wiley.com/doi/abs/10.1002/jgrd.50838 doi: https://doi.org/10.1002/jgrd.50838

Huang, H., Patricola, C. M., Bercos-Hickey, E., Zhou, Y., Rhoades, A., Risser, M. D., & Collins, W. D. (2021). Sources of subseasonal-to-seasonal predictability of atmospheric rivers and precipitation in the western United States. *Journal of Geophysical Research: Atmospheres*, *126*, e2020JD034053. doi: 10.1029/2020JD034053

Inda-Díaz, H. A., O'Brien, T. A., Zhou, Y., & Collins, W. D. (2021). Constraining and characterizing the size of atmospheric rivers: A perspective independent from the detection algorithm. *Journal of Geophysical Research: Atmospheres*, *126*(16), e2020JD033746. Retrieved from https://agupubs.onlinelibrary.wiley.com/doi/abs/10.1029/2020JD033746 (e2020JD033746 2020JD033746) doi: https://doi.org/10.1029/2020JD033746

Kim, J., Waliser, D. E., Neiman, P. J., Guan, B., Ryoo, J. M., & Wick, G. A. (2013). Effects of atmospheric river landfalls on the cold season precipitation in California. *Climate Dynamics*, *40*(1-2), 465–474. doi: 10.1007/s00382-012-1322-3

Lavers, D. A., Pappenberger, F., Richardson, D. S., & Zsoter, E. (2016). ECMWF Extreme Forecast Index for water vapor transport: A forecast tool for atmospheric rivers and extreme precipitation. *Geophysical Research Letters*, *43*(22), 11,852–11,858. doi: 10.1002/2016GL071320

Lavers, D. A., Ralph, F. M., Waliser, D. E., Gershunov, A., & Dettinger, M. D. (2015, jul). Climate change intensification of horizontal water vapor transport in CMIP5. *Geophysical Research Letters*, *42*(13), 5617–5625. Retrieved from http://doi.wiley.com/10.1002/2015GL064672 doi: 10.1002/2015GL064672

Lavers, D. A., & Villarini, G. (2013a). Atmospheric rivers and flooding over the central United States. *Journal of Climate*, *26*(20), 7829–7836. doi: 10.1175/JCLI-D-13-00212.1

Lavers, D. A., & Villarini, G. (2013b). The nexus between atmospheric rivers and extreme precipitation across Europe. *Geophysical Research Letters*, *40*(12), 3259–3264. doi: 10.1002/grl.50636

Lavers, D. A., Waliser, D. E., Ralph, F. M., & Dettinger, M. D. (2016). Predictability of horizontal water vapor transport relative to precipitation: Enhancing situational awareness for forecasting western U.S. extreme precipitation and flooding. *Geophysical Research Letters*, *43*(5), 2275–2282. doi: 10.1002/2016GL067765

Leung, L.-R., & Qian, Y. (2009). Atmospheric rivers induced heavy precipitation and flooding in the western U.S. simulated by the WRF regional climate model. *Geophysical Research Letters*, *36*(3), 1–6. doi: 10.1029/2008GL036445

Lintner, B. R., & Boos, W. R. (2019). Using atmospheric energy transport to quantitatively constrain south pacific convergence zone shifts during enso. *Journal of Climate*, *32*(6), 1839 - 1855. Retrieved from https://journals.ametsoc.org/view/journals/clim/32/6/jcli-d-18-0151.1.xml doi: 10.1175/JCLI-D-18-0151.1

Livneh, B., Bohn, T. J., Pierce, D. W., Munoz-Arriola, F., Nijssen, B., Vose, R., … Brekke, L. (2015, August). A spatially comprehensive, hydrometeorological data set for mexico, the u.s., and southern canada 1950–2013. *Scientific Data*, *2*(1). Retrieved from `https://doi.org/10.1038/sdata.2015.42` doi: 10.1038/sdata.2015.42

Livneh, Ben & National Center for Atmospheric Research Staff (Eds). (Last modified 12 Dec 2019). *ERA5: Fifth generation of ECMWF atmospheric reanalyses of the global climate.* https://climatedataguide.ucar.edu/climate-data/livneh-gridded-precipitation-and-other-meteorological-variables-continental-us-mexico.

Lora, J. M., Shields, C. A., & Rutz, J. J. (2020, oct). Consensus and Disagreement in Atmospheric River Detection: ARTMIP Global Catalogues. *Geophysical Research Letters*, *47*(20), 1–10. Retrieved from `https://onlinelibrary.wiley.com/doi/10.1029/2020GL089302` doi: 10.1029/2020GL089302

Matías Méndez and Víctor Magaña. (2010). Regional aspects of prolonged meteorological droughts over mexico and central america. *Journal of Climate*, *23*(5), 1175 - 1188. Retrieved from `https://journals.ametsoc.org/view/journals/clim/23/5/2009jcli3080.1.xml` doi: 10.1175/2009JCLI3080.1

Neiman, P. J., Ralph, F. M., White, A. B., Kingsmill, D. E., & Persson, P. O. (2002). The statistical relationship between upslope flow and rainfall in California's coastal mountains: Observations during CALJET. *Monthly Weather Review*, *130*(6), 1468–1492. doi: 10.1175/1520-0493(2002)130⟨1468:TSRBUF⟩2.0.CO;2

Neiman, P. J., Ralph, F. M., Wick, G. A., Lundquist, J. D., & Dettinger, M. D. (2008). Meteorological Characteristics and Overland Precipitation Impacts of Atmospheric Rivers Affecting the West Coast of North America Based on Eight Years of SSM/I Satellite Observations. *Journal of Hydrometeorology*, *9*(1), 22–47. doi: 10.1175/2007jhm855.1

Neiman, P. J., Ralph, M. F., Moore, B. J., Hughes, M., Mahoney, K. M., Cordeira, J. M., & Dettinger, M. D. (2013). The landfall and inland penetration of a flood-producing atmospheric river in Arizona. Part I: Observed synoptic-scale, orographic, and hydrometeorological characteristics. *Journal of Hydrometeorology*, *14*(2), 460–484. doi: 10.1175/JHM-D-12-0101.1

NOAA Physical Science Laboratory. (2008). *CPC global unified gauge-based analysis of daily precipitation.* Retrieved from `https://psl.noaa.gov/data/gridded/data.cpc.globalprecip.html`

O'Brien, T. A., Risser, M. D., Loring, B., Elbashandy, A. A., Krishnan, H., Johnson, J., ... Collins, W. D. (2020, dec). Detection of atmospheric rivers with inline uncertainty quantification: TECA-BARD v1.0.1. *Geoscientific Model Development*, *13*(12), 6131–6148. Retrieved from `https://www.geosci-model-dev-discuss.net/gmd-2020-55/#discussionhttps://gmd.copernicus.org/articles/13/6131/2020/` doi: 10.5194/gmd-13-6131-2020

O'Brien, T. A., Wehner, M. F., Payne, A. E., Shields, C. A., Rutz, J. J., Leung, L. R., ... Zhou, Y. (2021). Increases in future ar count and size: Overview of the artmip tier 2 cmip5/6 experiment. *Journal of Geophysical Research: Atmospheres*, e2021JD036013. Retrieved from `https://agupubs.onlinelibrary.wiley.com/doi/abs/10.1029/2021JD036013` doi: https://doi.org/10.1029/2021JD036013

Paltan, H., Waliser, D., Lim, W. H., Guan, B., Yamazaki, D., Pant, R., & Dadson, S. (2017). Global Floods and Water Availability Driven by Atmospheric Rivers. *Geophysical Research Letters*, *44*(20), 10,387–10,395. doi: 10.1002/2017GL074882

Payne, A. E., Demory, M.-E., Leung, L. R., Ramos, A. M., Shields, C. A., Rutz, J. J., ... Ralph, F. M. (2020, mar). Responses and impacts of atmospheric rivers to climate change. *Nature Reviews Earth & Environment*, *1*(3), 143–157. Retrieved from `http://dx.doi.org/10.1038/s43017-020-0030-5http://www.nature.com/articles/s43017-020-0030-5` doi:

10.1038/s43017-020-0030-5

Poli, P., Hersbach, H., Dee, D. P., Berrisford, P., Simmons, A. J., Vitart, F., ... Fisher, M. (2016). Era-20c: An atmospheric reanalysis of the twentieth century. *Journal of Climate*, *29*(11), 4083 - 4097. Retrieved from `https://journals.ametsoc.org/view/journals/clim/29/11/jcli-d-15-0556.1.xml` doi: 10.1175/JCLI-D-15-0556.1

Porter, J. R., & Semenov, M. A. (2005, November). Crop responses to climatic variation. *Philosophical Transactions of the Royal Society B: Biological Sciences*, *360*(1463), 2021–2035. Retrieved 2020-08-13, from `https://royalsocietypublishing.org/doi/10.1098/rstb.2005.1752` doi: 10.1098/rstb.2005.1752

Ralph, F., Rutz, J. J., Cordeira, J. M., Dettinger, M., Anderson, M., Reynolds, D., ... Smallcomb, C. (2019, feb). A scale to characterize the strength and impacts of atmospheric rivers. *Bulletin of the American Meteorological Society*, *100*(2), 269–289. doi: 10.1175/BAMS-D-18-0023.1

Ralph, F. M., Coleman, T., Neiman, P. J., Zamora, R. J., & Dettinger, M. D. (2013, apr). Observed Impacts of Duration and Seasonality of Atmospheric-River Landfalls on Soil Moisture and Runoff in Coastal Northern California. *Journal of Hydrometeorology*, *14*(2), 443–459. Retrieved from `https://journals.ametsoc.org/jhm/article/14/2/443/5819/Observed-Impacts-of-Duration-and-Seasonality-of` doi: 10.1175/JHM-D-12-076.1

Ralph, F. M., Dettinger, M., Lavers, D., Gorodetskaya, I. V., Martin, A., Viale, M., ... Cordeira, J. (2017). Atmospheric rivers emerge as a global science and applications focus. *Bulletin of the American Meteorological Society*, *98*(9), 1969 - 1973. Retrieved from `https://journals.ametsoc.org/view/journals/bams/98/9/bams-d-16-0262.1.xml` doi: 10.1175/BAMS-D-16-0262.1

Ralph, F. M., & Dettinger, M. D. (2011, aug). Storms, floods, and the science of atmospheric rivers. *Eos, Transactions American Geophysical Union*, *92*(32), 265–266. Retrieved from `https://onlinelibrary.wiley.com/doi/abs/10.1029/2011EO320001` doi: 10.1029/2011EO320001

Ralph, F. M., Dettinger, M. D., Cairns, M. M., Galarneau, T. J., & Eylander, J. (2018, apr). Defining "Atmospheric River": How the Glossary of Meteorology Helped Resolve a Debate. *Bulletin of the American Meteorological Society*, *99*(4), 837–839. Retrieved from `http://journals.ametsoc.org/doi/10.1175/BAMS-D-17-0157.1` doi: 10.1175/BAMS-D-17-0157.1

Ralph, F. M., Neiman, P. J., Kiladis, G. N., Weickmann, K., & Reynolds, D. W. (2010, nov). A Multiscale Observational Case Study of a Pacific Atmospheric River Exhibiting Tropical–Extratropical Connections and a Mesoscale Frontal Wave. *Monthly Weather Review*, *139*(4), 1169–1189. doi: 10.1175/2010mwr3596.1

Ralph, F. M., Neiman, P. J., & Rotunno, R. (2005). Dropsonde observations in low-level jets over the northeastern Pacific Ocean from CALJET-1998 and PACJET-2001: Mean vertical-profile and atmospheric-river characteristics. *Monthly Weather Review*, *133*(4), 889–910. doi: 10.1175/MWR2896.1

Ralph, F. M., Neiman, P. J., & Wick, G. A. (2004). Satellite and CALJET Aircraft Observations of Atmospheric Rivers over the Eastern North Pacific Ocean during the Winter of 1997/98. *Monthly Weather Review*, *132*(7), 1721–1745. Retrieved from `http://journals.ametsoc.org/doi/abs/10.1175/1520-0493{\%}282004{\%}29132{\%}3C1721{\%}3ASACAOO{\%}3E2.0.CO{\%}3B2` doi: 10.1175/1520-0493(2004)132⟨1721:SACAOO⟩2.0.CO;2

Ralph, F. M., Neiman, P. J., Wick, G. A., Gutman, S. I., Dettinger, M. D., Cayan, D. R., & White, A. B. (2006). Flooding on California's Russian River: Role of atmospheric rivers. *Geophysical Research Letters*, *33*(13), 3–7. doi: 10.1029/2006GL026689

Ralph, F. M., Rutz, J. J., Cordeira, J. M., Dettinger, M., Anderson, M., Reynolds, D., ... Smallcomb, C. (2019, feb). A Scale to Characterize the Strength and Impacts of Atmospheric Rivers. *Bulletin of the American Meteorological Society*, *100*(2), 269–289. Retrieved from `https://journals.ametsoc.org/bams/article/100/2/269/69196/A-Scale-to-Characterize-the-Strength-and-Impacts` doi: 10.1175/BAMS-D-18-0023.1

Romero-Rodríguez, D. A., Soto-Mardones, L. A., Cepeda-Morales, J., Rivera Caicedo, J. P., & Inda Díaz, E. A. (2020). Satellite-derived turbidity influence factors at small river mouths, tropical Pacific coast off México. *Advances in Space Research*. (Aceptado el 3 de agosto de 2020)

Rutz, J. J., James Steenburgh, W., & Martin Ralph, F. (2014, feb). Climatological characteristics of atmospheric rivers and their inland penetration over the western united states. *Monthly Weather Review*, *142*(2), 905–921. Retrieved from `https://journals.ametsoc.org/mwr/article/142/2/905/71947/Climatological-Characteristics-of-Atmospheric` doi: 10.1175/MWR-D-13-00168.1

Rutz, J. J., Shields, C. A., Lora, J. M., Payne, A. E., Guan, B., Ullrich, P., ... Viale, M. (2019, dec). The Atmospheric River Tracking Method Intercomparison Project (ARTMIP): Quantifying Uncertainties in Atmospheric River Climatology. *Journal of Geophysical Research: Atmospheres*, *124*(24), 13777–13802. Retrieved from `https://onlinelibrary.wiley.com/doi/abs/10.1029/2019JD030936` doi: 10.1029/2019JD030936

Simmons, A. J., & Burridge, D. M. (1981). An energy and angular-momentum conserving vertical finite-difference scheme and hybrid vertical coordinates. *Monthly Weather Review*, *109*(4), 758 - 766. Retrieved from `https://journals.ametsoc.org/view/journals/mwre/109/4/1520-0493_1981_109_0758_aeaamc_2_0_co_2.xml` doi: 10.1175/1520-0493(1981)109⟨0758:AEAAMC⟩2.0.CO;2

Smith, B. L., Yuter, S. E., Neiman, P. J., & Kingsmill, D. E. (2009). Water Vapor Fluxes and Orographic Precipitation over Northern California Associated with a Landfalling Atmospheric River. *Monthly Weather Review*, *138*(1), 74–100. doi: 10.1175/2009mwr2939.1

Viale, M., & Nuñez, M. N. (2011). Climatology of winter orographic precipitation over the subtropical central Andes and associated synoptic and regional characteristics. *Journal of Hydrometeorology*, *12*(4), 481–507. doi: 10.1175/2010JHM1284.1

Viale, M., Valenzuela, R., Garreaud, R. D., & Ralph, F. M. (2018). Impacts of Atmospheric Rivers on Precipitation in Southern South America. *Journal of Hydrometeorology*, *19*(10), 1671–1687. doi: 10.1175/jhm-d-18-0006.1

Viguera, B., Martínez-Rodríguez, M., Donatti, C., Harvey, C., & Alpízar, F. (2017). *Impactos del cambio climático en la agricultura de centroamérica, estrategias de mitigación y adaptación. materiales de fortalecimiento de capacidades técnicas del proyecto cascada (conservación internacional-catie).* Conservación Internacional. Retrieved from `https://www.conservation.org/docs/default-source/publication-pdfs/cascade_modulo-2-impactos-del-cambio-climatico-en-la-agricultura-de-centroamerica.pdf`

Waliser, D., & Guan, B. (2017). Extreme winds and precipitation during landfall of atmospheric rivers. *Nature Geoscience*, *10*(3), 179–183. doi: 10.1038/ngeo2894

Warner, M. D., Mass, C. F., & Salatheé, E. P. (2012). Wintertime extreme precipitation events along the Pacific Northwest Coast: Climatology and synoptic evolution. *Monthly Weather Review*, *140*(7), 2021–2043. doi: 10.1175/MWR-D-11-00197.1

Zhang, Z., Ralph, F. M., & Zheng, M. (2019). The Relationship Between Extratropical Cyclone Strength and Atmospheric River Intensity and Position. *Geophysical Research Letters*, *46*(3), 1814–1823. doi: 10.1029/2018GL079071

Zhu, Y., & Newell, R. E. (1998). A Proposed Algorithm for Moisture Fluxes from Atmospheric Rivers. *Monthly Weather Review*, *126*(3), 725–735. doi: 10.1175/1520-0493(1998)126⟨0725:apafmf⟩2.0.co;2

JOURNAL OF GEOPHYSICAL RESEARCH

Supporting Information for "Relationship Between Atmospheric Rivers and the Dry Season Extreme Precipitation in Central-Western Mexico"

H. A. Inda-Díaz[1], T. A. O'Brien[2,1]

[1]Climate and Ecosystem Sciences Division, Lawrence Berkeley National Laboratory, Berkeley, CA, USA

[2]Dept. of Earth and Atmospheric Sciences, Indiana University, Bloomington, IN, USA

Contents of this file

Corresponding author: T. A. O'Brien, Department of Earth and Atmospheric Sciences, Indiana University Bloomington. (obrienta@iu.edu)

Text S1. Long-term means

In Figures S1 through S5, we present the times where each of the ERA-20C climatological means in the 1900-2010 for sea level ressure (SLP), geopotential height (Z), integrated water vapor (IWV), and integrated vapor transport (IVT).

Text S2. Additional plots for composites and their anomalies

In Figures S6 through S17, we present additional plots for the AR + Extreme preciption, AR + No Extreme Precipitation, and Extreme Precipitation + No AR composites. Left columns show IVT, IWV, SLP, Z at 850 and 500 hPa, vertical velocity (ω), and the direction of IVT. The right column shows the anomalies of each composite with respect to the climatological means.

Text S3. Time Correlation between AR and Extreme Precipitation Events

In Figures S18 through S25, we present the times where each of the composites is present at `Loc1` for the entire 1900-2010 period. We notice that AR detection (blue circle markers) are in general around the same dates that the extreme precipitation events (purple cross markers), in some cases before or after, but around each other. It is possible that an ARDTs tuned for tropical ARs would better detect ARs near CWM. Moreover, in future works, we could explore different reanalysis or precipitation data that, together with a tropical ARDT, could mean an even more significant correlation between extreme dry-season precipitation and ARs in CWM. The captions from S18 apply for Figures S19-S25.

Long-term Means

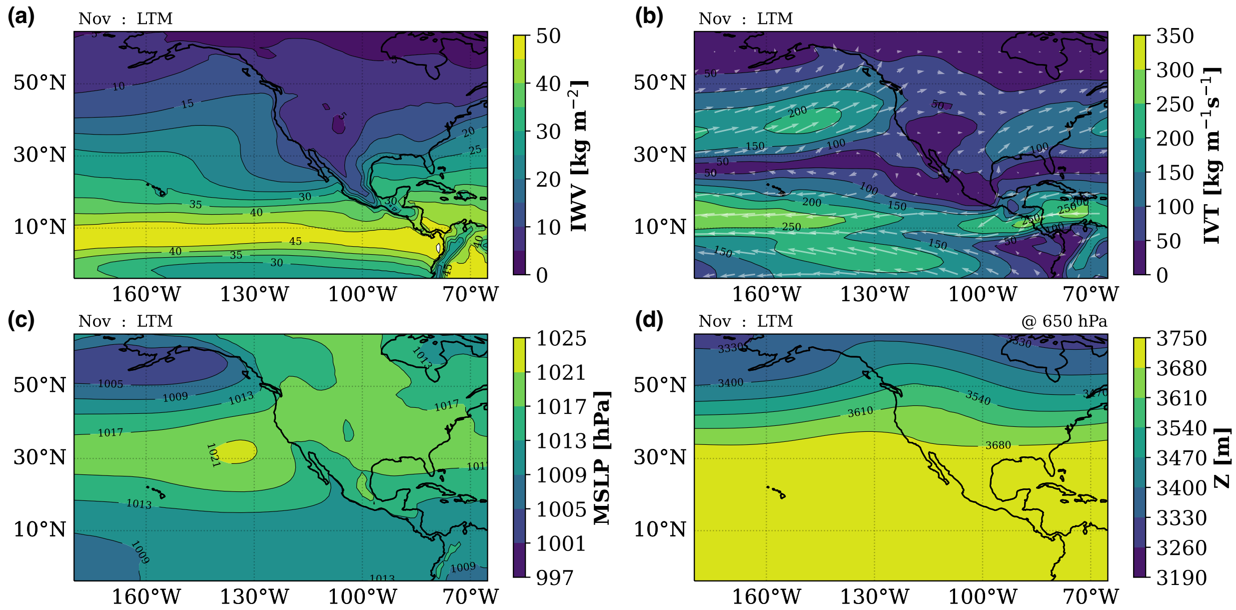

Figure S1. Long-term mean for 1900-2010. (a) Integrated water vapor (IWV), (b) integrated vapor transport (IVT), (c) mean sea level pressure (MSLP), (d) geopotential height at 650 hPa

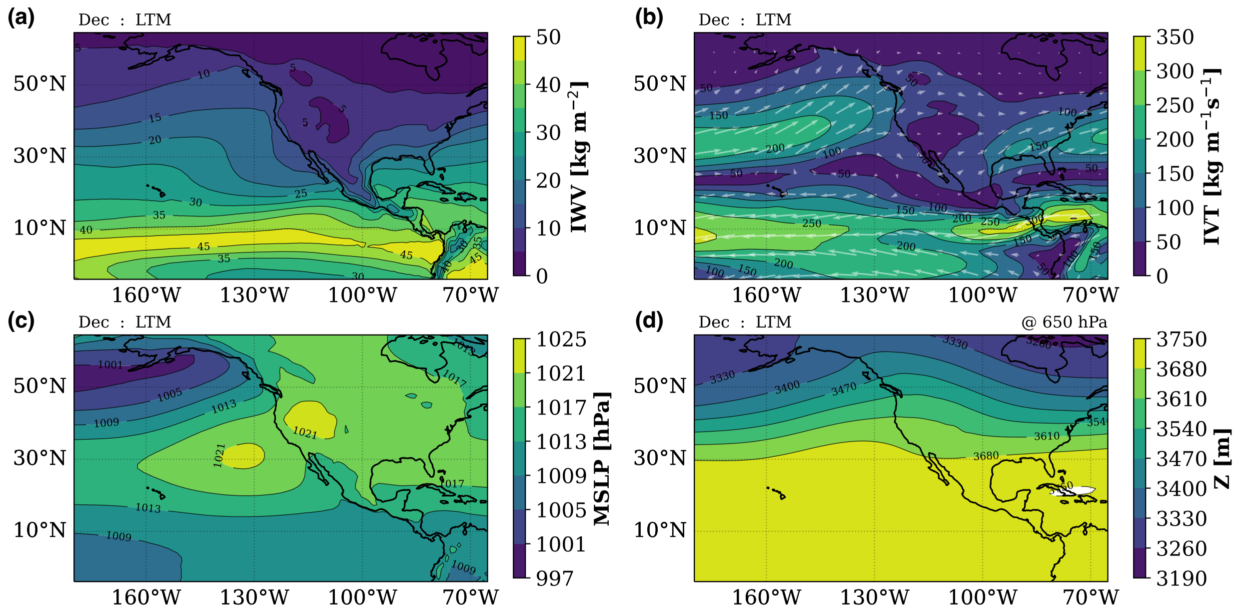

Figure S2. Long-term mean for 1900-2010. (a) Integrated water vapor (IWV), (b) integrated vapor transport (IVT), (c) mean sea level pressure (MSLP), (d) geopotential height at 650 hPa

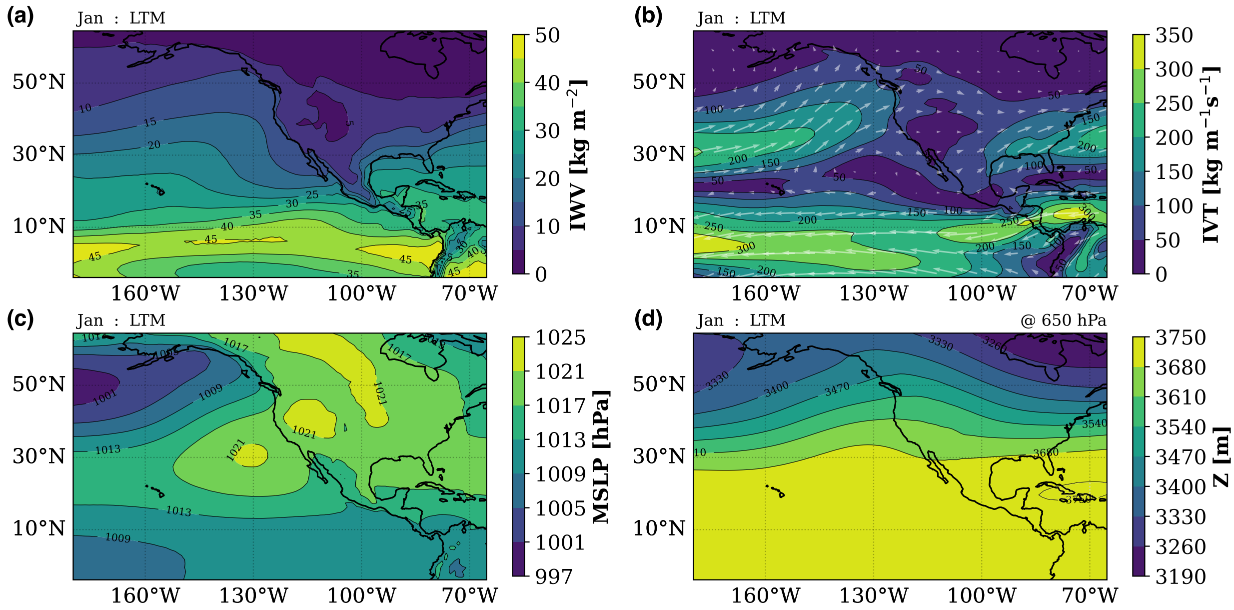

Figure S3. Long-term mean for 1900-2010. (a) Integrated water vapor (IWV), (b) integrated vapor transport (IVT), (c) mean sea level pressure (MSLP), (d) geopotential height at 650 hPa

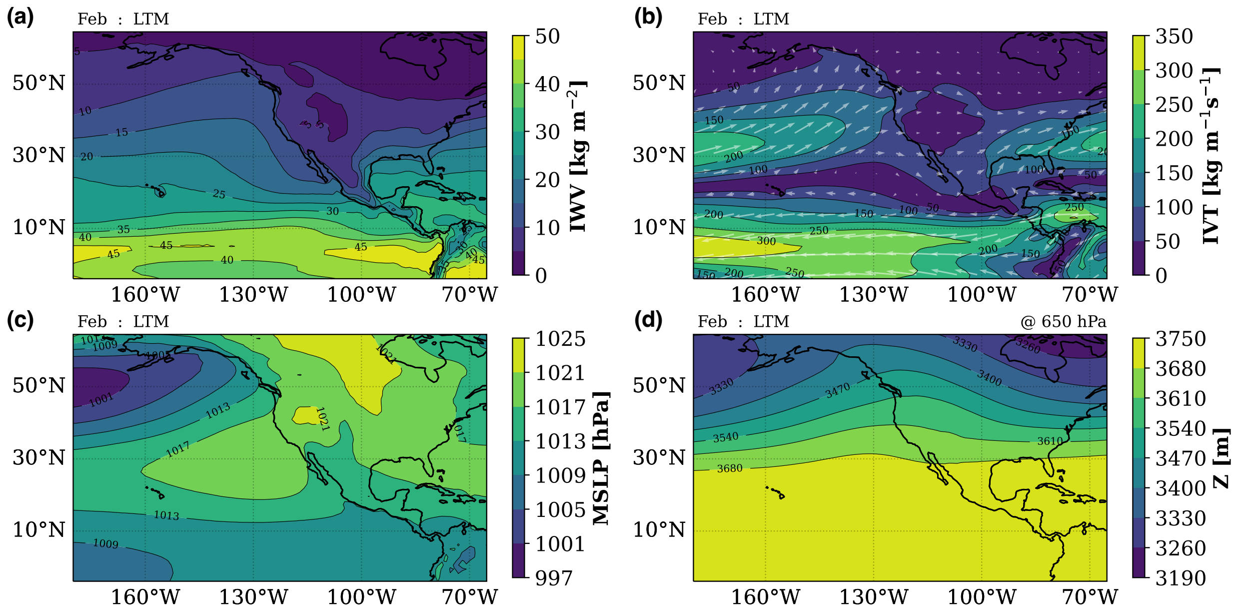

Figure S4. Long-term mean for 1900-2010. (a) Integrated water vapor (IWV), (b) integrated vapor transport (IVT), (c) mean sea level pressure (MSLP), (d) geopotential height at 650 hPa

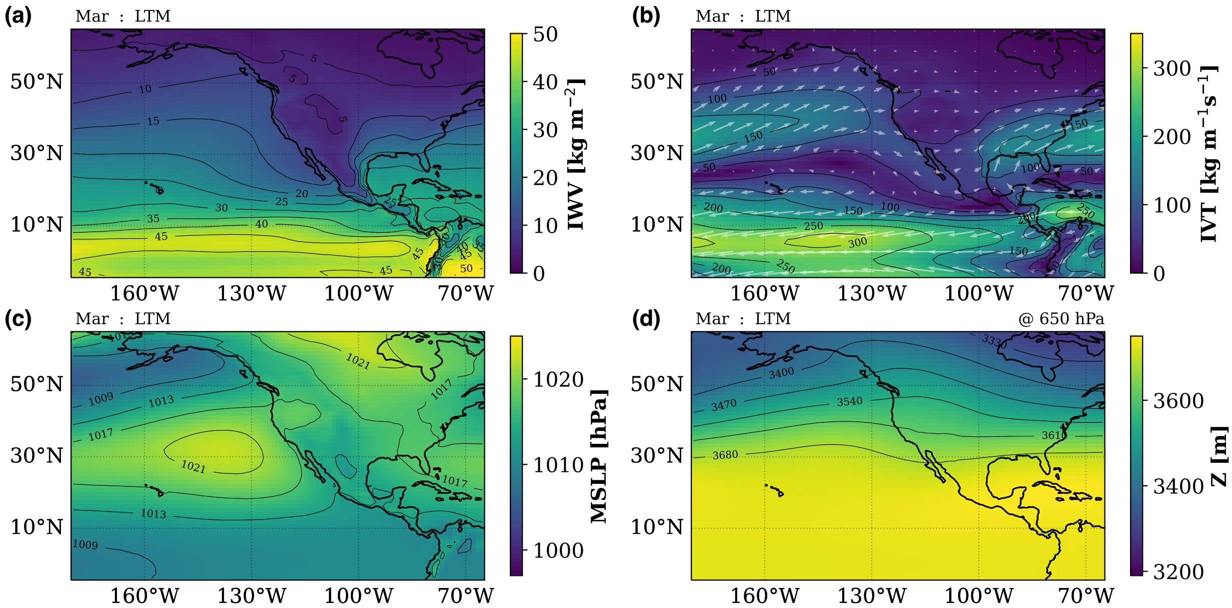

Figure S5. Long-term mean for 1900-2010. (a) Integrated water vapor (IWV), (b) integrated vapor transport (IVT), (c) mean sea level pressure (MSLP), (d) geopotential height at 650 hPa

AR + Extreme Precipitation Composite at Loc1

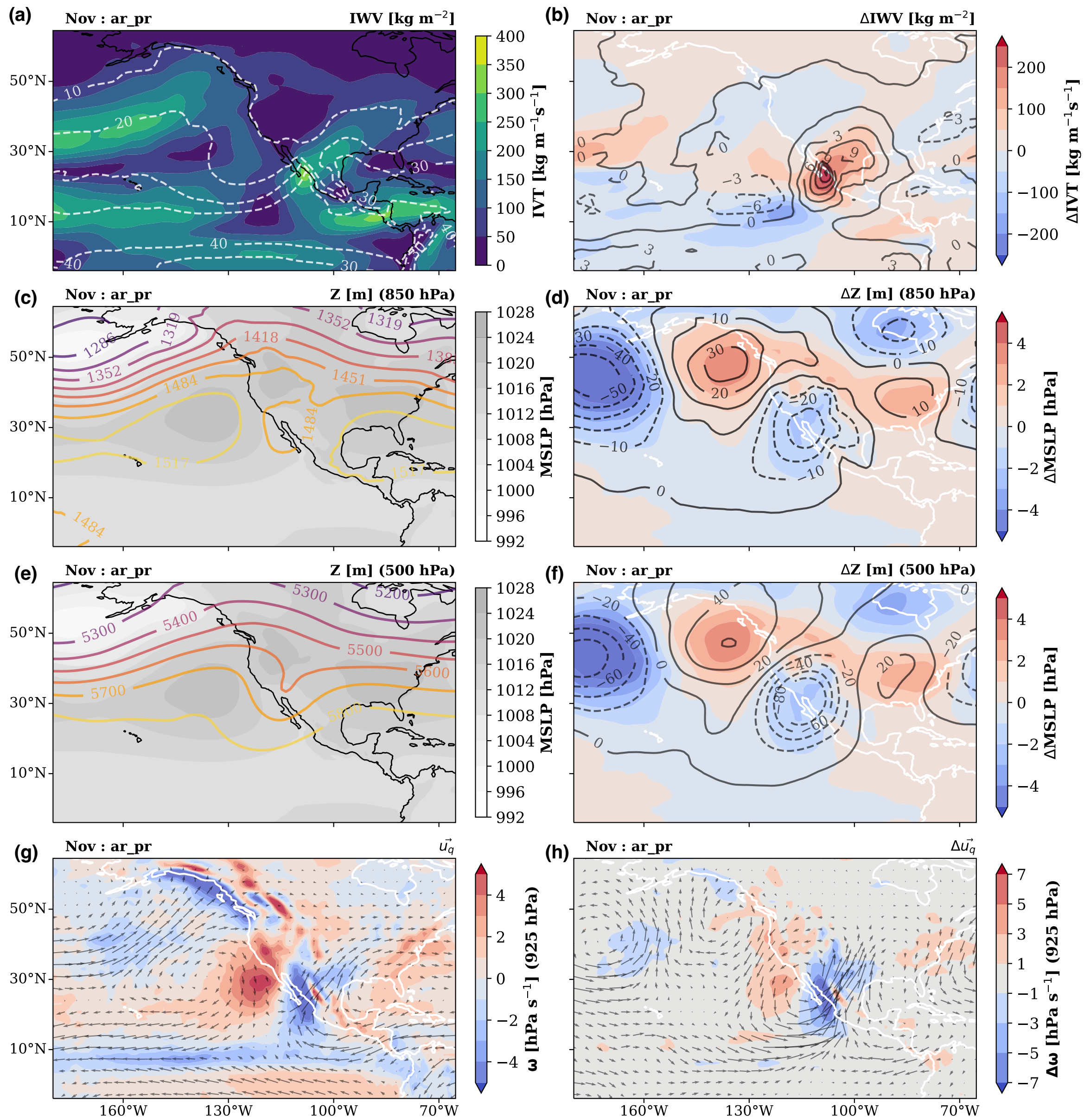

Figure S6. State of the atmosphere during AR landfalling and extreme precipitation at `Loc1` in November. Black contours variables are specified on the top-right of each plot. Left column: IWV, IVT, mean sea level pressure, geopotential height at 850 and 500 hPA, IVT direction (u_q), and ω at 650 hPa. Right column: anomalies with respect to the long-term mean for the same variables.

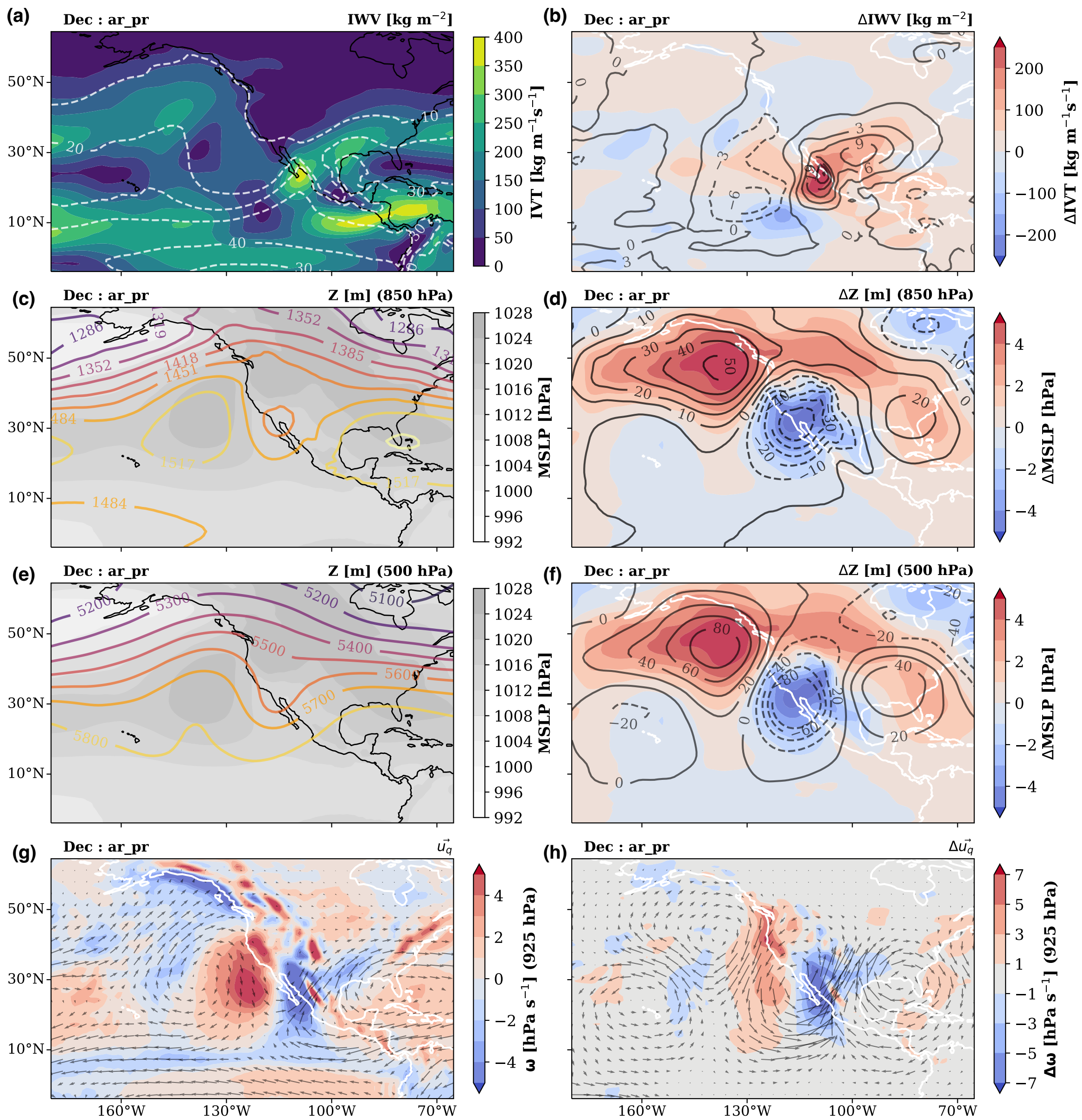

Figure S7. State of the atmosphere during AR landfalling and extreme precipitation at `Loc1` in December. Black contours variables are specified on the top-right of each plot. Left column: IWV, IVT, mean sea level pressure, geopotential height at 850 and 500 hPA, IVT direction (u_q), and ω at 650 hPa. Right column: anomalies with respect to the long-term mean for the same variables.

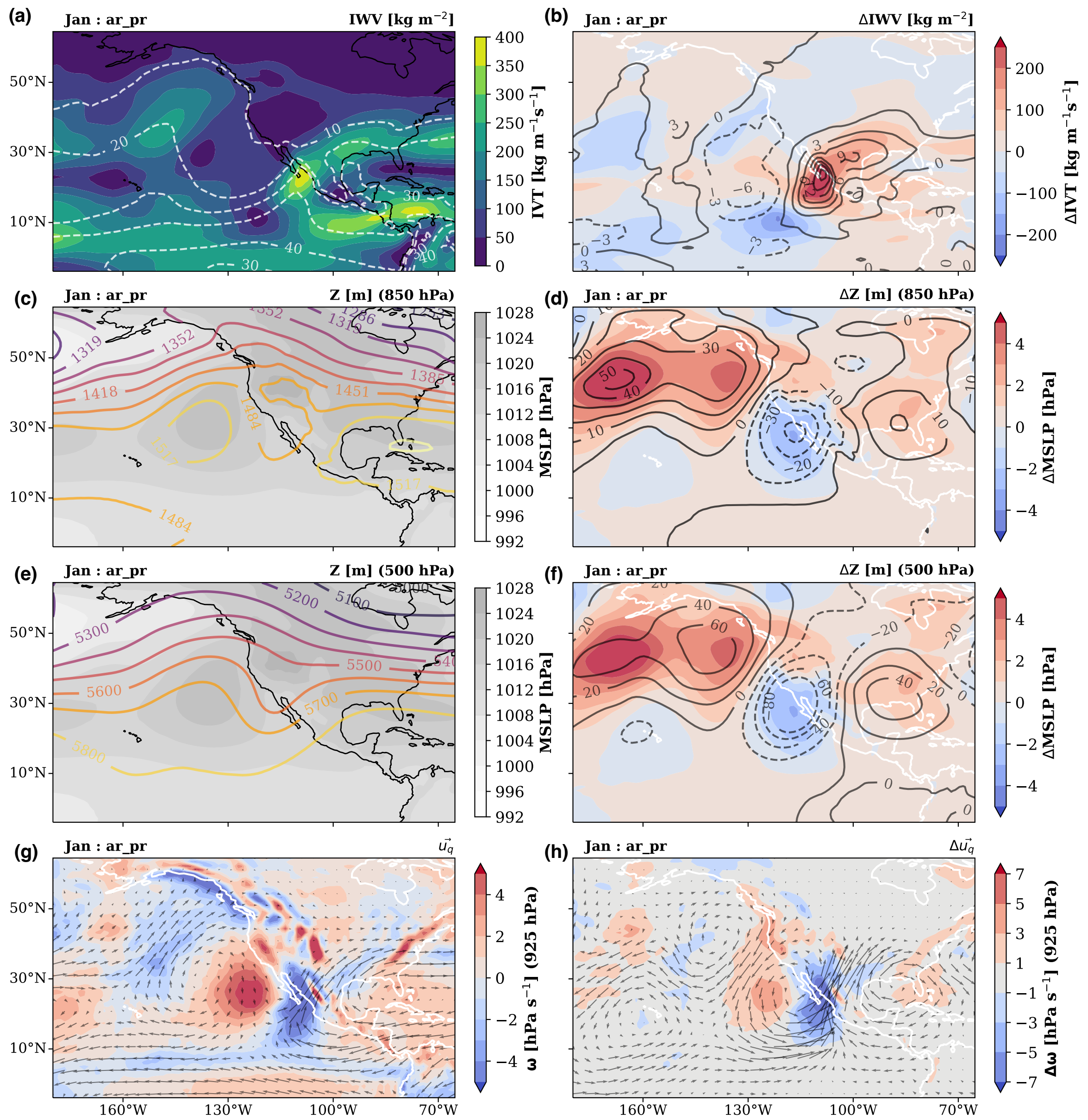

Figure S8. State of the atmosphere during AR landfalling and extreme precipitation at `Loc1` in January. Black contours variables are specified on the top-right of each plot. Left column: IWV, IVT, mean sea level pressure, geopotential height at 850 and 500 hPA, IVT direction (u_q), and ω at 650 hPa. Right column: anomalies with respect to the long-term mean for the same variables.

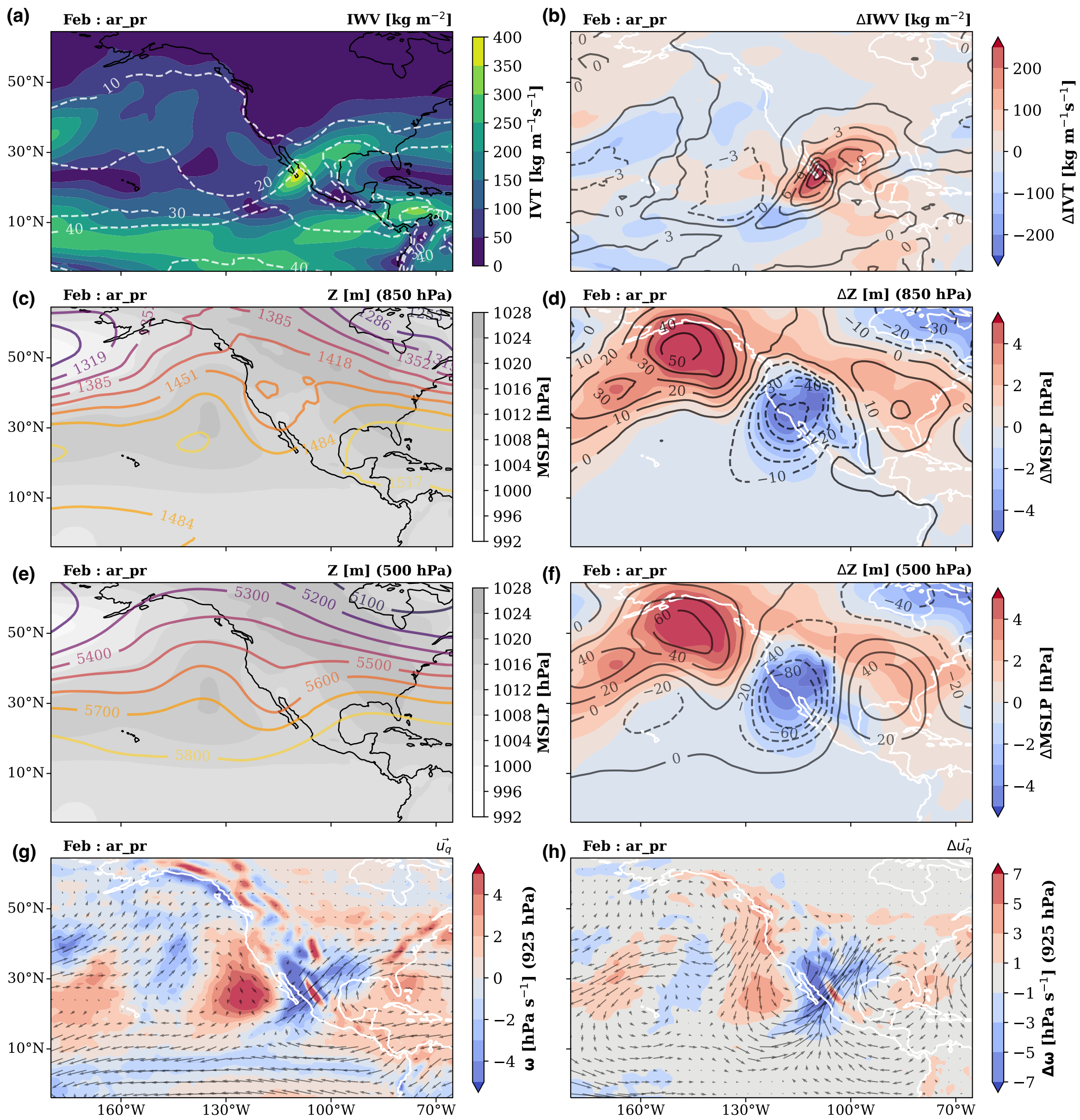

Figure S9. State of the atmosphere during AR landfalling and extreme precipitation at `Loc1` in February. Black contours variables are specified on the top-right of each plot. Left column: IWV, IVT, mean sea level pressure, geopotential height at 850 and 500 hPA, IVT direction (u_q), and ω at 650 hPa. Right column: anomalies with respect to the long-term mean for the same variables.

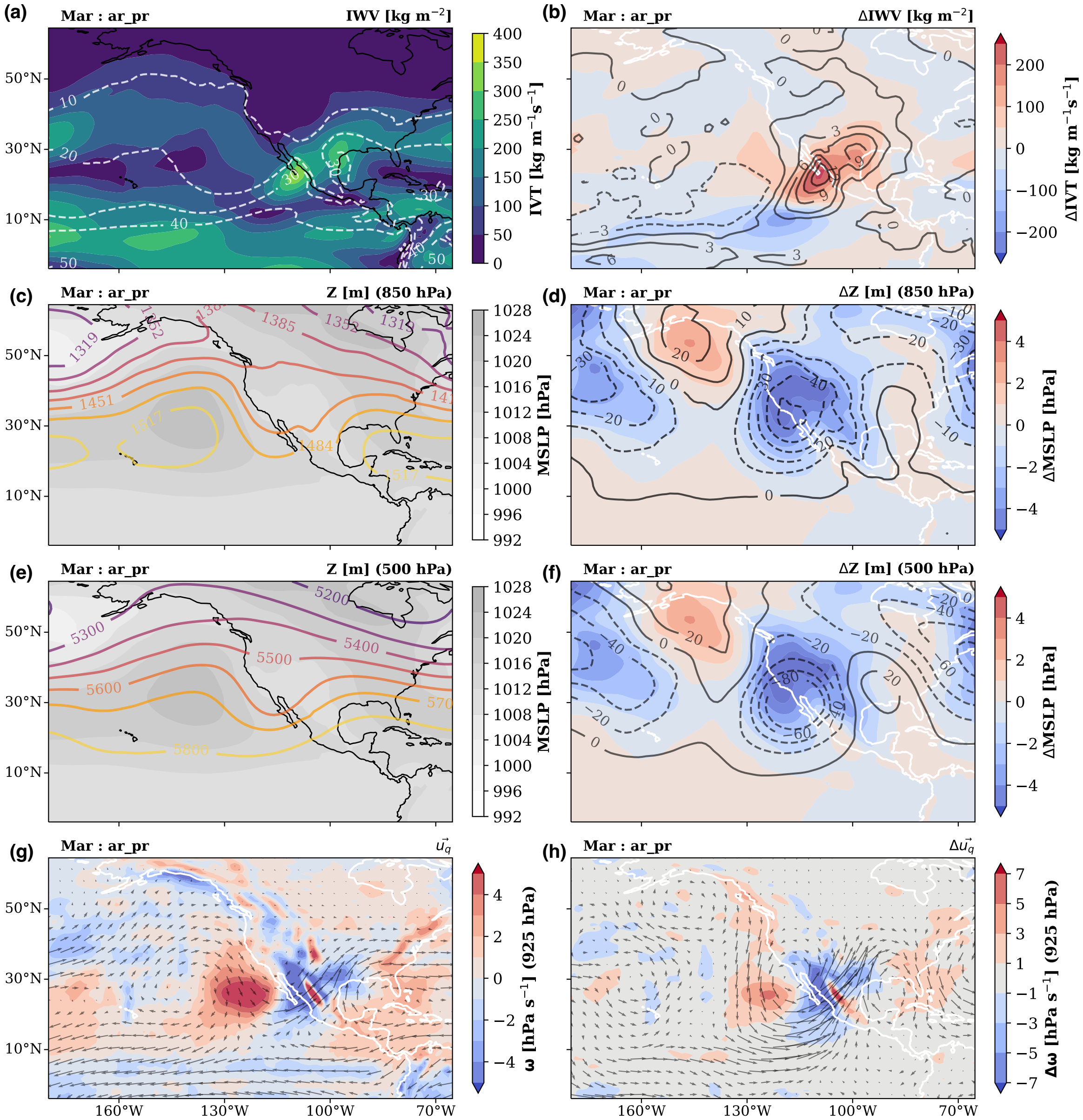

Figure S10. State of the atmosphere during AR landfalling and extreme precipitation at `Loc1` in March. Black contours variables are specified on the top-right of each plot. Left column: IWV, IVT, mean sea level pressure, geopotential height at 850 and 500 hPA, IVT direction (u_q), and ω at 650 hPa. Right column: anomalies with respect to the long-term mean for the same variables.

AR + Extreme Precipitation Composite at Loc2

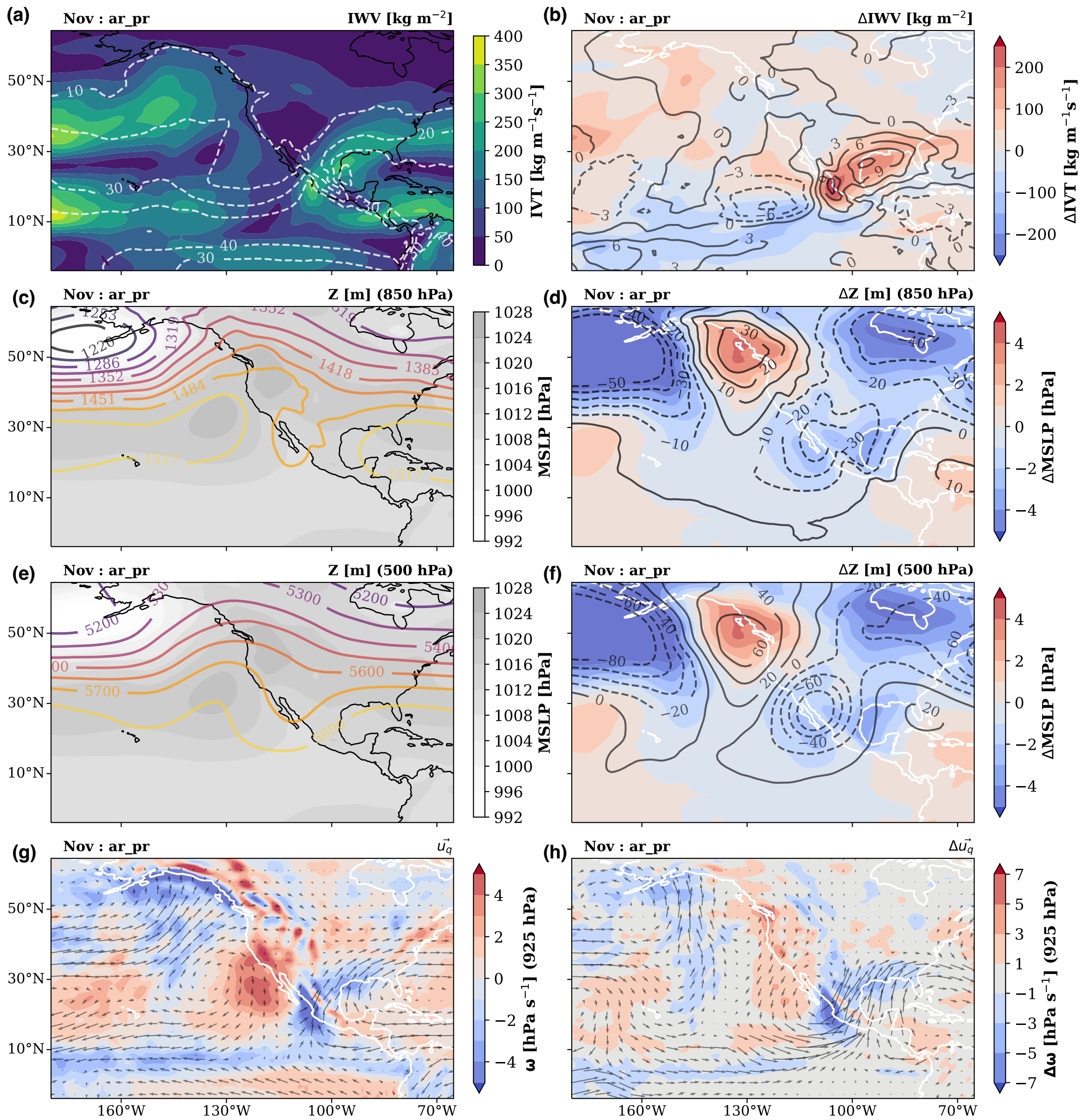

Figure S11. State of the atmosphere during AR landfalling and extreme precipitation at `Loc2` in November. Black contours variables are specified on the top-right of each plot. Left column: IWV, IVT, mean sea level pressure, geopotential height at 850 and 500 hPA, IVT direction (u_q), and ω at 650 hPa. Right column: anomalies with respect to the long-term mean for the same variables.

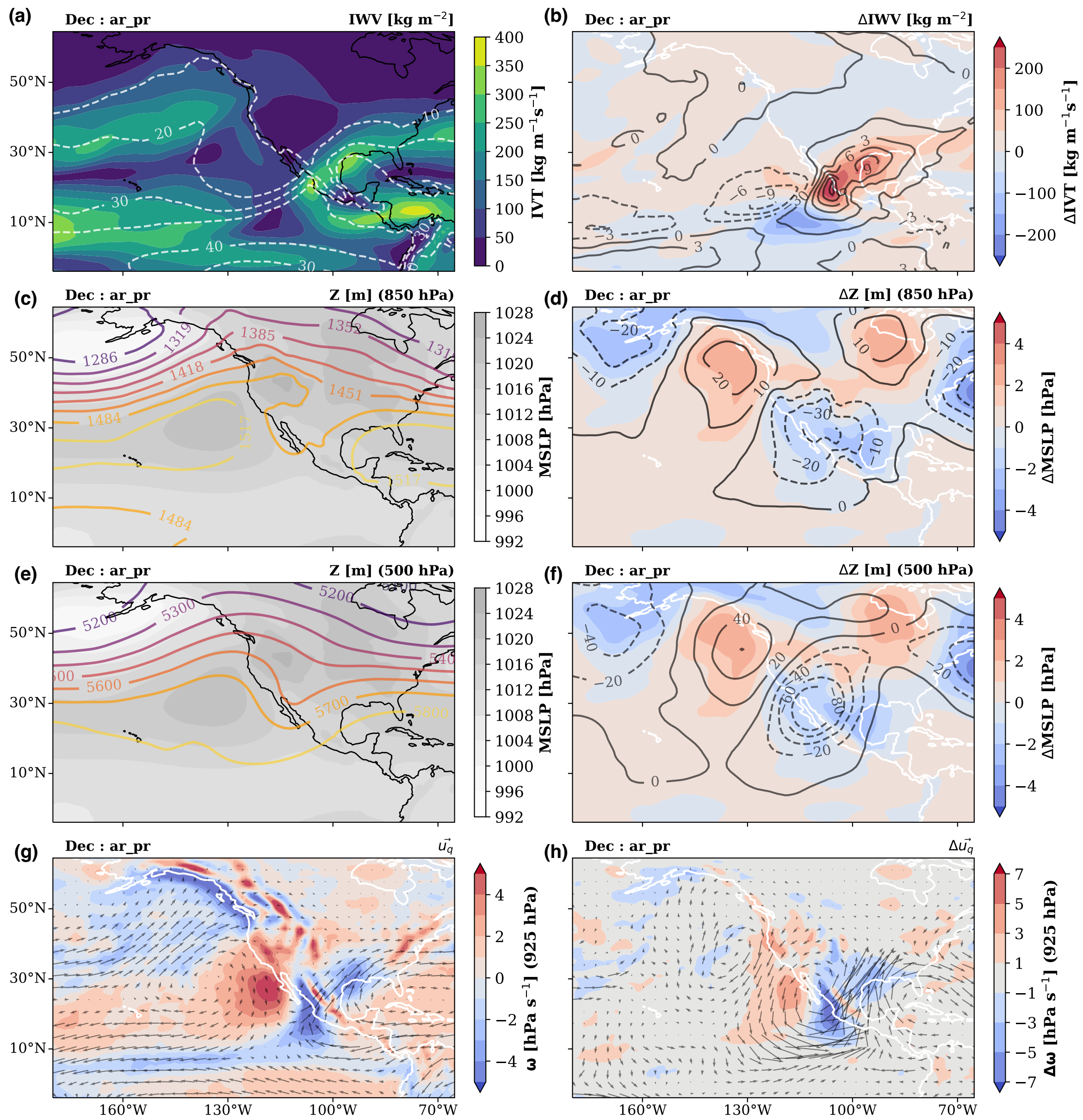

Figure S12. State of the atmosphere during AR landfalling and extreme precipitation at `Loc2` in December. Black contours variables are specified on the top-right of each plot. Left column: IWV, IVT, mean sea level pressure, geopotential height at 850 and 500 hPA, IVT direction (u_q), and ω at 650 hPa. Right column: anomalies with respect to the long-term mean for the same variables.

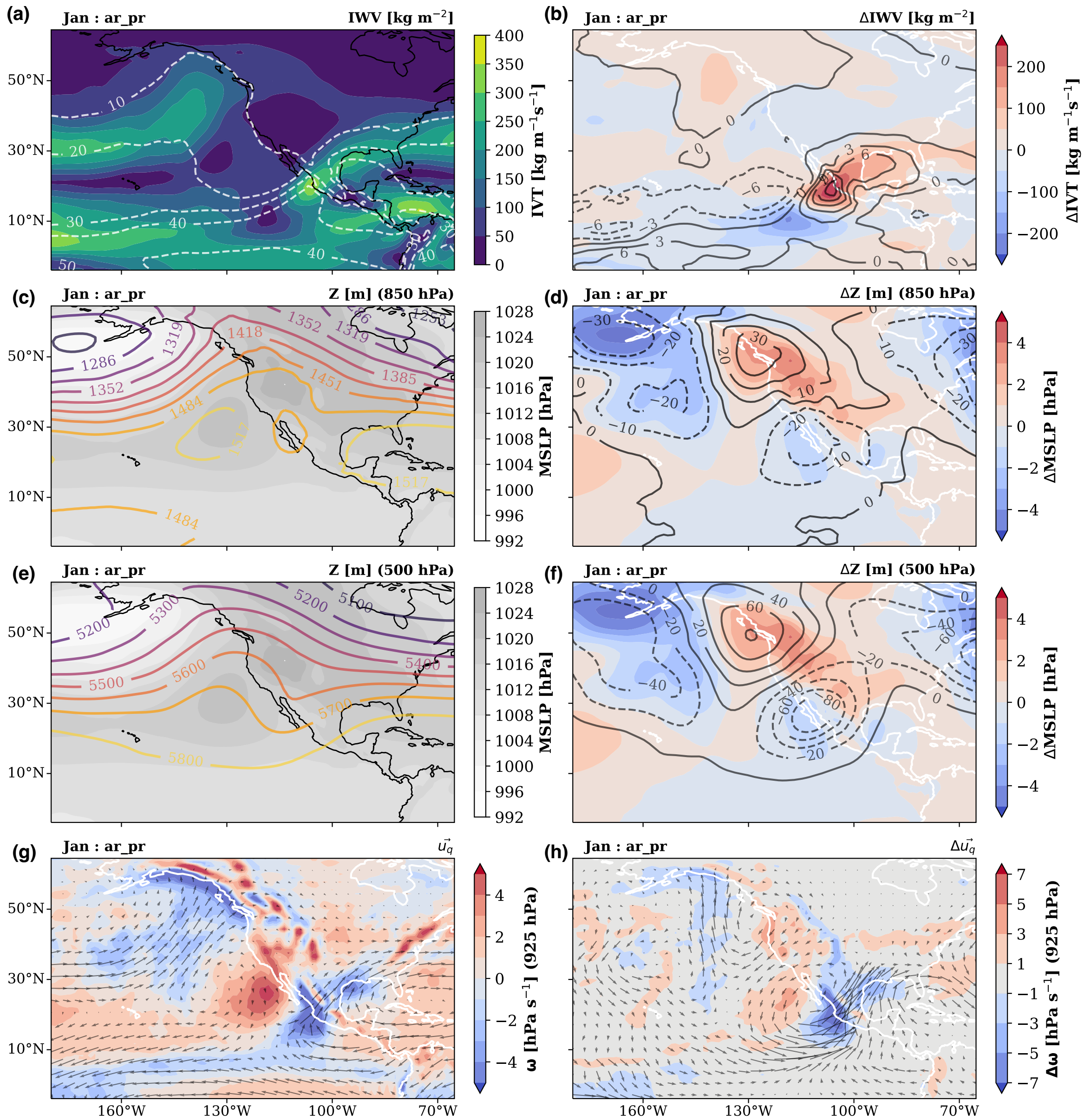

Figure S13. State of the atmosphere during AR landfalling and extreme precipitation at `Loc2` in January. Black contours variables are specified on the top-right of each plot. Left column: IWV, IVT, mean sea level pressure, geopotential height at 850 and 500 hPA, IVT direction (u_q), and ω at 650 hPa. Right column: anomalies with respect to the long-term mean for the same variables.

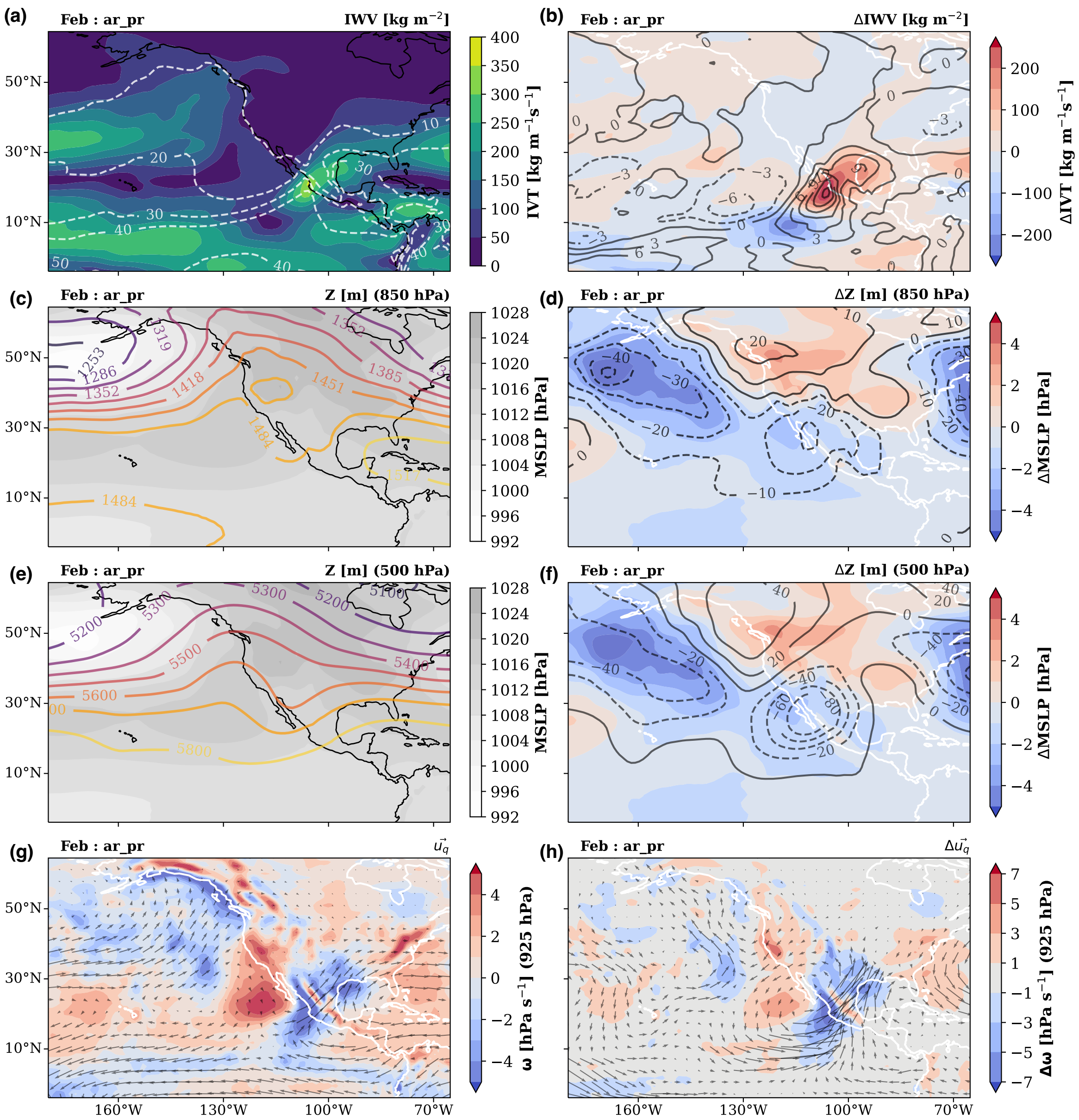

Figure S14. State of the atmosphere during AR landfalling and extreme precipitation at Loc2 in February. Black contours variables are specified on the top-right of each plot. Left column: IWV, IVT, mean sea level pressure, geopotential height at 850 and 500 hPA, IVT direction (u_q), and ω at 650 hPa. Right column: anomalies with respect to the long-term mean for the same variables.

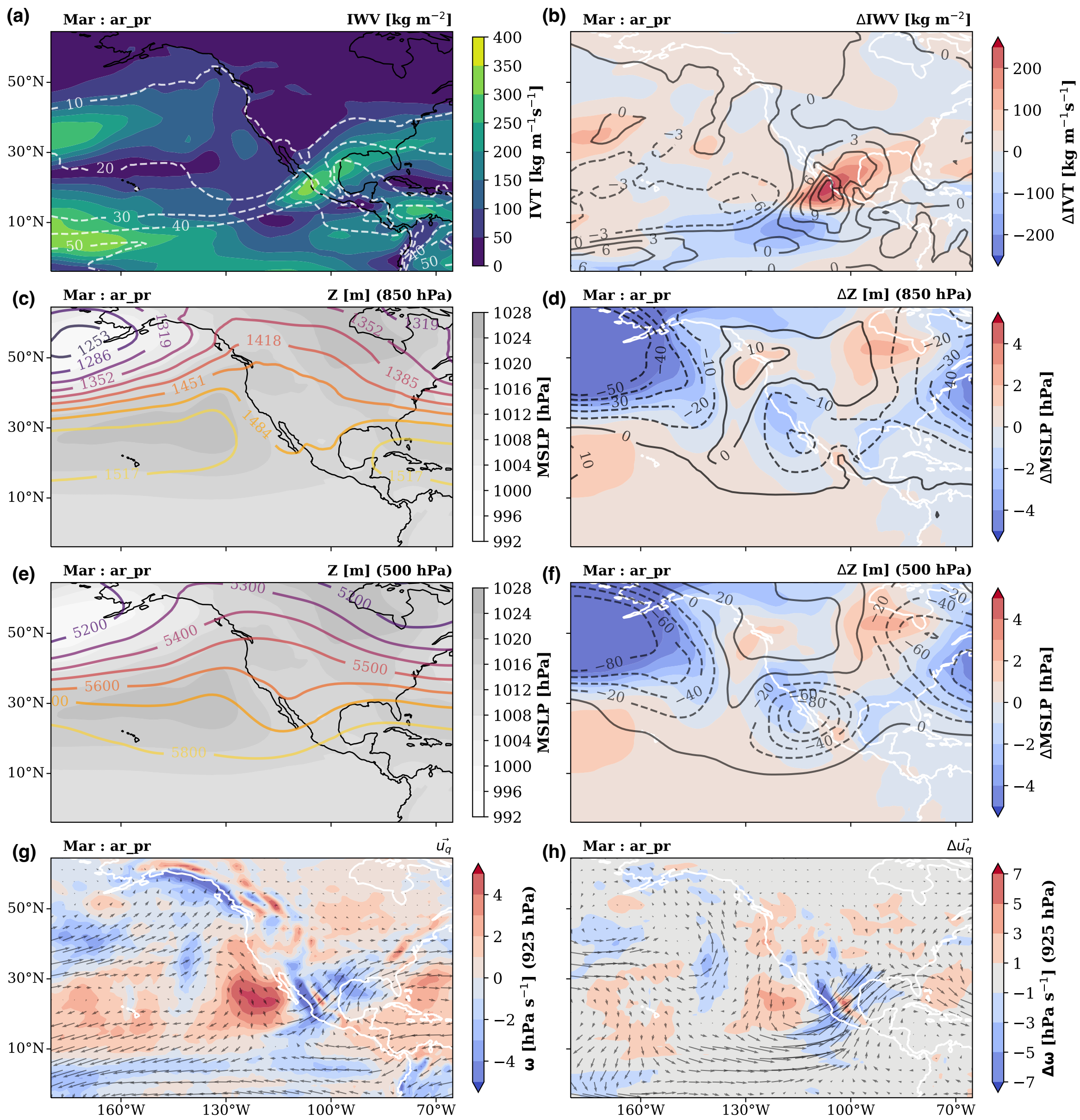

Figure S15. State of the atmosphere during AR landfalling and extreme precipitation at Loc2 in March. Black contours variables are specified on the top-right of each plot. Left column: IWV, IVT, mean sea level pressure, geopotential height at 850 and 500 hPA, IVT direction (u_q), and ω at 650 hPa. Right column: anomalies with respect to the long-term mean for the same variables.

AR + No Precipitation Composite

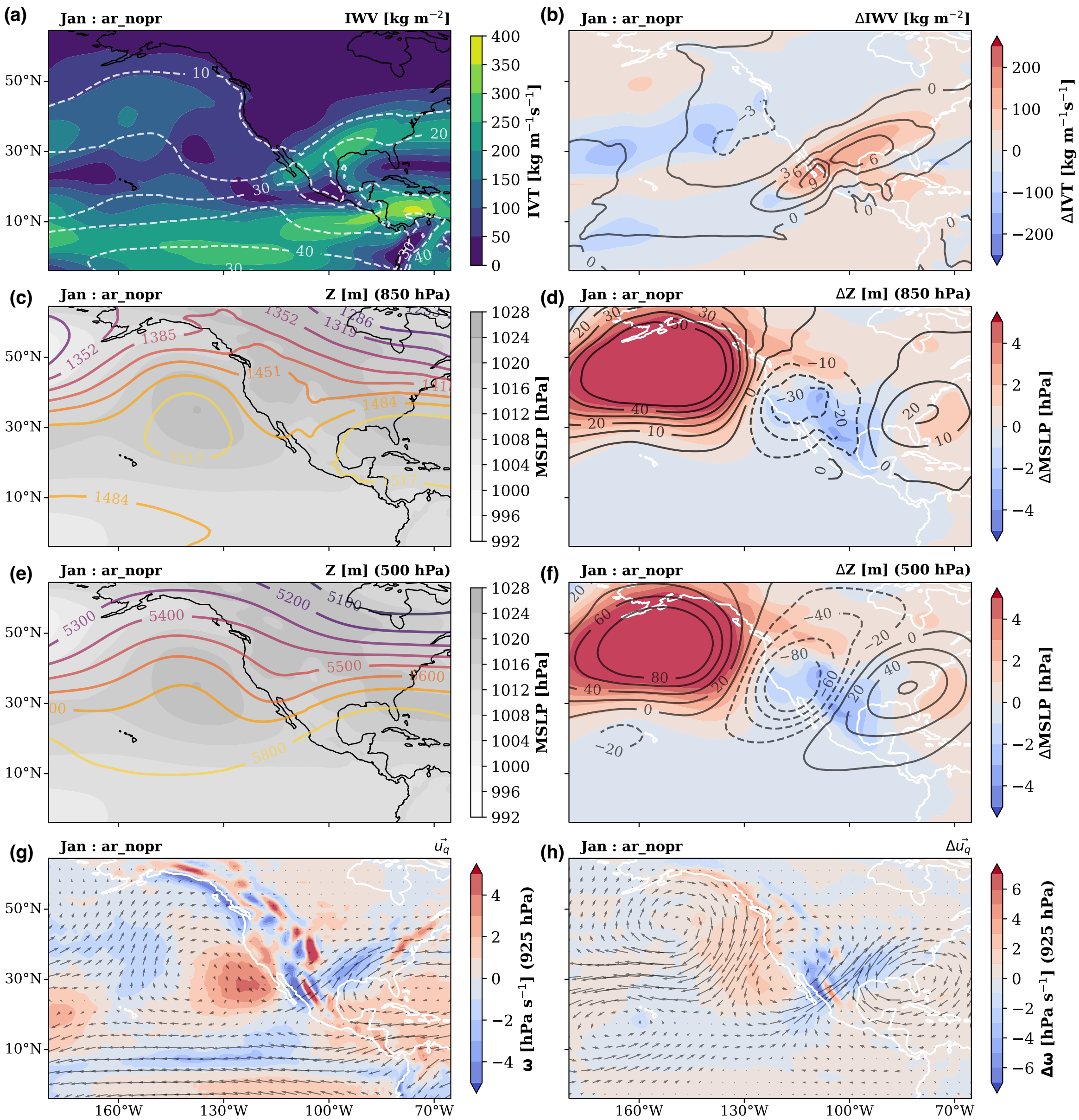

Figure S16. State of the atmosphere during AR landfalling and without extreme precipitation at `Loc1` in January. Black contours variables are specified on the top-right of each plot. Left column: IWV, IVT, mean sea level pressure, geopotential height at 850 and 500 hPA, IVT direction (u_q), and ω at 650 hPa. Right column: anomalies with respect to the long-term mean for the same variables.

Precipitation + no AR Composite

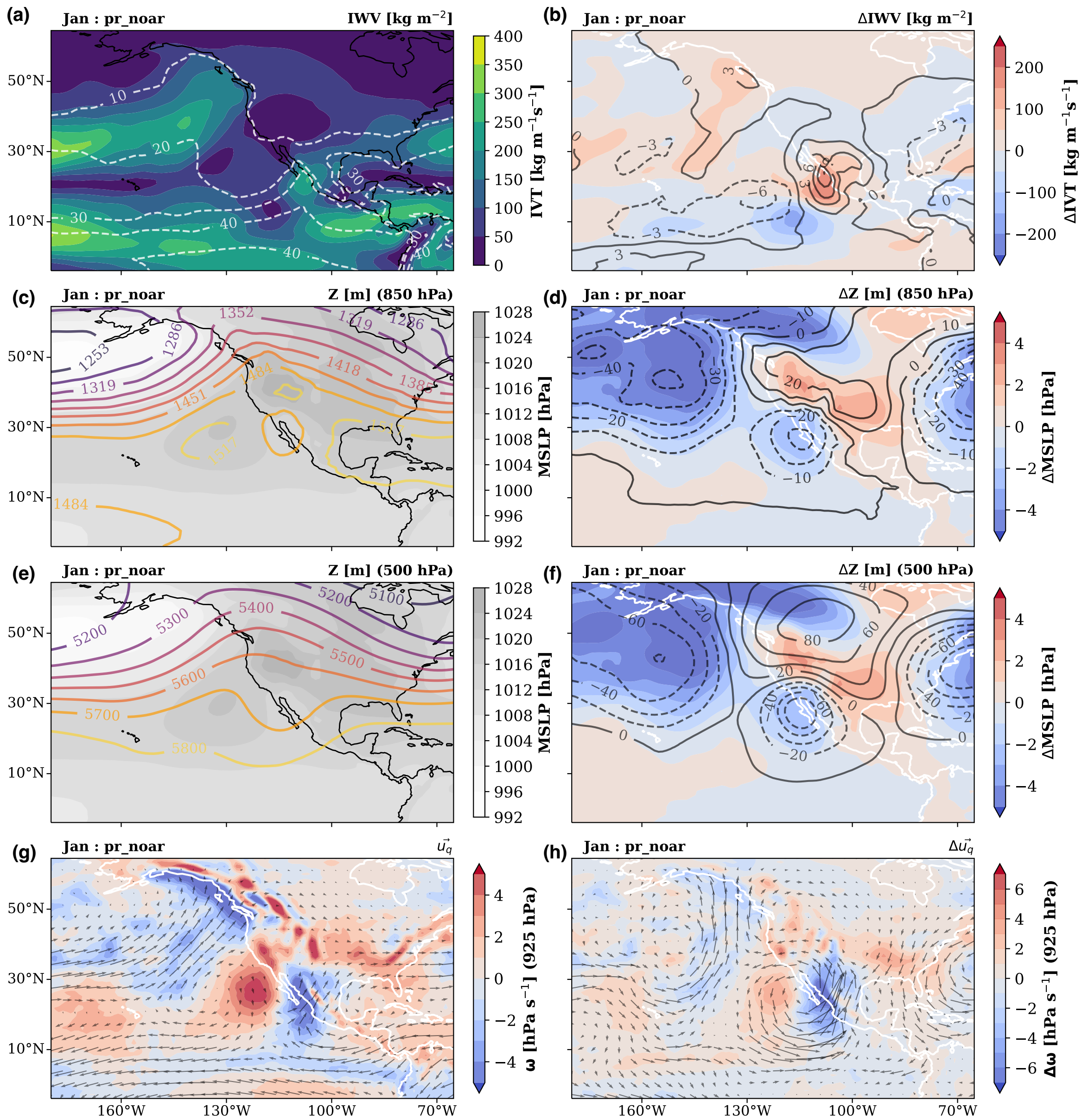

Figure S17. State of the atmosphere during extreme precipitation without AR landfalling conditions at `Loc1` in January. Black contours variables are specified on the top-right of each plot. Left column: IWV, IVT, mean sea level pressure, geopotential height at 850 and 500 hPA, IVT direction (u_q), and ω at 650 hPa. Right column: anomalies with respect to the long-term mean for the same variables.

Time Correlation between AR and Extreme Precipitation Events

Figure S18. Time of event for each composite (*ar*, *ar_pr*, *ar_nopr*, *pr_noar*, and *pr*). Each subfigure shows a year in the 1900-2010 period to be able to clearly look at the overlap of events across composites. Blue circle markers represent *ar*, orange squares *ar_pr*, green triangles *ar_nopr*, red stars *pr_noar*, and purple crosses *pr*.

The same caption applies for Figures S19 through S25

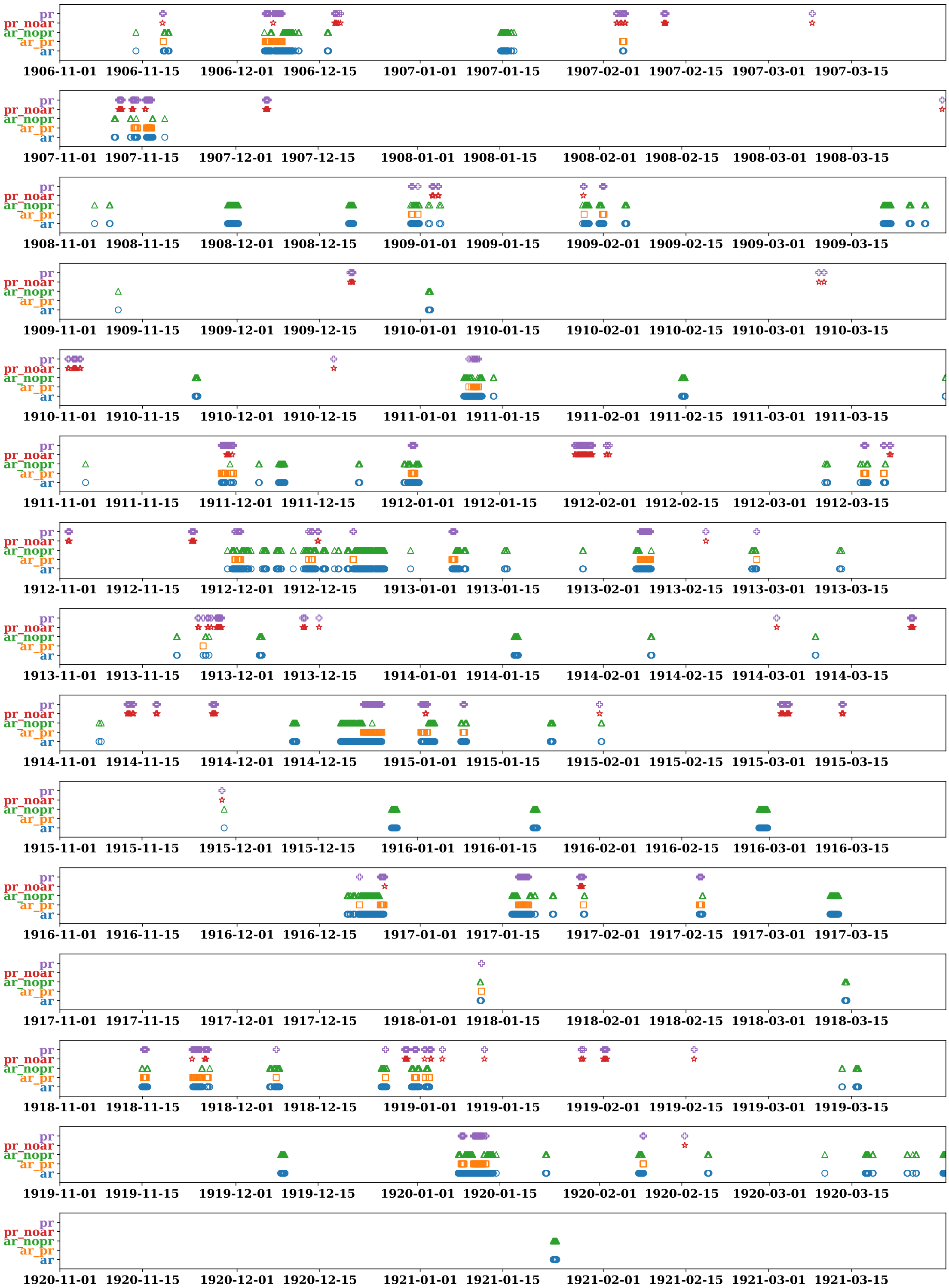

Figure S19. Same caption as Figure S18

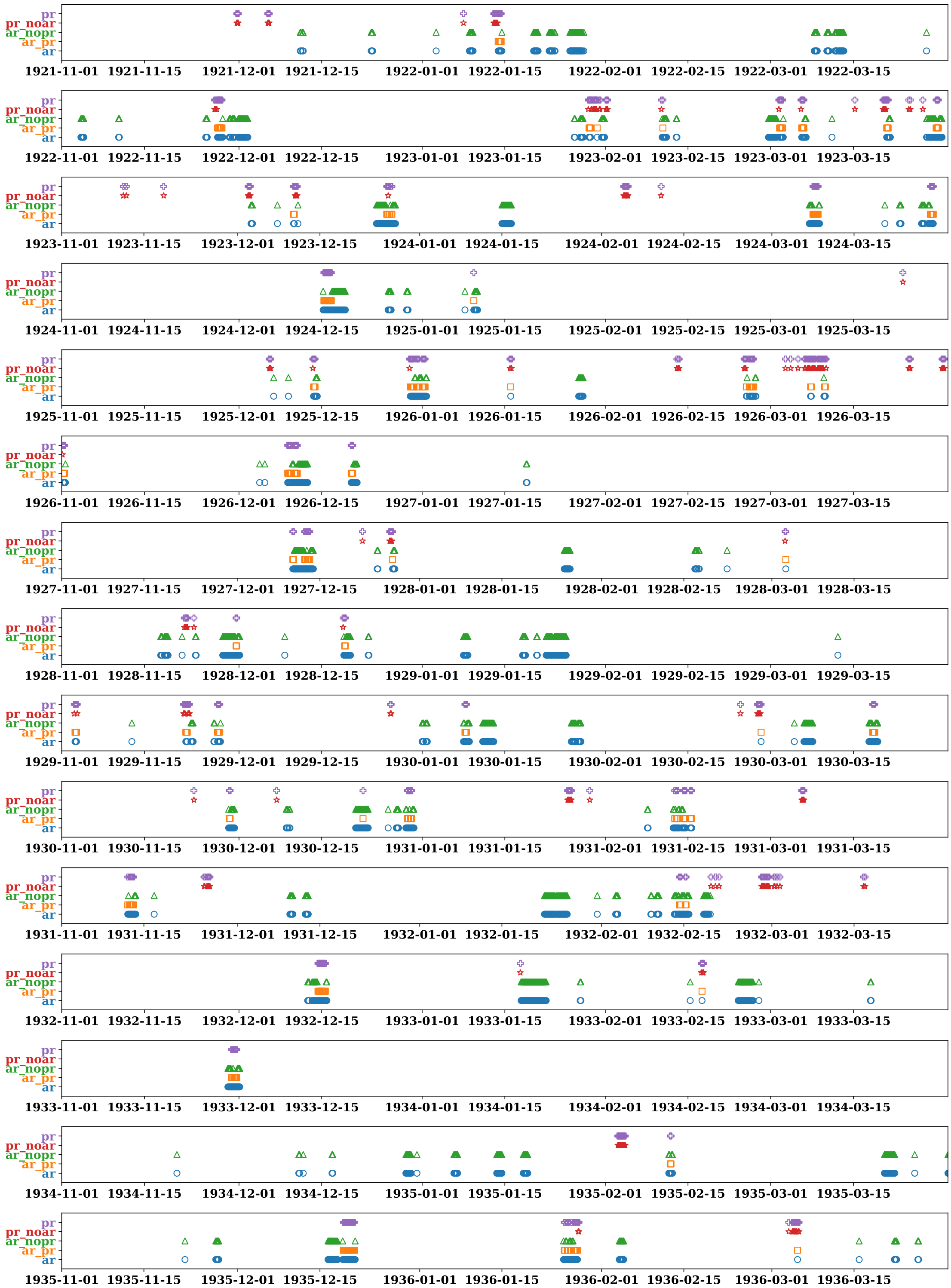

Figure S20. Same caption as Figure S18

Figure S21. Same caption as Figure S18

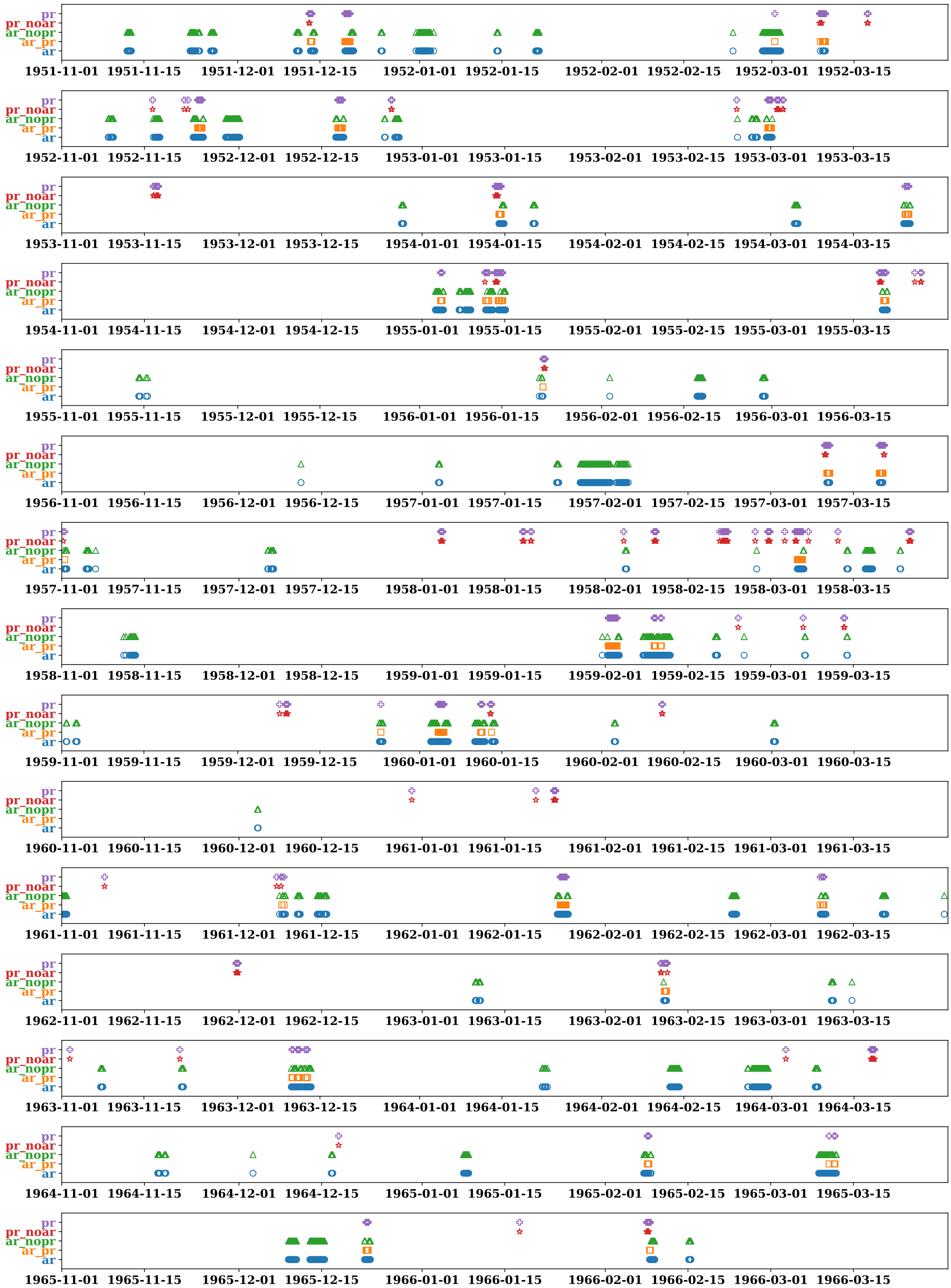

Figure S22. Same caption as Figure S18

Figure S23. Same caption as Figure S18

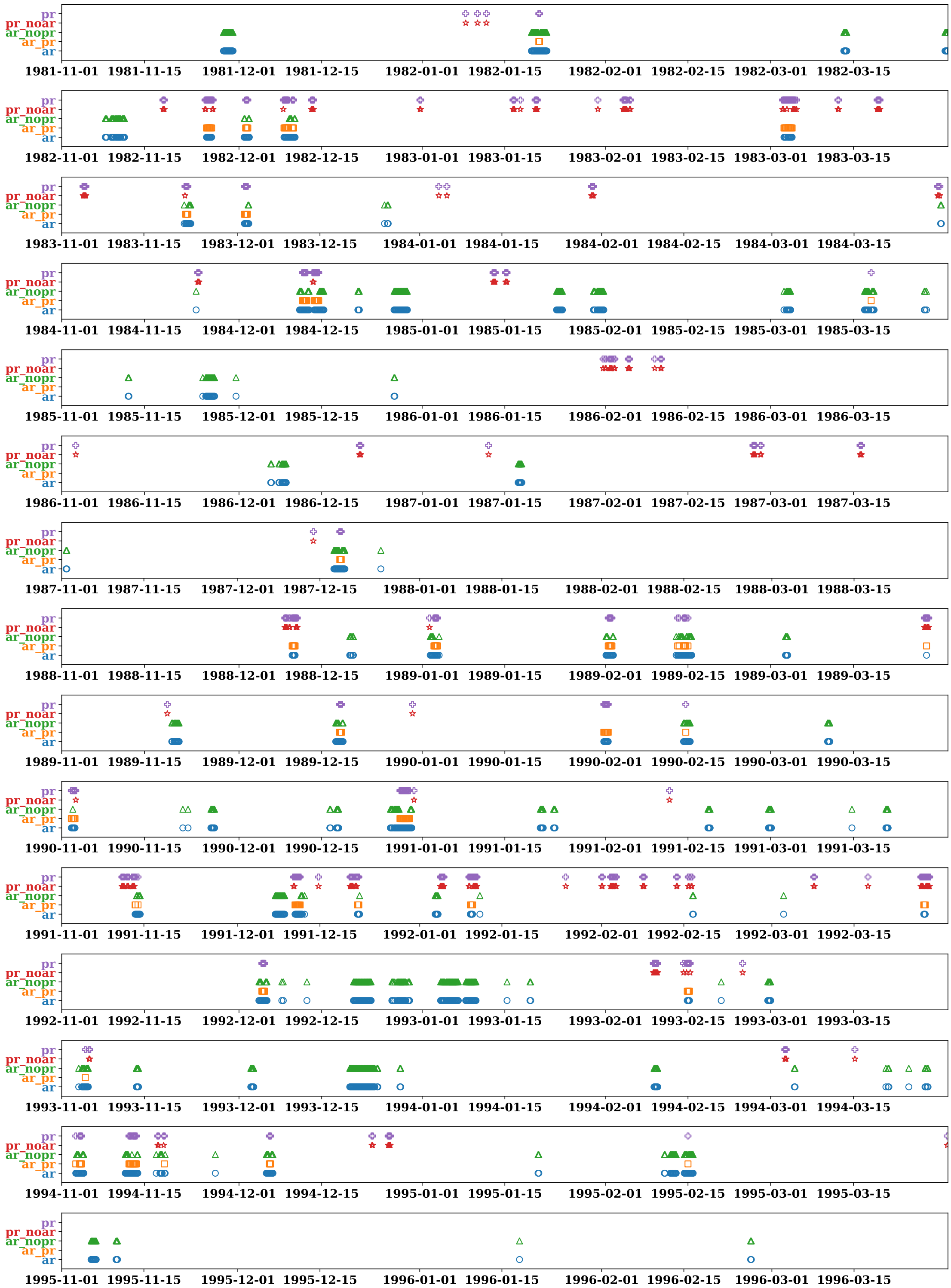

Figure S24. Same caption as Figure S18

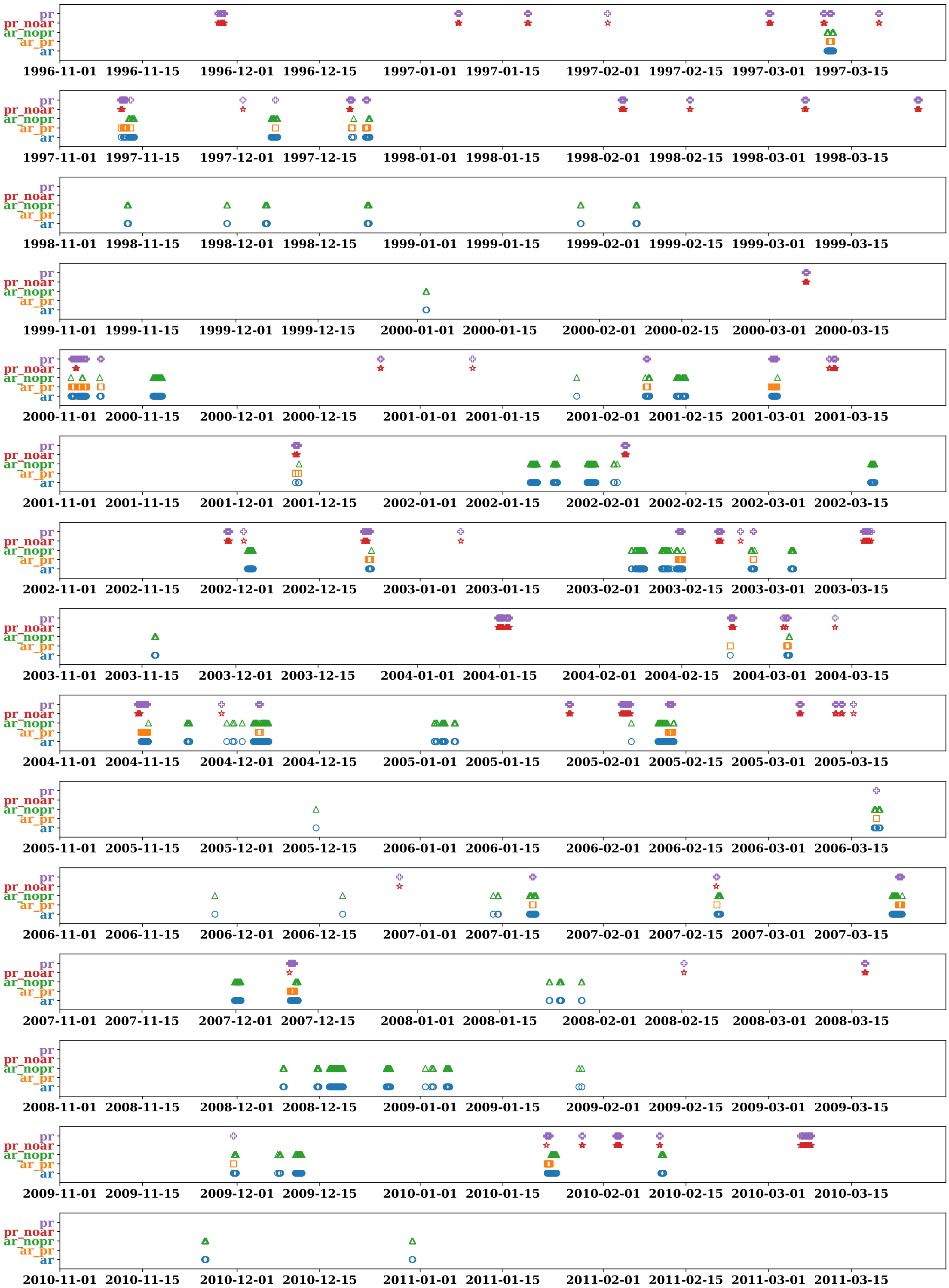

Figure S25. Same caption as Figure S18